

Dynamic Critical Behavior of the Chayes–Machta Algorithm for the Random-Cluster Model

I. Two Dimensions

Timothy M. Garoni

*Department of Mathematics and Statistics
University of Melbourne
Vic. 3010, AUSTRALIA
T.GARONI@MS.UNIMELB.EDU.AU*

Giovanni Ossola

*Department of Physics
New York City College of Technology
300 Jay Street
Brooklyn, NY 11201, USA
GOSSOLA@CITYTECH.CUNY.EDU*

Marco Polin

*Department of Applied Mathematics and Theoretical Physics
University of Cambridge
Wilberforce Road
Cambridge CB3 0WA, UK
M.POLIN@DAMTP.CAM.AC.UK*

Alan D. Sokal*

*Department of Physics
New York University
4 Washington Place
New York, NY 10003, USA
SOKAL@NYU.EDU*

April 4, 2011

Abstract

We study, via Monte Carlo simulation, the dynamic critical behavior of the Chayes–Machta dynamics for the Fortuin–Kasteleyn random-cluster model, which generalizes the Swendsen–Wang dynamics for the q -state Potts ferromagnet to non-integer $q \geq 1$. We consider spatial dimension $d = 2$ and $1.25 \leq q \leq 4$ in steps of 0.25, on lattices up to 1024^2 , and obtain estimates for the dynamic critical exponent z_{CM} . We present evidence that when $1 \leq q \lesssim 1.95$ the Ossola–Sokal conjecture $z_{\text{CM}} \geq \beta/\nu$ is violated, though we also present plausible fits compatible with this conjecture. We show that the Li–Sokal bound $z_{\text{CM}} \geq \alpha/\nu$ is close to being sharp over the entire range $1 \leq q \leq 4$, but is probably non-sharp by a power. As a byproduct of our work, we also obtain evidence concerning the corrections to scaling in static observables.

Key Words: Random-cluster model, Potts model, Chayes–Machta algorithm, Swendsen–Wang algorithm, cluster algorithm, dynamic critical behavior.

*Also at Department of Mathematics, University College London, London WC1E 6BT, United Kingdom.

Contents

1	Introduction	3
2	The Swendsen–Wang and Chayes–Machta algorithms	7
2.1	Swendsen–Wang algorithm	8
2.2	Chayes–Machta algorithm	9
3	Observables and autocorrelation times	11
3.1	Autocorrelation functions and autocorrelation times	11
3.2	Observables to be measured	12
4	Statistical analysis of the Monte Carlo data	15
5	Description of the simulations	19
6	Data analysis: Static quantities	20
6.1	Corrections to finite-size-scaling	21
6.2	The correlation length ξ	23
6.3	The susceptibility χ	24
6.4	The largest cluster C_1	25
6.5	The specific heat C_H	25
7	Data analysis: Dynamic quantities	28
7.1	Dependence on k	28
7.2	Summary of qualitative behavior	29
7.3	Dynamic critical exponent $z_{\text{int},\mathcal{E}'}$	30
7.4	Sharpness of Li–Sokal bound	34
7.5	Test of Ossola–Sokal conjecture	35
7.6	Dynamic critical exponents $z_{\text{int},\mathcal{O}}$ for other \mathcal{O}	36
8	Discussion	37

1 Introduction

Since nontrivial models in statistical mechanics are rarely exactly solvable, Monte Carlo (MC) simulations have become a standard tool for obtaining information on phase diagrams and critical exponents [1–3]. Unfortunately, MC simulations typically suffer from severe *critical slowing-down* [4,5], so that the computational efficiency tends rapidly to zero as the critical point is approached. More precisely, the autocorrelation (relaxation) time τ diverges in the critical limit, most often like $\tau \sim \xi^z$, where ξ is the spatial correlation length. The dynamic critical exponent z depends on both the model being investigated and the MC algorithm being used. For local algorithms one typically has $z \approx 2$.

An important advance was made in 1987 with the invention of the Swendsen–Wang (SW) cluster algorithm [6] for simulating the ferromagnetic q -state Potts model [7–9] at integer $q \geq 2$. The SW algorithm is based on passing back and forth between the Potts spin representation and the Fortuin–Kasteleyn (FK) bond representation [10–15]. More precisely, one introduces a joint probability distribution [14] of spin and bond variables, whose marginal on the spins (integrating out the bonds) is the Potts spin model and whose marginal on the bonds (integrating out the spins) is the FK random-cluster model [15]; one then updates this joint distribution by alternately applying the two conditional distributions (see Section 2.1 below for details).

Since a local move in one set of variables can have highly nonlocal effects in the other, it is not surprising that the SW algorithm might have less critical slowing-down than the conventional local algorithms. And this is in fact the case: although the SW algorithm does not eliminate critical slowing-down, it does radically reduce it compared to local algorithms. Much effort has therefore been devoted, for both theoretical and practical reasons, to understanding the dynamic critical behavior of the SW algorithm as a function of the spatial dimension d and the number q of Potts spin states. The best information on the dynamic critical exponent z_{SW} prior to the present work is summarized in Table 1. Unfortunately, it is very difficult to develop a physical understanding from the small number of non-trivial “data points” at our disposal: second-order non-mean-field transitions occur only for $(d, q) = (2, 2), (2, 3), (2, 4), (3, 2)$ and $(4, 2)$.¹

A further advance was made in 1998 by Chayes and Machta (CM) [25], who devised a cluster algorithm for simulating the FK random-cluster model at any *real* value $q \geq 1$. The idea behind the CM algorithm is very similar to that of SW, but now one starts with the random-cluster (bond) measure and introduces auxiliary color (spin) variables on the sites, so that we again have a joint model of spins and bonds, analogous to the one employed in the SW algorithm. Although the marginal measure on the spins no longer has any obvious physical interpretation when q is noninteger, the joint measure can still be used to construct an efficient cluster algorithm, by alternately applying the conditional distributions exactly as in standard SW. The CM algorithm thus generalizes the SW algorithm and in fact reduces to (a slight variant of) it when q is an integer: see Section 2.2 for details. Indeed, the CM algorithm can be thought of as a “natural”

¹ A continuous (second-order) transition occurs also in the Ising ($q = 2$) model in dimensions $d > 4$, but here the static behavior is mean-field. One expects the dynamic critical exponents likewise to be dimension-independent for $d \geq 4$ (with possible multiplicative logarithmic corrections at $d = 4$).

	Estimates of z_{SW}			
	$q = 1$	$q = 2$	$q = 3$	$q = 4$
$d = 1$	0	0	0	0
$d = 2$	0	0.222 ± 0.007	0.514 ± 0.006	$1 (\times \log^{??})$
$d = 3$	0	0.46 ± 0.03	—	—
$d = 4$	0	$1 (\times \log^{??})$	—	—

Table 1: Best estimates of the dynamic critical exponent z for the Swendsen–Wang algorithm prior to the present work. Estimates are taken from [16] for $d = 2$, $q = 2$; [17] for $d = 2$, $q = 3$; [18, 19] for $d = 2$, $q = 4$; [20] for $d = 3$, $q = 2$; and [21–24] for $d = 4$, $q = 2$. Error bars are one standard deviation, and include statistical errors only.

interpolation of the SW algorithm to noninteger q (though unfortunately only for $q \geq 1$). Thus, by using the CM algorithm we can study the dynamic critical behavior of the SW–CM dynamic universality class as a function of the *continuous* variable q throughout the range $1 \leq q \leq q_c(\mathcal{L})$, where $q_c(\mathcal{L})$ is the maximum q for which the transition is second-order on the given lattice \mathcal{L} .² This vastly enhances our ability to make theoretical sense of the numerical results.

In the present paper we perform high-precision MC simulations of the random-cluster model on the square lattice ($d = 2$), for $1.25 \leq q \leq 4$ in steps of 0.25, using the CM algorithm. Our main goal is to gain better insight into the SW–CM dynamic universality class in two dimensions by studying the behavior as a function of the continuous variable q . We estimate numerically several dynamic critical exponents for each value of q , and we attempt to understand their behavior as a function of q . As a byproduct we also obtain new information on corrections to scaling in the *static* quantities. In the companion paper [27] we carry out an analogous study for the simple-cubic lattice ($d = 3$) at $q = 1.5, 1.8, 2.2$; and in a forthcoming paper [28] we will analyze the case of the complete graph (Curie–Weiss model).³

One advantage of considering $d = 2$ is of course is that we have available a remarkable amount of information concerning the static behavior of the random-cluster model as a function of q . This information includes the exact location [30, 31] of the transition point on the square lattice, namely $p_c = \sqrt{q}/(1 + \sqrt{q})$, and the knowledge that the transition is second-order for $0 \leq q \leq 4$ and first-order for $q > 4$. Furthermore, the leading and next-to-leading thermal and magnetic critical exponents are known exactly (though non-

² We stress that $q_c(\mathcal{L})$ is *not* necessarily the same for all lattices of a given dimension d ; the first-order or second-order nature of the transition is a *non-universal* question. See [26] for further discussion. For the standard two-dimensional lattices (square, triangular and hexagonal) we have $q_c(\mathcal{L}) = 4$.

³ A brief summary of the preliminary results in this trio of papers has appeared in letter form [29].

rigorously) for the entire range $0 \leq q \leq 4$ [32–34]:

$$y_{T1} = \frac{3g - 6}{g} \quad (1.1)$$

$$y_{T2} = \frac{4g - 16}{g} \quad (1.2)$$

$$y_{H1} = \frac{(g + 2)(g + 6)}{8g} \quad (1.3)$$

$$y_{H2} = \frac{(g - 2)(g + 10)}{8g} \quad (1.4)$$

where g is the Coulomb-gas coupling defined by $q = 4 \cos^2(\pi g/4)$ and $2 \leq g \leq 4$.⁴ For the standard critical exponents this implies

$$1/\nu = y_{T1} = \frac{3g - 6}{g} \quad (1.5)$$

$$\Delta_1 = -y_{T2} = \frac{16 - 4g}{g} \quad (1.6)$$

$$d_F = y_{H1} = \frac{(g + 2)(g + 6)}{8g} \quad (1.7)$$

$$\alpha/\nu = 2y_{T1} - d = \frac{4g - 12}{g} \quad (1.8)$$

$$\beta/\nu = d - y_{H1} = \frac{(g - 2)(6 - g)}{8g} \quad (1.9)$$

$$\gamma/\nu = 2y_{H1} - d = \frac{12 + g^2}{4g} \quad (1.10)$$

(Here Δ_1 is the leading correction-to-scaling exponent, defined e.g. by corrections $\sim L^{-\Delta_1}$ in finite volume at criticality; and d_F is the cluster fractal dimension.) The numerical values of these critical exponents for the values of q employed in our simulations are collected for reference in Table 2.

A key theoretical result concerning the SW dynamics is the Li–Sokal bound [35], which states that

$$\tau_{\text{int},\mathcal{N}}, \tau_{\text{exp},\mathcal{N}} \geq \text{const} \times C_H \quad (1.11)$$

where $\tau_{\text{int},\mathcal{N}}$ and $\tau_{\text{exp},\mathcal{N}}$ are, respectively, the integrated and exponential autocorrelation times for the observable \mathcal{N} = number of occupied bonds, and C_H is the specific heat. (For the precise definitions of τ_{int} and τ_{exp} , see Section 3.1.) It follows from this lower bound

⁴ See [19, Appendix A.1] for further discussion and references. Note that there is a typographical error in equation (A.10) of [19], which should read $\Delta_{r,s} = ([2(s-r) + sx]^2 - x^2)/(8[(2+x)])$. We remark that the same formulae for $4 \leq g \leq 6$ give the exponents $y_{T1}, y_{T2}, y_{H1}, y_{H2}$ of the tricritical Potts model [32, 33].

that the SW algorithm *cannot* completely eliminate critical slowing-down if the specific heat is divergent at criticality. In particular, (1.11) implies the lower bound

$$z_{\text{int},\mathcal{N}}, z_{\text{exp}} \geq \alpha/\nu \quad (1.12)$$

for the dynamic critical exponents of the SW algorithm, where α/ν is the static exponent for the specific heat. Now, simple “Fortuin–Kasteleyn identities” show that $\text{var}(\mathcal{N})/V$ is a specific-heat-like quantity and provides a natural continuation of the notion of specific heat to random-cluster models. It turns out that the Li–Sokal bound (1.11) with this definition of specific heat can be easily extended from the SW to the CM algorithm at arbitrary real $q \geq 1$, as we show in [27, Appendix A].

The physical mechanism underlying the Li–Sokal proof is the slow evolution of \mathcal{N} , which is an “energy-like” observable. Previous studies in two dimensions for $q = 2, 3, 4$ have shown empirically that the Li–Sokal bound is very close to being sharp for all three values of q [16, Section 6] [17–19]; and we will show here that this is the case also for noninteger q throughout the range $1 \leq q \leq 4$ (see Sections 7.3 and 7.4). For the three-dimensional Ising model, by contrast, the Li–Sokal bound is very far from sharp [20]. Therefore there must be another mechanism, beyond the one captured in the Li–Sokal proof, that is principally responsible for the critical slowing-down in three dimensions. A few years ago, Ossola and Sokal [20] suggested that this as-yet-not-understood mechanism causing slowness might perhaps be somehow related to the typical size of the largest cluster. More specifically, they conjectured that perhaps the SW dynamics for any Potts ferromagnet in any dimension satisfies

$$\tau_{\text{SW}} \stackrel{?}{\geq} \text{const} \times \frac{L^d}{C_1} \quad (1.13)$$

where C_1 is the expected number of sites in the largest cluster. If true, this would imply the critical-exponent inequality

$$z_{\text{SW}} \stackrel{?}{\geq} \beta/\nu, \quad (1.14)$$

where β/ν is the static exponent for the magnetization. Indeed, Coddington and Baillie [23] had earlier suggested that the inequality (1.14) holds as an *equality* for the Ising models in dimensions $d = 2, 3, 4$. The numerical results reported by Ossola and Sokal [20] for the three-dimensional Ising model are consistent with this conjectured equality, though they also present plausible fits consistent with $z_{\text{SW}} < \beta/\nu$ (i.e. violation of their conjectured inequality). Finally, an analytical treatment [24] of the SW dynamics for the Ising model on the complete graph suggests that $z_{\text{SW}} = \beta/\nu$ in this case also (namely, $z_{\text{SW}} = \beta/\nu = 1$).

Alas, by considering the Ossola–Sokal conjecture within the more general framework of the Chayes–Machta dynamics, one can see at a glance that it is probably false! To start with, for $q = 1$ on any lattice, the Swendsen–Wang–Chayes–Machta algorithm reduces to independent sampling for independent bond percolation, so that $z_{\text{CM}} = 0$; but in general $\beta/\nu > 0$ for percolation, which shows that the Ossola–Sokal conjecture (1.14) is false for $q = 1$. Moreover, it is reasonable to believe that z_{CM} is a continuous function of q : if so, then for q slightly greater than 1 one has either z_{CM} identically zero or else z_{CM} very close

to zero; and in either case one would have $z_{\text{CM}} < \beta/\nu$, so that the Ossola–Sokal conjecture would be violated also for q in some interval above 1.⁵ Our numerical results in this paper (see Section 7.3) suggest that in $d = 2$ the Ossola–Sokal conjecture fails for $1 \leq q \lesssim 1.95$; indeed, for $1 \leq q \lesssim 1.6$ we apparently have $z_{\text{CM}} = 0$ exactly, while of course $\beta/\nu > 0$. (But see Section 7.5 for an alternative fit that is compatible with the Ossola–Sokal conjecture.) Likewise, the numerical results for $d = 3$ to be presented in [27] for $q = 1.5$ and $q = 1.8$ strongly suggest that the Ossola–Sokal conjecture is violated for these values of q and hence presumably for all $q \lesssim 2$, but that it holds as a strict inequality $z_{\text{CM}} > \beta/\nu$ when $q = 2.2$ and hence presumably for all q in the range $2 \lesssim q \leq q_c(\mathbb{Z}^3)$. Indeed, in $d = 3$ it is found that z_{CM} is a strongly increasing function of q , while β/ν varies very slowly with q ; the two curves presumably cross somewhere near $q = 2$. Finally, in our forthcoming paper [28] we will extend the method of [24] to cover the CM dynamics on the complete graph for all q in the range $1 \leq q \leq 2$. We find that there are two markedly different behaviors depending on q : for $1 \leq q < 2$ we have $z_{\text{CM}} = 0 < \beta/\nu = 1$, while for $q = 2$ we have $z_{\text{CM}} = \beta/\nu = 1$. In particular, the Ossola–Sokal conjecture (1.14) is violated when $1 \leq q < 2$ for the CM dynamics on the complete graph.

It therefore seems that the mechanism causing slowness of SW–CM in three dimensions is *not* related in any simple way to the size of the largest cluster, contrary to the intuition of Ossola and Sokal.⁶ And so we are back to square one: no one seems to have the slightest idea what is the physical mechanism dominating the critical slowing-down of the SW–CM dynamics in dimensions $d \geq 3$.

The present paper is organized as follows: In Section 2 we briefly review the Swendsen–Wang algorithm and then present a simple explanation of the Chayes–Machta algorithm. In Section 3 we define the observables and autocorrelation times that we measured in our simulations, while in Section 4 we discuss our methods of statistical data analysis. In Section 5 we summarize the characteristics of our MC simulations. In Section 6 we analyze our numerical data for the static observables, with an emphasis on detecting corrections to scaling and estimating their exponents and amplitudes. In Section 7 we analyze our numerical data for the dynamic quantities (i.e. autocorrelation times), with an emphasis on estimating the dynamic critical exponent z_{CM} as a function of q ; in particular we test the Ossola–Sokal conjecture and the sharpness of the Li–Sokal bound. Finally, in Section 8 we briefly discuss our results and the prospects for future work.

2 The Swendsen–Wang and Chayes–Machta algorithms

In this section we describe a family of algorithms for simulating the FK random-cluster model at any real $q \geq 1$, which generalize slightly the original algorithms introduced by Chayes and Machta [25]. We begin (Section 2.1) by reviewing the Swendsen–Wang

⁵ It is of course conceivable that z_{CM} is discontinuous at $q = 1$: for instance, one might have $z_{\text{CM}} = \beta/\nu$ exactly for all q near 1, but with an amplitude that vanishes as $q \downarrow 1$. In Section 7.5 we will test this scenario against our data.

⁶ Or at least, no such relation seems to hold for *all* q . It is still conceivable that such a relation might hold for $q = 2$ only, or for all $q \geq 2$.

[6] algorithm for simulating the ferromagnetic q -state Potts model at integer $q \geq 2$, with emphasis on the perspective afforded by the joint probability distribution of spins and bonds (sometimes known as the Edwards–Sokal coupling [14]). We then present (Section 2.2) our version of the Chayes–Machta algorithm and a proof of its validity. For an alternative (and rather more general) presentation of the Chayes–Machta algorithm, see [27].

2.1 Swendsen–Wang algorithm

Let $G = (V, E)$ be a finite graph with vertex set V and edge set E , and let q be an integer ≥ 2 . The q -state Potts model on G with nearest-neighbor couplings $\beta = \{\beta_e\}_{e \in E}$ is defined by the Gibbs measure

$$\pi_{\beta, q}(\boldsymbol{\sigma}) \propto \exp\left(\sum_{e \in E} \beta_e \delta_e(\boldsymbol{\sigma})\right) \quad (2.1a)$$

$$\propto \prod_{e \in E} [(1 - p_e) + p_e \delta_e(\boldsymbol{\sigma})], \quad (2.1b)$$

for $\boldsymbol{\sigma} \in \{1, 2, \dots, q\}^V$, where $p_e = 1 - e^{-\beta_e}$ for each $e \in E$ and

$$\delta_e(\boldsymbol{\sigma}) = \delta_{\sigma_x, \sigma_y} \text{ for } e = \langle xy \rangle. \quad (2.2)$$

One rather natural way to elucidate the Swendsen–Wang (SW) algorithm is via the Edwards–Sokal coupling [14] of the Potts and random-cluster models. Recall first that the random-cluster model [15], introduced by Fortuin and Kasteleyn [10–13], is a correlated bond-percolation model defined on a finite graph $G = (V, E)$ for parameter $q > 0$ (not necessarily an integer) and edge probabilities $\mathbf{p} = \{p_e\}_{e \in E}$, by the probability measure

$$\phi_{\mathbf{p}, q}(\mathbf{n}) \propto q^{k(\mathbf{n})} B_{\mathbf{p}}(\mathbf{n}), \quad (2.3)$$

for $\mathbf{n} \in \{0, 1\}^E$, where

$$B_{\mathbf{p}}(\mathbf{n}) = \prod_{e \in E: n_e=1} p_e \prod_{e \in E: n_e=0} (1 - p_e) \quad (2.4)$$

and $k(\mathbf{n})$ is the number of connected components (“clusters”) in the spanning subgraph whose edges are those with $n_e = 1$ (we call these “components of \mathbf{n} ” for short). The Potts and random-cluster models are intimately related, in the sense that correlation functions of the Potts spins can be expressed in terms of connectivity functions of the random-cluster model. The Edwards–Sokal coupling is a joint measure on the space of spin and bond configurations, defined by

$$\mu_{\mathbf{p}, q}(\mathbf{n}, \boldsymbol{\sigma}) \propto \prod_{e \in E} [(1 - p_e) \delta_{n_e, 0} + p_e \delta_{n_e, 1} \delta_e(\boldsymbol{\sigma})]. \quad (2.5)$$

It is easy to show [5, 14] that the marginal measure $\sum_{\mathbf{n}} \mu_{\mathbf{p},q}(\mathbf{n}, \cdot)$ on the spins is the Potts measure (2.1), and the marginal measure $\sum_{\sigma} \mu_{\mathbf{p},q}(\cdot, \sigma)$ on the bonds is the random-cluster measure (2.3). Explicit forms for the conditional measures are also easily computed:

$$\mu_{\mathbf{p},q}(\sigma|\mathbf{n}) = \Delta(\mathbf{n}, \sigma) q^{-k(\mathbf{n})} \quad (2.6)$$

$$\mu_{\mathbf{p},q}(\mathbf{n}|\sigma) = \Delta(\mathbf{n}, \sigma) B_{\mathbf{p}}(\mathbf{n}) \quad (2.7)$$

where

$$\Delta(\mathbf{n}, \sigma) = \begin{cases} 1 & \text{if } \delta_e(\sigma) = 1 \text{ for all } e \text{ with } n_e = 1 \\ 0 & \text{otherwise} \end{cases} \quad (2.8)$$

In words, $\Delta(\mathbf{n}, \sigma)$ is the indicator for the event that “we draw occupied bonds only between vertices with the same spin value”.

The SW algorithm simulates the Edwards–Sokal measure (2.5), and hence both the Potts and random-cluster models, by alternately updating the spins conditioned on the bonds using (2.6) and the bonds conditioned on the spins using (2.7). In words, the spin-updating rule (2.6) states that, independently for each cluster, we choose a new spin value uniformly at random from the q possible choices and assign this spin value to all vertices in the cluster; while the bond-updating rule (2.7) states that on each subgraph induced by the vertices of a given spin value we update the bonds via independent bond percolation.

2.2 Chayes–Machta algorithm

Consider the random-cluster model defined on a finite graph $G = (V, E)$ by (2.3). Recall that to arrive at the SW algorithm for the Potts model, one introduces auxiliary bond variables and then considers the joint model of Potts spins on the vertices and auxiliary bond variables on the edges. The SW algorithm updates this joint model by alternately applying its two conditional measures (bond variables given spins and spin variables given bonds). Here we do the reverse: starting from the random-cluster model (2.3), we introduce auxiliary color variables on the vertices of G and then consider the joint model of our original bond variables and the new auxiliary color variables; we will then update this joint model by alternately applying its conditional measures. To this end, let us introduce color variables on the sites taking values in some finite set S , i.e. $\sigma \in S^V$. For each $\alpha \in S$, we choose a number $q_\alpha \geq 0$, and write $\mathbf{q} = \{q_\alpha\}_{\alpha \in S}$. We can now introduce the coupled probability measure

$$\mu_{\mathbf{p},\mathbf{q}}(\mathbf{n}, \sigma) \propto \Delta(\mathbf{n}, \sigma) B_{\mathbf{p}}(\mathbf{n}) \prod_{\alpha \in S} q_\alpha^{k_\alpha(\sigma, \mathbf{n})}. \quad (2.9)$$

Here $\Delta(\mathbf{n}, \sigma)$ is again given by (2.8) but now with $\sigma \in S^V$, i.e. it is the indicator of the event “we draw occupied bonds only between vertices of the same color”; and we denote by $k_\alpha(\sigma, \mathbf{n})$ the number of components of \mathbf{n} that are colored α by σ . Note that $k_\alpha(\sigma, \mathbf{n})$ is well-defined whenever $\Delta(\mathbf{n}, \sigma) \neq 0$. From the definition (2.9) we can observe the following:

- 1) The marginal measure $\sum_{\sigma} \mu_{\mathbf{p},q}(\cdot, \sigma)$ on the bond variables is the random-cluster measure with parameter $q = \sum_{\alpha \in S} q_{\alpha}$.
- 2) The conditional measure of σ given \mathbf{n} is as follows: Independently for each component of \mathbf{n} , randomly choose a value $\alpha \in S$ with probability q_{α}/q and impose it on all vertices in that component.
- 3) Every coloring σ defines a partition of the vertex set into $V = \bigcup_{\alpha \in S} V_{\alpha}$, where V_{α} is the set of all sites $v \in V$ colored α by σ . The conditional measure of \mathbf{n} given σ is then simply the product over $\alpha \in S$ of random-cluster measures with parameter q_{α} on the induced subgraphs $G[V_{\alpha}]$. All bonds not lying within a single $G[V_{\alpha}]$ are forced to be unoccupied.

Now suppose that for each $\alpha \in S$ and each induced subgraph $H \subseteq G$, we have a valid Monte Carlo algorithm for updating the random-cluster model with parameter q_{α} on H . We can then apply the following algorithm to simulate the joint model (2.9), and therefore, via Observation 1, the random-cluster model with parameter $q = \sum_{\alpha \in S} q_{\alpha}$:

Algorithm 1 (Random-cluster algorithm).

1. *Given a bond configuration, choose a new color configuration using the conditional measure described in Observation 2.*
2. *Given the new color configuration, for each $\alpha \in S$ update the random-cluster model on $G[V_{\alpha}]$ with parameter q_{α} , using the given algorithm.*

Note that for any $\alpha \in S$, one valid Monte Carlo update is to do nothing (i.e. perform the identity operation), since detailed balance is satisfied trivially. Furthermore, if q_{α} happens to equal 1, one can use a Bernoulli update, i.e. erase the bonds on $G[V_{\alpha}]$ and choose new ones via independent bond percolation. But if one has some other way of updating a random-cluster measure with parameter q_{α} , then that is fine too. A number of special cases of Algorithm 1 are now clear:

1. If q is an integer, $S = \{1, \dots, q\}$, $q_{\alpha} = 1$ for all α , and one uses Bernoulli updates for every α , then Algorithm 1 is simply the standard SW algorithm.
2. If q is an integer, $S = \{1, \dots, q\}$, $q_{\alpha} = 1$ for all α , and one uses Bernoulli updates for $1 \leq \alpha \leq k$ and do-nothing updates for $k + 1 \leq \alpha \leq q$ (where k is any integer satisfying $1 \leq k \leq q$), then Algorithm 1 is a variant of the SW algorithm in which only the first k colors are “active”.
3. If $q \geq 1$, $S = \{active, inactive\}$, $q_{active} = 1$, $q_{inactive} = q - 1$, and one uses a Bernoulli update for $\alpha = active$ and a do-nothing update for $\alpha = inactive$, then Algorithm 1 is the original Chayes–Machta algorithm presented in [25].
4. If $q \geq k \geq 1$ with k an integer, $S = \{1, \dots, k, inactive\}$, $q_{\alpha} = 1$ for $1 \leq \alpha \leq k$, $q_{inactive} = q - k$, and one uses a Bernoulli update for $1 \leq \alpha \leq k$ and a do-nothing update for $\alpha = inactive$, this is the generalized algorithm presented in [25, pp. 482–483].

Note that since each of these cases involves performing Bernoulli updates, they all require $q \geq 1$. For a given value of $q \geq 1$, Case 4 provides a family of algorithms, indexed by the integer k , for simulating the random-cluster model. We call this “the Chayes–Machta algorithm with k active colors”. Any choice of $1 \leq k \leq \lfloor q \rfloor$ is legitimate, though it seems reasonable to expect that $k = \lfloor q \rfloor$ should be the most efficient. Indeed, our numerical simulations suggest that in practice the autocorrelation time is approximately proportional to $1/k$ (see Section 7.1 below).

3 Observables and autocorrelation times

In this section we recall the definitions of the various autocorrelation times (Section 3.1) and then list the observables that we measured in our simulations (Section 3.2).

3.1 Autocorrelation functions and autocorrelation times

Consider an observable \mathcal{O} in the random-cluster model, i.e. a real-valued function of $\mathbf{n} \in \{0, 1\}^E$. Then a realization of the Chayes–Machta (CM) Markov chain gives rise to a time series $\mathcal{O}(t)$, where each unit of time corresponds to one step of the CM algorithm. The autocovariance function of \mathcal{O} is defined to be

$$C_{\mathcal{O}\mathcal{O}}(t) = \langle \mathcal{O}(0)\mathcal{O}(t) \rangle - \langle \mathcal{O} \rangle^2, \quad (3.1)$$

where the expectation is taken in equilibrium. The normalized autocorrelation function of \mathcal{O} is then

$$\rho_{\mathcal{O}\mathcal{O}}(t) = \frac{C_{\mathcal{O}\mathcal{O}}(t)}{C_{\mathcal{O}\mathcal{O}}(0)}. \quad (3.2)$$

From $\rho_{\mathcal{O}\mathcal{O}}(t)$ we define the integrated autocorrelation time as

$$\tau_{\text{int},\mathcal{O}} = \frac{1}{2} \sum_{t=-\infty}^{\infty} \rho_{\mathcal{O}\mathcal{O}}(t) \quad (3.3)$$

and the exponential autocorrelation time as

$$\tau_{\text{exp},\mathcal{O}} = \limsup_{|t| \rightarrow \infty} \frac{-|t|}{\log \rho_{\mathcal{N}\mathcal{N}}(t)}. \quad (3.4)$$

Finally, the exponential autocorrelation time of the system is defined as

$$\tau_{\text{exp}} = \sup_{\mathcal{O}} \tau_{\text{exp},\mathcal{O}}, \quad (3.5)$$

where the supremum is taken over all observables \mathcal{O} . This autocorrelation time thus measures the decay rate of the slowest mode of the system. All observables that are not orthogonal to this slowest mode satisfy $\tau_{\text{exp},\mathcal{O}} = \tau_{\text{exp}}$.

It is important to remember that there is not just one autocorrelation time, but many: namely τ_{exp} as well as $\tau_{\text{int},\mathcal{O}}$ for each \mathcal{O} . In all but the most trivial Markov chains these

autocorrelation times are *not* equal. Correspondingly, there are many dynamic critical exponents: namely z_{exp} as well as $z_{\text{int},\mathcal{O}}$ for each \mathcal{O} . These exponents *may* in some cases be equal, but they need not be; this is a detailed dynamical question, and the answer will vary from algorithm to algorithm and model to model.

More information on the principles of Markov-chain Monte Carlo and the relations between these autocorrelation times can be found in [5].

3.2 Observables to be measured

We now take the graph G to be the d -dimensional simple-hypercubic lattice of linear size L with periodic boundary conditions; we denote this graph by \mathbb{Z}_L^d in order to emphasize that addition of coordinates is always taken mod L . When the precise form of the graph G is unimportant to our definitions, we denote the vertex set and edge set as simply $V(G)$ and $E(G)$, respectively.

For $x_1, \dots, x_m \in V(G)$, not necessarily all distinct, we denote by $\gamma_{x_1 \dots x_m}$ the indicator for the event that the vertices x_1, \dots, x_m are all in the same cluster, i.e.

$$\gamma_{x_1 \dots x_m}(\mathbf{n}) = \begin{cases} 1 & \text{if } x_1 \leftrightarrow x_2 \leftrightarrow x_3 \leftrightarrow \dots \leftrightarrow x_m \text{ in configuration } \mathbf{n} \\ 0 & \text{otherwise} \end{cases} \quad (3.6)$$

and $x \leftrightarrow y$ denotes that x is connected to y by at least one path of occupied bonds. In particular, $\tau(x, y) = \langle \gamma_{xy} \rangle$ is the ‘‘two-point connectivity function’’, i.e. the probability that x is connected to y . On \mathbb{Z}_L^d we write $\tau(x) = \tau(x, 0)$, and translational invariance gives us $\tau(x, y) = \tau(x - y)$ for all $x, y \in \mathbb{Z}_L^d$.

We measured the following observables in our MC simulations:

- The number of occupied bonds

$$\mathcal{N} = \sum_{e \in E(G)} n_e \quad (3.7)$$

- The nearest-neighbor connectivity (which is an energy-like observable [17])

$$\mathcal{E}' = \sum_{\langle xy \rangle \in E(G)} \gamma_{xy} \quad (3.8)$$

- The cluster-size moments

$$\mathcal{S}_m = \sum_{C \in K(\mathbf{n})} |C|^m \quad (3.9a)$$

$$= \sum_{x_1, \dots, x_m \in V(G)} \gamma_{x_1 \dots x_m}(\mathbf{n}), \quad (3.9b)$$

where the size $|C|$ of a cluster means the number of vertices. In this work we measured \mathcal{S}_m for $m = 2, 4, 6, 8$;

- The size \mathcal{C}_i of the i th largest cluster. In this work we measured \mathcal{C}_i for $i = 1, 2, 3$;
- An observable used to compute the Fourier transform of $\tau(x, y)$ evaluated at the smallest non-zero momentum $(2\pi/L, 0, \dots, 0)$:

$$\mathcal{F}' = \frac{1}{d} \sum_{j=1}^d \sum_{x, y \in \mathbb{Z}_L^d} \gamma_{xy} e^{2\pi i(x_j - y_j)/L} \quad (3.10a)$$

$$= \frac{1}{d} \sum_{j=1}^d \sum_{C \in K(\mathbf{n})} \left| \sum_{x \in C} e^{2\pi i x_j / L} \right|^2 \quad (3.10b)$$

From these observables we computed the following quantities:

- The bond density

$$N = \frac{\langle \mathcal{N} \rangle}{B}, \quad (3.11)$$

where $B = |E|$ is the total number of edges in the graph G (i.e. $B = dL^d$ for $G = \mathbb{Z}_L^d$);

- The connectivity density

$$E' = \frac{\langle \mathcal{E}' \rangle}{B} \quad (3.12)$$

- The specific heat. There are a number of sensible definitions for specific heat, and we considered the following (see Remark 3.1 below):

$$C_H^{(1)} = \frac{1}{B} \text{var}(\mathcal{N}) \quad (3.13)$$

$$C_H^{(2)} = \frac{d}{p^2} [C_H^{(1)} - (1-p)N] \quad (3.14)$$

$$C_H^{(3)} = \frac{q^2}{(q-1)^2} C_H^{(2)} \quad (3.15)$$

In this paper we used $C_H = C_H^{(2)}$ in agreement with [16, 17].

- The expected size of the i th largest cluster,

$$C_i = \langle \mathcal{C}_i \rangle \quad (3.16)$$

We expect that in the critical region $C_i \sim L^{d-\beta/\nu}$ as $L \rightarrow \infty$, for any fixed i ;

- The susceptibility (see Remark 3.2 below)

$$\chi = \frac{\langle \mathcal{S}_2 \rangle}{L^d} \quad (3.17)$$

In the random-cluster model, χ is the mean size of the cluster containing any specified point.

- The Fourier transform of the two-point connectivity function $\tau(x)$, evaluated at the smallest nonzero momentum, $(2\pi/L, 0, \dots, 0)$:

$$F = \tilde{\tau}(p) \Big|_{p=(2\pi/L, 0, \dots, 0)} = \frac{\langle \mathcal{F}' \rangle}{L^d} \quad (3.18)$$

- The finite-size second-moment correlation length (see Remark 3.3 below):

$$\xi = \frac{1}{2 \sin(\pi/L)} \left(\frac{\chi}{F} - 1 \right)^{1/2} \quad (3.19)$$

Remark 3.1. The definition $C_H^{(1)}$ of the specific heat seems quite natural from the perspective of the random-cluster model, in which we view the bond variables as fundamental; in particular, it arises in a very direct way in the proof of the Li–Sokal bound for the CM algorithm [27, Appendix]. The definitions $C_H^{(2)}$ and $C_H^{(3)}$, by contrast, are designed to reduce to more familiar expressions in terms of the energy of the Potts spin model when q is an integer. Specifically, if q is an integer we have

$$C_H^{(2)} = \frac{1}{V} \text{var} \left(\sum_{\langle xy \rangle \in E} \delta_{\sigma_x, \sigma_y} \right) \quad (3.20)$$

$$C_H^{(3)} = \frac{1}{V} \text{var} \left(\sum_{\langle xy \rangle \in E} \sigma_x \cdot \sigma_y \right) \quad (3.21)$$

where $\sigma_x \in \{1, 2, \dots, q\}$ and $\sigma_x \in \mathbb{R}^{q-1}$ is a Potts spin in the hypertetrahedral representation, so that

$$\sigma_x \cdot \sigma_y = \frac{q \delta_{\sigma_x, \sigma_y} - 1}{q - 1}. \quad (3.22)$$

Remark 3.2. We note that for $q \in \{2, 3, \dots\}$, the Fortuin–Kasteleyn identity $\langle \sigma_x \cdot \sigma_y \rangle = \langle \gamma_{xy} \rangle$ shows that $\langle \mathcal{M}^2 \rangle = \langle \mathcal{S}_2 \rangle$, where \mathcal{M}^2 is the squared magnetization, and hence χ is simply equal to the magnetic susceptibility.

Remark 3.3. In terms of $\tilde{\tau}(p)$ the definition (3.19) has the general form

$$\xi = \frac{1}{2 \sin(\pi/L)} \left(\frac{\tilde{\tau}(0, \dots, 0)}{\tilde{\tau}(2\pi/L, 0, \dots, 0)} - 1 \right)^{1/2} \quad (3.23)$$

and applies equally well to the integer q case where we interpret $\tau(x)$ as the spin-spin correlation function. A very nice account of the origin of the definition (3.23) of the finite-size correlation length, relating it to the thermodynamic second-moment correlation length is given in [36, Part III]; see also [37, 38].

The prime on \mathcal{F}' is employed to distinguish it from another estimator for F , often denoted \mathcal{F} , which can be defined in terms of Potts spins when $q \in \{2, 3, \dots\}$: see e.g. [17]. We note that \mathcal{F}' could profitably be used even in Swendsen–Wang simulations of the Potts model, as an alternative to \mathcal{F} .

Remark 3.4. For any $q > 0$ and any $\langle xy \rangle \in E(G)$ we have the identity

$$q \langle n_{xy} \rangle = p [(q - 1) \langle \gamma_{xy} \rangle + 1]. \quad (3.24)$$

This is most easily seen by first considering the Edwards–Sokal joint measure when q is an integer ≥ 2 , and then combining the identities $\langle n_{xy} \rangle = p \langle \delta_{\sigma_x, \sigma_y} \rangle$ and $\langle \gamma_{xy} \rangle = \langle \sigma_x \cdot \sigma_y \rangle$ together with (3.22). See e.g. [5]. This clearly proves (3.24) for all $q \in \{2, 3, \dots\}$; and since both sides are rational functions of q , it follows that the equality must hold for all $q \in \mathbb{C}$. Summing over all edges we then obtain

$$\langle \mathcal{N} \rangle = p \frac{q-1}{q} \langle \mathcal{E}' \rangle + \frac{p}{q} B. \quad (3.25)$$

As a consistency check on the correctness of our simulations we numerically tested the identity (3.25) to high precision by measuring the observable

$$\mathcal{N} - p \frac{q-1}{q} \mathcal{E}' - \frac{p}{q} B. \quad (3.26)$$

Clearly this observable should have mean zero, and in all our simulations this was observed to be the case within statistical errors.

4 Statistical analysis of the Monte Carlo data

Consider a generic observable \mathcal{O} with expectation $\langle \mathcal{O} \rangle = \mu_{\mathcal{O}}$. Suppose that, after equilibration, we have a sequence of T Monte Carlo measurements of \mathcal{O} , denoted $\{\mathcal{O}_t\}_{t=1}^T$. Since the Monte Carlo process is assumed equilibrated, the $\{\mathcal{O}_t\}_{t=1}^T$ are a sample from a stationary stochastic process (also called a stationary time series). In this section we recall the basic principles of statistical time-series analysis, and describe the standard estimators for various quantities associated with \mathcal{O} . For more details, see e.g. [5, 39].

The natural estimator for the expectation $\mu_{\mathcal{O}}$ is the sample mean

$$\bar{\mathcal{O}} = \frac{1}{T} \sum_{t=1}^T \mathcal{O}_t. \quad (4.1)$$

This is an unbiased estimator and has a variance

$$\text{var}(\bar{\mathcal{O}}) = \frac{1}{T^2} \sum_{s,t=1}^T C_{\mathcal{O}\mathcal{O}}(t-s) \quad (4.2a)$$

$$= \frac{1}{T} \sum_{t=-(T-1)}^{T-1} \left(1 - \frac{|t|}{T}\right) C_{\mathcal{O}\mathcal{O}}(t) \quad (4.2b)$$

$$\approx \frac{1}{T} 2 \tau_{\text{int}, \mathcal{O}} C_{\mathcal{O}\mathcal{O}}(0) \quad \text{for } T \gg \tau_{\text{int}, \mathcal{O}}. \quad (4.2c)$$

This implies that the variance of $\bar{\mathcal{O}}$ is a factor $2 \tau_{\text{int}, \mathcal{O}}$ larger than it would be if the measurements were uncorrelated. Therefore, in order to obtain accurate error bars for

the estimator of the static quantity $\mu_{\mathcal{O}}$, we must obtain an accurate estimate of the dynamic quantity $\tau_{\text{int},\mathcal{O}}$.

The natural estimator for the autocovariance function is

$$\widehat{C}_{\mathcal{O}\mathcal{O}}(t) = \frac{1}{T-|t|} \sum_{s=1}^{T-|t|} (\mathcal{O}_s - \mu_{\mathcal{O}})(\mathcal{O}_{s+t} - \mu_{\mathcal{O}}) \quad (4.3)$$

if the expectation $\mu_{\mathcal{O}}$ is known, and

$$\widehat{\widehat{C}}_{\mathcal{O}\mathcal{O}}(t) = \frac{1}{T-|t|} \sum_{s=1}^{T-|t|} (\mathcal{O}_s - \overline{\mathcal{O}})(\mathcal{O}_{s+t} - \overline{\mathcal{O}}) \quad (4.4)$$

if $\mu_{\mathcal{O}}$ is unknown. The estimator $\widehat{C}_{\mathcal{O}\mathcal{O}}(t)$ is unbiased, and the bias of $\widehat{\widehat{C}}_{\mathcal{O}\mathcal{O}}(t)$ is of order $1/T$. To leading order for $T \gg \tau_{\text{int},\mathcal{O}}$ the covariance matrices of $\widehat{C}_{\mathcal{O}\mathcal{O}}$ and $\widehat{\widehat{C}}_{\mathcal{O}\mathcal{O}}$ are equal and it can be shown [39, 40] that

$$\begin{aligned} \text{cov}(\widehat{C}_{\mathcal{O}\mathcal{O}}(t), \widehat{C}_{\mathcal{O}\mathcal{O}}(u)) &= \frac{1}{T} \sum_{s=-\infty}^{\infty} [C_{\mathcal{O}\mathcal{O}}(s)C_{\mathcal{O}\mathcal{O}}(s+u-t) + C_{\mathcal{O}\mathcal{O}}(s+u)C_{\mathcal{O}\mathcal{O}}(s-t) \\ &\quad + \kappa(t, s, s+u)] + o(1/T), \end{aligned} \quad (4.5)$$

where $t, u \geq 0$ and κ is the connected 4-point autocorrelation function

$$\begin{aligned} \kappa(r, s, t) &= \langle (\mathcal{O}_i - \mu_{\mathcal{O}})(\mathcal{O}_{i+r} - \mu_{\mathcal{O}})(\mathcal{O}_{i+s} - \mu_{\mathcal{O}})(\mathcal{O}_{i+t} - \mu_{\mathcal{O}}) \rangle \\ &\quad - C_{\mathcal{O}\mathcal{O}}(r)C_{\mathcal{O}\mathcal{O}}(t-s) - C_{\mathcal{O}\mathcal{O}}(s)C_{\mathcal{O}\mathcal{O}}(t-r) - C_{\mathcal{O}\mathcal{O}}(t)C_{\mathcal{O}\mathcal{O}}(s-r). \end{aligned} \quad (4.6)$$

Similarly, the natural estimator for the autocorrelation function is

$$\widehat{\rho}_{\mathcal{O}\mathcal{O}}(t) = \frac{\widehat{C}_{\mathcal{O}\mathcal{O}}(t)}{\widehat{C}_{\mathcal{O}\mathcal{O}}(0)} \quad (4.7)$$

if $\mu_{\mathcal{O}}$ is known, and

$$\widehat{\widehat{\rho}}_{\mathcal{O}\mathcal{O}}(t) = \frac{\widehat{\widehat{C}}_{\mathcal{O}\mathcal{O}}(t)}{\widehat{\widehat{C}}_{\mathcal{O}\mathcal{O}}(0)} \quad (4.8)$$

if $\mu_{\mathcal{O}}$ is unknown. Both the estimators $\widehat{\rho}_{\mathcal{O}\mathcal{O}}(t)$ and $\widehat{\widehat{\rho}}_{\mathcal{O}\mathcal{O}}(t)$ have bias of order $1/T$. The covariance matrices of $\widehat{\rho}_{\mathcal{O}\mathcal{O}}$ and $\widehat{\widehat{\rho}}_{\mathcal{O}\mathcal{O}}$ are the same to leading order for large T . If the process is Gaussian, this covariance matrix is given in the large T limit by [39]

$$\begin{aligned} \text{cov}(\widehat{\rho}_{\mathcal{O}\mathcal{O}}(t), \widehat{\rho}_{\mathcal{O}\mathcal{O}}(u)) &= \frac{1}{T} \sum_{s=-\infty}^{\infty} [\rho_{\mathcal{O}\mathcal{O}}(s)\rho_{\mathcal{O}\mathcal{O}}(s+t-u) + \rho_{\mathcal{O}\mathcal{O}}(s+u)\rho_{\mathcal{O}\mathcal{O}}(s-t) \\ &\quad + 2\rho_{\mathcal{O}\mathcal{O}}(t)\rho_{\mathcal{O}\mathcal{O}}(u)\rho_{\mathcal{O}\mathcal{O}}^2(s) - 2\rho_{\mathcal{O}\mathcal{O}}(t)\rho_{\mathcal{O}\mathcal{O}}(s)\rho_{\mathcal{O}\mathcal{O}}(s-u) \\ &\quad - 2\rho_{\mathcal{O}\mathcal{O}}(u)\rho_{\mathcal{O}\mathcal{O}}(s)\rho_{\mathcal{O}\mathcal{O}}(s-t)] + o(1/T). \end{aligned} \quad (4.9)$$

If the process is not Gaussian, then there are additional terms proportional to the fourth cumulant $\kappa(s, t, t-u)$. The simplest assumption is to assume the stochastic process to

be “not too far from Gaussian” and simply drop all the terms involving κ . This is what we will do. If this assumption is not justified, then we are introducing a bias into the estimate of $\text{cov}(\widehat{\rho}_{\mathcal{O}\mathcal{O}}(t), \widehat{\rho}_{\mathcal{O}\mathcal{O}}(u))$.

Finally, we take the estimator for the integrated autocorrelation time to be [41]

$$\widehat{\tau}_{\text{int},\mathcal{O}} = \frac{1}{2} \sum_{t=-M}^M \widehat{\rho}_{\mathcal{O}\mathcal{O}}(t) \quad (4.10)$$

if $\mu_{\mathcal{O}}$ is known, or the analogous object defined in terms of $\widehat{\rho}_{\mathcal{O}\mathcal{O}}$ is $\mu_{\mathcal{O}}$ is unknown; here $M (\leq T - 1)$ is a suitably chosen number, which we call the *window width*. One’s first thought might be to use all the data, i.e. take $M = T - 1$; but this turns out to be a very bad estimator, which has a variance of order 1 even as $T \rightarrow \infty$. Loosely speaking (see e.g. [39, 41]), this is because the terms in $\widehat{\rho}_{\mathcal{O}\mathcal{O}}(t)$ with large t (namely, $t \gg \tau_{\text{exp},\mathcal{O}}$) have variance of order $1/T$ that does not vanish as t grows, cf. (4.9), and there are of order T of them. These terms thus contribute much “noise” but very little “signal”, since $\rho_{\mathcal{O}\mathcal{O}}(t)$ is tiny when $t \gg \tau_{\text{exp},\mathcal{O}}$. To obtain a good estimator, we should instead choose the window width M to be large enough so that we do not lose too much “signal”, i.e. $\rho_{\mathcal{O}\mathcal{O}}(t)$ is tiny for all $t > M$, but not too much larger than this. In general, a window of width M creates a bias given by

$$\text{bias}(\widehat{\tau}_{\text{int},\mathcal{O}}) = -\frac{1}{2} \sum_{|t|>M} \rho_{\mathcal{O}\mathcal{O}}(t) + o(1/T). \quad (4.11)$$

The variance of the estimator $\widehat{\tau}_{\text{int},\mathcal{O}}$ can be computed from (4.9); assuming that $\tau_{\text{int},\mathcal{O}} \ll M \ll T$, the final result is [41]

$$\text{var}(\widehat{\tau}_{\text{int},\mathcal{O}}) \approx \frac{2(2M + 1)}{T} \tau_{\text{int},\mathcal{O}}^2. \quad (4.12)$$

To choose the window width M we used the automatic windowing algorithm introduced in [41], in which one sets

$$M = \min\{m \in \mathbb{Z} : m \geq c \widehat{\tau}_{\text{int},\mathcal{O}}(m)\} \quad (4.13)$$

where c is a suitably chosen constant. If the normalized autocorrelation function is approximately a pure exponential, then a choice in the range $c \approx 6 - 8$ is reasonable. Indeed [17], if we take $\rho_{\mathcal{O}\mathcal{O}}(t) = e^{-|t|/\tau}$ and minimize the mean-square error

$$\text{MSE}(\widehat{\tau}_{\text{int},\mathcal{O}}) \equiv \text{bias}(\widehat{\tau}_{\text{int},\mathcal{O}})^2 + \text{var}(\widehat{\tau}_{\text{int},\mathcal{O}}) \quad (4.14)$$

using (4.11)/(4.12), we find that the optimal window width is

$$M_{\text{opt}} = \frac{\tau}{2} \log\left(\frac{n}{2\tau}\right) - 1. \quad (4.15)$$

For $n/\tau \approx 10^4, 10^5, 10^6, 10^7, 10^8$ with $\tau \gg 1$, we have $M_{\text{opt}}/\tau \approx 4.26, 5.41, 6.56, 7.71, 8.86$, respectively.

In this paper we chose $c = 6$ for the observable \mathcal{E}' , which has the slowest-decaying autocorrelation function of all the observables we measured and whose autocorrelation function is in fact very close to a pure exponential. We then used the same window width M , computed by applying the automatic windowing algorithm to \mathcal{E}' , for all the other observables. We think that this procedure is preferable to applying the automatic windowing algorithm directly to the other observables, since some of the latter have an autocorrelation decay that is far from a pure exponential (this is especially so for \mathcal{F}' , \mathcal{C}_2 and \mathcal{C}_3).

Remark 4.1. If $\{\mathcal{O}^{(1)}, \dots, \mathcal{O}^{(m)}\}$ is a family of observables, we estimate composite observables of the form $f(\langle \mathcal{O}^{(1)} \rangle, \dots, \langle \mathcal{O}^{(m)} \rangle)$ by $f(\overline{\mathcal{O}^{(1)}}, \dots, \overline{\mathcal{O}^{(m)}})$ and approximate the corresponding variance by assuming the fluctuations from the mean are small, so that

$$\text{var } f(\overline{\mathcal{O}^{(1)}}, \dots, \overline{\mathcal{O}^{(m)}}) \approx g^2 \text{var } \overline{Z}, \quad (4.16)$$

where

$$Z_t = \sum_{i=1}^m a_i \mathcal{O}_t^{(i)} \quad (4.17)$$

$$a_i = \frac{1}{g(\langle \mathcal{O}_1 \rangle, \dots, \langle \mathcal{O}_m \rangle)} \frac{\partial f}{\partial x_i}(\langle \mathcal{O}_1 \rangle, \dots, \langle \mathcal{O}_m \rangle) \quad (4.18)$$

and $g = g(\langle \mathcal{O}_1 \rangle, \dots, \langle \mathcal{O}_m \rangle)$ is just a convenient common factor of the derivatives of f , which may be simply 1 in practice. Obviously in practice we compute a_i using $\overline{\mathcal{O}_i}$ in place of $\langle \mathcal{O}_i \rangle$. We used this method to compute the estimate and standard error of ξ .

In principle we can also estimate the specific heat using this procedure, but in practice it turns out that a better estimator for the specific heat is provided by

$$\widehat{C}_H = \frac{1}{B} (\mathcal{N} - \langle \mathcal{N} \rangle)^2. \quad (4.19)$$

The mean of (4.19) is clearly $C_H^{(1)}$ [cf. (3.13)], and its variance determines the error bar on the resulting estimate of $C_H^{(1)}$. We prefer this estimator since it avoids computing the quantity $\overline{\mathcal{N}^2} - \overline{\mathcal{N}}^2$ which can be a numerically perilous object when $\overline{\mathcal{N}^2}$ and $\overline{\mathcal{N}}^2$ are close in value.

Remark 4.2. For the larger values of L we actually performed a number of independent runs rather than one long run. The best estimate of each autocorrelation function $\rho_{\mathcal{O}\mathcal{O}}(t)$ was then computed, for each fixed t , by averaging the $\widehat{\rho}_{\mathcal{O}\mathcal{O}}(t)$ from the individual runs, with weights proportional to the run lengths. The windowing procedure described above was then applied to this best estimate of $\rho_{\mathcal{O}\mathcal{O}}(t)$ in order to obtain the final value for the integrated autocorrelation time.

5 Description of the simulations

We implemented the Chayes–Machta (CM) algorithm for the random-cluster model on an $L \times L$ square lattice with periodic boundary conditions. We performed all our runs at the exact critical temperature $p_c = \sqrt{q}/(1 + \sqrt{q})$. We studied lattice sizes $16 \leq L \leq 1024$ in powers of 2, and parameters $1.25 \leq q \leq 4$ in steps of 0.25. For each (q, L) pair we studied all values of k (the number of active colors) in the range $1 \leq k \leq \lfloor q \rfloor$. We thus performed 189 runs in total.

For each triplet (q, k, L) we performed between 2×10^7 and 10^8 CM iterations: more precisely, we performed 10^8 iterations for $16 \leq L \leq 256$, 5×10^7 iterations for $L = 512$, and 2×10^7 iterations for $L = 1024$. In terms of the autocorrelation time $\tau_{\text{exp}} \approx \tau_{\text{int}, \mathcal{E}'}$, our total data set at each triplet (q, k, L) ranges in length from $\approx 7 \times 10^7 \tau$ on the smallest lattices at small q (i.e. $L = 16$, $q = 1.25$) to $\approx 7 \times 10^3 \tau$ on the largest lattices at large q (i.e. $L = 1024$, $q = 4$, $k = 1$); in 90% of cases (171 out of 189 runs) our run length is at least $10^5 \tau$. These statistics are high enough to permit a high accuracy in our estimates of the static (error $\lesssim 0.1\%$) and dynamic (error $\lesssim 1\%$) quantities, except for the largest lattices at large q .

Our results for the principal static observables, obtained by combining the data for all available k values for each pair (q, L) , are reported in Tables 3–7. Our results for the dynamic quantities $\tau_{\text{int}, \mathcal{O}}$ for the case $k = 1$ and the most important observables \mathcal{O} are reported in Tables 8–14. The complete set of static and dynamic data, for all observables and all values of k , is contained as a file `cm2data.tar.gz` in the preprint version of this paper at [arXiv.org](https://arxiv.org).⁷

The initial configuration of each run was all-bonds-occupied, except for the run at $(q, k, L) = (3.75, 3, 1024)$, for which it was all-bonds-vacant. The number of iterations discarded at the beginning of each run in order to allow the system to reach equilibrium was $j \times 10^5$ for $j = 1, 2, 3$ or 4 , except for eight runs ($2 \leq q \leq 2.75$, $L = 256$ and $k = 1, 2$) for which it was 10^4 .⁸ Thus, the discard interval was in all cases at least $100 \tau_{\text{int}, \mathcal{E}'}$ and in most cases at least $1000 \tau_{\text{int}, \mathcal{E}'}$. Since our data suggest that τ_{exp} is very close to $\tau_{\text{int}, \mathcal{E}'}$, it follows that our discard interval was in all cases at least $100 \tau_{\text{exp}}$, which is more than sufficient for the systematic error from thermalization to be negligible.⁹

Our program was written in Fortran 77 and run on a 1266 MHz Pentium III Tualatin processor using the `g77` Fortran compiler. Our program requires approximately $(12 + 26d)L^d$ bytes memory for a lattice of linear size L in d dimensions. The CPU time required by our program was approximately $0.35 \mu\text{s}/\text{iteration}/\text{lattice site}$; this value is weakly dependent on the lattice size and on k and q . In particular, the CPU time per site rises sharply on very small lattices due to the “fixed costs” of the algorithm (i.e. those that

⁷ The `tar` file unpacks to make a directory `cm2data` with subdirectories `static` and `dynamic`. Each of these subdirectories is in turn subdivided according to the value of q and, in the dynamic case, the value of k . Individual files have names like `C1_Q1.25.txt` or `tau_C1_Q4_K1.txt` and have three fields on each line: L , value and error bar.

⁸ Please don’t ask why the discard interval was chosen in this erratic way — we don’t remember anymore!

⁹ Unless there exists a vastly slower mode of which we are unaware, so that in fact $\tau_{\text{exp}} \gg \tau_{\text{int}, \mathcal{E}'}$.

do not scale with the volume); it rises gradually on lattices $L \gtrsim 128$ due to “cache misses” coming from the nonlocal nature of the Chayes–Machta algorithm, when the lattice no longer fits in the computer’s 512 KB cache. The complete set of runs reported in this paper used approximately 14 yr CPU time.

One delicate issue concerns the choice of the pseudo-random-number generator. We learned by bitter experience [42] that linear congruential pseudo-random-number generators can cause systematic errors in Monte Carlo simulations using the Swendsen–Wang (or Chayes–Machta) algorithm, if the lattice size is a multiple of a very large power of 2 and one random number is used per bond in a periodic manner. These systematic errors arise from correlations within a single bond-update half-sweep: see [42] for details. These errors can be eliminated (or at least radically reduced) by updating the bonds in a random order or in an aperiodic manner, and by using a generator of large modulus (e.g. 60 or more bits). In the present project, therefore, we used a linear congruential generator

$$x_{n+1} = ax_n + c \pmod{m} \quad (5.1)$$

with modulus $m = 2^{64}$, increment $c = 1$, and multiplier $a = 3202034522624059733$. This multiplier gives good results on the spectral test in low dimensions [43]. Moreover — and perhaps even more importantly — we used an “aperiodic” updating, in which the random-number subroutine is called *only* if the two spins are equal and of an “active color”, i.e. for an edge $e = \langle xy \rangle$

```

if  $\sigma_x = \sigma_y \leq k$  then
  if  $\text{ran}() \leq p$  then
     $n_e \leftarrow 1$ 
  else
     $n_e \leftarrow 0$ 
  endif
endif

```

To the best of our knowledge [42] these choices suffice to make the systematic errors negligible.

6 Data analysis: Static quantities

Our general methodology for analyzing the Monte Carlo data (both static and dynamic) is as follows: For each quantity Q of interest we impose an ansatz of the form

$$Q(L) = A_1 L^{p_1} + A_2 L^{p_2} + \dots + A_k L^{p_k} \quad (6.1)$$

(or a logarithmic variant thereof), where some of the parameters may be fixed and others free. The precise ansatz will be motivated in each case by finite-size-scaling theory, possibly together with some exactly known exponents. Typically our ansätze will have 2–4 free parameters. We then perform the nonlinear fits corresponding to the chosen ansatz by using MATHEMATICA’s function `NonlinearModelFit`. As a precaution against

correction-to-scaling terms that we have failed to include in our chosen ansatz, we impose a lower cutoff $L \geq L_{\min}$ on the data points admitted in the fit, and we systematically study the effect on the χ^2 value of increasing L_{\min} . In general, our preferred fit for any given ansatz corresponds to the smallest L_{\min} for which the goodness of fit is reasonable and for which subsequent increases in L_{\min} do not cause the χ^2 value to drop by vastly more than one unit per degree of freedom. In practice, by “reasonable” we mean that the confidence level is $\gtrsim 10\text{--}20\%$.¹⁰ We do not allow fits with zero degrees of freedom, since there would then be no way of testing the goodness of fit. As a last step, we consider the effect of including different terms in the ansatz, by comparing the fits obtained with different ansätze.

The exact values of the static critical exponents are of course already known [cf. (1.5)–(1.10)]. Our analysis of the static Monte Carlo data therefore has three major goals:

1. To test how accurately we would be able to estimate the static critical exponents if we did *not* know them exactly. Here our knowledge of the exact values allows us to evaluate systematic errors (including those due to unknown causes) as well as statistical ones. This study of the static critical exponents serves as a comparison case for our subsequent study of the dynamic critical exponents (Section 7 below). In particular, the behavior of the autocorrelation times is closely related to that of the specific heat, as is evident from the Li–Sokal bound (1.11) and the empirical fact of its near-sharpness.
2. To estimate universal amplitude ratios such as $x^* = \lim_{L \rightarrow \infty} \xi(L)/L$.
3. To study the structure of the corrections to scaling. In particular, are we able to see the leading non-analytic correction-to-scaling term $L^{-\Delta_1}$ with exponent given by (1.6)? And what additional corrections are present? Depending on the observable, one might expect to see analytic corrections such as L^{-1} or regular background contributions.

We begin by summarizing the finite-size-scaling (FSS) ansätze that motivate our fits (Section 6.1). We then study successively the correlation length ξ (Section 6.2), the susceptibility χ (Section 6.3), the largest cluster C_1 (Section 6.4), and the specific heat C_H (Section 6.5).

6.1 Corrections to finite-size-scaling

Let us work exactly at the critical point, and consider a quantity $Q(L)$ whose asymptotic behavior as $L \rightarrow \infty$ is

$$Q(L) = AL^\psi (1 + \text{corrections}), \quad (6.2)$$

¹⁰ “Confidence level” is the probability that χ^2 would exceed the the observed value, assuming that the underlying statistical model is correct. An unusually low confidence level (e.g. less than 5%) thus suggests that the underlying statistical model is *incorrect*; in our context it suggests that the terms we have chosen to retain in the ansatz (6.1) are insufficient to explain our data, i.e. there are unincluded corrections to scaling whose contribution is comparable to or larger than the statistical errors in our data.

where $\psi > 0$ is the leading critical exponent and A is the leading critical amplitude.¹¹ Then finite-size-scaling (FSS) theory predicts the following types of contributions to the “corrections” in (6.2):¹²

1. “Non-analytic” corrections to scaling L^{y_i} coming from irrelevant scaling fields, i.e. those with $y_i < 0$. The leading such contribution is given by $y_i = y_{T2} = -\Delta_1$ [cf. (1.6)]. There are also higher-order “non-analytic” terms of the general form $L^{y_i+y_j+\dots}$, but these are so far down as to be undetectable in our data.
2. “Analytic” corrections to scaling coming from nonlinear mixing between the thermal and magnetic scaling fields. The leading such contribution behaves as $L^{y_{T1}-2y_{H1}} = L^{(\alpha-1-\gamma)/\nu}$.
3. A regular background term $L^{-\psi}$ [i.e. a contribution of order L^0 to $Q(L)$].
4. Corrections with negative integer exponents, i.e. L^{-1} , L^{-2} , etc. Some theoretical frameworks [44] suggest that these contributions are absent.¹³

Looking at the known exact values (1.5)–(1.10) of these exponents (see Table 2), we can predict the pattern of corrections to scaling for different observables:

- For strongly divergent quantities such as the susceptibility ($\psi = \gamma/\nu \approx 1.75$) and the mean cluster size ($\psi = d - \beta/\nu \approx 1.88$), the strongest correction to scaling at large L is expected to come from the leading irrelevant term $L^{-\Delta_1}$ whenever $q > (3 + \sqrt{5})/2 \approx 2.618$; indeed, this behavior will hold for all $q \gtrsim 1.294$ (resp. $q \gtrsim 1.136$) if the L^{-1} correction is absent. However, for $q \lesssim 1.5$ the irrelevant, regular-background and L^{-2} contributions are all of roughly the same order and will be extremely difficult to disentangle.
- The same pattern is expected to hold for the correlation length, since it is built out of the more fundamental quantities χ and F [cf. (3.19)] and therefore inherits their corrections to scaling (we expect F to behave like χ in this context).
- For weakly divergent quantities such as the specific heat for $q \geq 2$, the strongest correction to scaling at large L is expected to come from the regular background term when $2 \leq q < 2 + \sqrt{2} \approx 3.414$ and from the leading irrelevant term when $q > 2 + \sqrt{2}$.

¹¹ For the specific heat we have $\psi = \alpha/\nu < 0$ when $q < 2$. The same formulae will apply in this case, but the meanings of “dominant” and “subdominant” will be interchanged.

¹² See e.g. [16, Section 3] for a review and citations to the original literature. We are also indebted to Youjin Deng for extremely helpful discussions of these points.

¹³ See [16, Section 3.2] for further discussion. Interestingly, a recent study [45] of percolation on two-dimensional lattices, using both transfer-matrix and Monte Carlo methods, found no evidence of any L^{-1} correction but found indirect evidence of an L^{-2} correction (namely, an apparent term $L^{-2} \log L$ that could result from mixing between the L^{-2} and $L^{y_{T2}} = L^{-2}$ terms when $q = 1$).

- For non-divergent quantities such as the specific heat for $q < 2$, the dominant contribution is the regular background, and the leading singular term $L^{\alpha/\nu}$ becomes the principal subdominant contribution.

One very interesting question concerns the presence or absence of the correction-to-scaling term $L^{-\Delta_1} = L^{-4/3}$ in the case of the Ising model ($q = 2$). Plausible physical arguments [46] suggest that such a correction should be present in at least some models in the Ising universality class, even though special symmetries might cause it to be absent in simple exactly-soluble models such as the nearest-neighbor square-lattice model. A transfer-matrix study of the square-lattice random-cluster model for $q \approx 2$ suggested [46] that such a correction is indeed present for all $q \neq 2$ but has an amplitude that vanishes linearly with $q - 2$ when $q \rightarrow 2$. If this is the case, then this correction will be observable in derivatives d/dq of standard Potts-model observables evaluated at $q = 2$. Note also that such derivatives can be expressed as bond observables in the random-cluster model; therefore, in this scenario, at least some bond observables in the $q = 2$ random-cluster model will exhibit the correction-to-scaling term $L^{-4/3}$.

6.2 The correlation length ξ

Finite-size-scaling (FSS) theory predicts that $\xi(L)/L$ for the random-cluster model on a torus tends to a universal value $x^*(q)$ as $L \rightarrow \infty$.¹⁴ More precisely, we expect the behavior

$$\xi/L = x^* + BL^{-p} + \dots \quad (6.3)$$

where $p > 0$ is one of the correction exponents discussed in the preceding subsection. For $q = 2$, the exact value of x^* is known from conformal-invariance theory [47, 48] together with numerical integration [49] to be

$$x^*(q = 2) = 0.9050488292 \pm 0.0000000004. \quad (6.4)$$

For $q \neq 2$ the exact value of x^* is unknown. In this section we will use our Monte Carlo data to estimate the universal values $x^*(q)$ and to test the agreement of the corrections to scaling with the FSS ansatz (6.3).

In Table 15 we report fits of ξ/L to the ansätze x^* and $x^* + BL^{-p}$. For $q = 1.25$ and 1.50 , the fits to both ansätze are excellent, and the estimated values of p agree closely with the known exact values of Δ_1 ; the correction-to-scaling amplitude B is positive and more than three standard deviations away from zero. In particular, there is no evidence of any L^{-1} correction. For $q = 1.75$, the behavior is similar but the quality of the fit is poorer (possibly due to a statistical fluctuation that made the $L = 1024$ point 2σ too high). For $2 \leq q \leq 3.25$, the fits to a constant are excellent provided that L_{\min} is chosen large enough, but the fits to the ansatz $x^* + BL^{-p}$ are mostly badly behaved: either they fail completely to converge (as for $q = 3.25$), or they exhibit estimates for p that seem much too low ($q = 2$) or much too high ($q = 2.5, 3$) or somewhat too high ($q = 2.25$);

¹⁴ In general this value depends on the aspect ratio of the torus. Here we are considering only the case of aspect ratio 1.

only $q = 2.75$ behaves well in these respects. Also, the estimated correction amplitudes B are mostly within two standard deviations of zero. Examination of plots of these fits (see Figure 1) suggests that the problem arises because ξ/L is a very flat and possibly nonmonotonic function of L at large L in this range of q .¹⁵ This suggests that the ansatz (6.3) might be too simple, and that we are seeing the combined effect of two (or more) correction-to-scaling terms of opposite sign. However, our statistical errors are too large for us to resolve this question clearly. For $3.5 \leq q \leq 4$, by contrast, the fits to both ansätze are again excellent, and the estimated values of p agree well with the known exact values of Δ_1 (except at $q = 4$, where the corrections to scaling $\log \log L / \log L$ and $1 / \log L$ [19] are mimicked by a small inverse power of L). Moreover, the correction-to-scaling amplitude B is now clearly negative. This suggests that B passed through zero somewhere in the range $2 \lesssim q \lesssim 3.4$ and was small throughout this range, thereby explaining why our fits to $x^* + BL^{-p}$ were so unstable.

It is curious that our estimate for $x^*(q = 2)$ agrees slightly *less well* in absolute terms with the exact value (6.4) than the estimate a decade ago by Salas and Sokal [49], despite the fact that our raw-data error bars are a factor of 3–7 smaller than theirs. Most likely we were the unlucky victim of a statistical fluctuation on our $L = 512$ and $L = 1024$ data points that placed them roughly $2\text{--}3\sigma$ and 1σ too low, respectively, thereby causing us to choose $L_{\min} = 512$ rather than 256 in the fit to a constant and hence to privilege these discrepant values [see Figure 1(b)].

6.3 The susceptibility χ

In Table 16 we report fits of the susceptibility χ to the pure-power-law ansatz $AL^{\gamma/\nu}$, just to see how accurately we would be able to estimate the exponent γ/ν if we did not know its exact value. The last two columns show the deviation of the estimated γ/ν from the known exact value (1.10), in absolute terms and in units of its standard deviation.

For small q we are able to estimate γ/ν with extraordinary accuracy: both statistical and systematic errors are of order 0.0001 or less. However, as q grows, both the systematic and the statistical errors grow: the statistical errors grow because the critical slowing-down is becoming gradually worse (see Section 7 below); and the systematic errors grow (even faster than the statistical errors) because the corrections to scaling are becoming much stronger as the correction-to-scaling exponent Δ_1 decreases (see Table 2). As a consequence, at $q \approx 3$ the statistical and systematic errors are of order 0.0003 and 0.001, respectively; at $q = 3.75$ the errors are roughly twice this; and at $q = 4$ the statistical and systematic errors are of order 0.0015 and 0.01, respectively. (The large systematic errors at $q = 4$ are of course not surprising in view of the multiplicative logarithmic correction $(\log L)^{-1/8}$ and the additive logarithmic corrections $\log \log L / \log L$, $1 / \log L$, etc. [19]. Indeed, what is somewhat surprising is that the systematic errors are not larger! See Section 6.5 below for the case of the specific heat.)

We next imposed the known exact value (1.10) of γ/ν and attempted to extract the corrections to scaling. Table 17 shows fits of $\chi/L^{\gamma/\nu}$ to the ansätze A and $A + BL^{-p}$.

¹⁵ Or, perhaps, the statistical errors are just too large, compared to the small “signal”, for us to estimate the corrections to scaling accurately.

Plots for some selected values of q are shown in Figure 2. For $q = 1.25$ and 1.5 , the correction to scaling at small L is clearly positive in sign, though very small in absolute magnitude (of order 0.001 at $L = 16$): see Figure 2(a). This suggests that the correction-to-scaling exponent is fairly large, in agreement with the theoretical prediction. However, the fits produce unusually small estimates for the correction exponent p ; this is a possible behavior of the “effective exponent” when there are two correction-to-scaling terms of opposite sign (e.g. L^{-1} and $L^{-\Delta_1}$). For $q = 1.75$ and 2 , the corrections to scaling are small and erratic and it was not possible to fit them to a single inverse power; indeed, for $q = 2$ the behavior may be nonmonotonic in L [see Figure 2(b)], suggesting again the presence of two correction-to-scaling terms of opposite sign. For $q \geq 2.25$ the correction to scaling is clearly negative in sign, and it gets larger in absolute magnitude as q grows (evaluated at $L = 16$, the magnitude of the correction grows from ≈ 0.003 at $q = 2.25$ to ≈ 0.018 at $q = 3.75$); furthermore, the fits produce estimates for the correction exponent p that are in decent agreement with the exact value of Δ_1 . At $q = 4$ the correction to scaling is extremely strong (as expected) and it is not possible to fit it to an inverse power.

In summary, for $q \geq 2.25$ we obtain modest evidence that a correction $L^{-\Delta_1}$ is present, with negative amplitude. For $q \leq 2$ we are unable to say much about the corrections to scaling except that the amplitude is probably positive for $q \leq 1.5$ (we say “probably” because it is not clear that the positive contribution at small L comes from the *same* correction-to-scaling term that is dominant at large L). But our data are at least compatible with the scenario [46] that the correction-to-scaling amplitude passes through zero at $q = 2$.

6.4 The largest cluster C_1

In Table 18 we report fits of the mean size of the largest cluster, $C_1 = \langle C_1 \rangle$, to the pure-power-law ansatz $AL^{d-\beta/\nu}$, just to see how accurately we would be able to estimate the exponent β/ν if we did not know its exact value. The last two columns show the deviation of the estimated β/ν from the known exact value (1.9), in absolute terms and in units of its standard deviation.

The results are extremely similar to those obtained for the susceptibility. For small q , both the statistical and the systematic errors are of order 0.0001 or less. As q grows, the statistical errors grow and the systematic errors grow even more. But the results are remarkably good except at $q = 4$.

6.5 The specific heat C_H

In Table 19 we report fits of the specific heat C_H to the ansätze $AL^{\alpha/\nu}$ and $AL^{\alpha/\nu} + B$. The exact value (1.8) of α/ν is shown for comparison in the next-to-last column. The last two columns show the deviation of the estimated α/ν (taken from the fit $AL^{\alpha/\nu} + B$) from the known exact value, in absolute terms and in units of its standard deviation.

For $q \lesssim 2.75$ the fits to a pure power law are horrible. This is not surprising: after all, for $q < 2$ the specific heat increases to a finite value as $L \rightarrow \infty$, so the fit will indicate a positive value of α/ν (but with a ridiculously poor goodness of fit) while the true value of

α/ν is actually negative. And for $2 < q \lesssim 2.75$ the additive constant is very important, so a pure power law has poor goodness of fit.

Good fits to $AL^{\alpha/\nu} + B$ can be obtained for all values of q other than $q = 2$ by appropriate choice of L_{\min} . For $q = 2$ the fit fails to converge: initial guesses with $A > 0$, $B < 0$ and α/ν slightly positive always get driven to $\alpha/\nu \downarrow 0$ with $A \approx -B \uparrow +\infty$. The fit is therefore suggesting the correct behavior $C_H \approx A \log L + B$. Indeed, a fit to this ansatz is good already for $L_{\min} = 64$ and yields

$$A = 0.6371(9), B = 0.1732(42) \quad (\chi^2 = 1.49, 3 \text{ DF, CL} = 68\%), \quad (6.5)$$

in good agreement with the known exact values $A = 2/\pi \approx 0.6366$ and $B \approx 0.1778$ [50, 51].¹⁶ If we fit instead to $A \log^2 L + B \log L + C$, we get a good fit for $L_{\min} = 32$,

$$A = -0.0012(6), B = 0.6493(55), C = 0.1415(125) \quad (\chi^2 = 2.36, 3 \text{ DF, CL} = 50\%), \quad (6.6)$$

in which the extremely small value of A correctly suggests that the $\log^2 L$ term is absent.

Although the fits to $AL^{\alpha/\nu} + B$ are good for all $q \neq 2$, some of the estimated values of α/ν deviate significantly from the known exact value (see the last two columns of Table 19). For $q < 2$ the estimates of α/ν are surprisingly good, given that we are estimating a subleading singular contribution underneath a nonsingular background. For $2.25 \leq q \leq 2.75$ the estimates of α/ν are also excellent. However, for $q \geq 3$ the estimates of α/ν deviate by more than three standard deviations from the exact value. This may be due to the effect of corrections to scaling: in particular, those governed by the exponent Δ_1 , whose known exact value is given by (1.6). Indeed, for $q > 2 + \sqrt{2} \approx 3.414$ ($g > 7/2$) we have $\Delta_1 < \alpha/\nu$, so that the correction-to-scaling contribution $L^{\alpha/\nu - \Delta_1}$ is larger than the nonsingular background. For $3 \leq q \leq 3.75$ we therefore tried fits to the ansätze $AL^{\alpha/\nu} + BL^{\alpha/\nu - \Delta_1}$ and $AL^{\alpha/\nu} + BL^{\alpha/\nu - \Delta_1} + C$, in which Δ_1 is fixed at its known exact value and α/ν is free:

(i) For $q = 3$ it is silly not to include the constant background, since $\alpha/\nu - \Delta_1 = -0.4 \ll 0$; nevertheless, we obtain a good fit to $AL^{\alpha/\nu} + BL^{\alpha/\nu - \Delta_1}$ when $L_{\min} = 64$:

$$\alpha/\nu = 0.4152(15), A = 1.397(14), B = -2.346(153) \quad (\chi^2 = 0.75, 2 \text{ DF, CL} = 69\%). \quad (6.7)$$

However, the estimate for α/ν is 10 standard deviations away from the correct value! If we include the constant background we get a good fit already when $L_{\min} = 16$,

$$\alpha/\nu = 0.4036(34), A = 1.555(44), B = -0.787(188), C = -0.795(152) \quad (\chi^2 = 1.07, 3 \text{ DF, CL} = 78\%), \quad (6.8)$$

and the estimate for α/ν is in excellent agreement with the correct answer.

¹⁶ These values of A and B can be extracted from [50] or [51] after translating their conventions to ours. We use the definition $C_H^{(2)}$ of specific heat [cf. (3.14)]. Salas [51] uses the definition $C_H^{(3)}$ [cf. (3.15)], which is 4 times ours when $q = 2$. Ferdinand and Fisher use $C_H^{(3)}$ multiplied by K^2 , where K is the nearest-neighbor coupling in the Ising normalization; the critical point is given by $K_c = \frac{1}{2} \log(1 + \sqrt{2})$.

(ii) For $q = 3.25$ the correction-to-scaling contribution is only slightly smaller than the nonsingular background, and it will probably be difficult for the fit to separate the two. The fit to $AL^{\alpha/\nu} + BL^{\alpha/\nu-\Delta_1}$ is good already when $L_{\min} = 16$,

$$\alpha/\nu = 0.4972(7) \quad A = 1.201(5) \quad B = -0.945(19) \quad (\chi^2 = 2.58, 4 \text{ DF, CL} = 63\%) , \quad (6.9)$$

but the estimate for α/ν is almost six standard deviations away from the correct value ≈ 0.5013 . If we include the constant background we also get a good fit when $L_{\min} = 16$,

$$\alpha/\nu = 0.4988(44), \quad A = 1.186(42), \quad B = -1.089(396), \quad C = 0.133(365) \\ (\chi^2 = 2.45, 3 \text{ DF, CL} = 49\%) , \quad (6.10)$$

but the estimate for the constant C is consistent with zero. The estimate for α/ν is now less than one standard deviation away from the correct value, but this is principally because the standard deviation has become much larger, not because the estimated value has actually moved much closer to the true value!

(iii) For $q = 3.5$ the correction-to-scaling contribution is now slightly larger than the nonsingular background, and it will again likely be difficult for the fit to separate the two. The fit to $AL^{\alpha/\nu} + BL^{\alpha/\nu-\Delta_1}$ is good when $L_{\min} = 64$,

$$\alpha/\nu = 0.5945(39), \quad A = 0.926(25), \quad B = -0.017(91) \quad (\chi^2 = 0.91, 2 \text{ DF, CL} = 64\%) , \quad (6.11)$$

but the estimate for the correction-to-scaling amplitude B is consistent with zero. Indeed, the result from this fit is virtually identical to what was obtained from the ansatz $AL^{\alpha/\nu} + B$, and the estimate for α/ν is again about four standard deviations away from the correct value ≈ 0.6101 . By contrast, the fit to $AL^{\alpha/\nu} + BL^{\alpha/\nu-\Delta_1} + C$ is good already when $L_{\min} = 16$,

$$\alpha/\nu = 0.6095(67), \quad A = 0.805(43), \quad B = 2.961(368), \quad C = -3.509(390) \\ (\chi^2 = 2.32, 3 \text{ DF, CL} = 51\%) , \quad (6.12)$$

and the estimate for α/ν is now in excellent agreement with the correct answer. Interestingly, the estimates for the amplitudes B and C are *not* consistent with zero; rather, they are strongly nonzero but of opposite signs. Clearly, what happened is that when we performed a fit with a single correction term (whether B or $BL^{\alpha/\nu-\Delta_1}$, which are anyway nearly the same) this *pair* of correction terms combined to make an “effective” correction term (in the given range of L) with a nearly zero amplitude; but this gave a *biased* estimate of the leading exponent α/ν . What is slightly surprising is that our fit was able to separate the correction-to-scaling contribution $BL^{\approx 0.090}$ from the nonsingular background C . Perhaps the stunning agreement of the estimated value of α/ν with the exact answer is a fluke and ought not be taken too seriously.

(iv) For $q = 3.75$ the correction-to-scaling contribution is significantly larger than the nonsingular background. The fit to $AL^{\alpha/\nu} + BL^{\alpha/\nu-\Delta_1}$ is good when $L_{\min} = 64$,

$$\alpha/\nu = 0.7181(90), \quad A = 0.568(42), \quad B = 0.413(76) \quad (\chi^2 = 1.26, 2 \text{ DF, CL} = 53\%) , \quad (6.13)$$

and the estimate for α/ν is only about two standard deviations away from the true value ≈ 0.7376 . By contrast, the fit to $AL^{\alpha/\nu} + BL^{\alpha/\nu - \Delta_1} + C$ is good already when $L_{\min} = 16$:

$$\alpha/\nu = 0.7856(237), A = 0.288(68), B = 1.085(64), C = -1.046(37) \\ (\chi^2 = 0.30, 3 \text{ DF}, \text{CL} = 96\%) . \quad (6.14)$$

Here the estimated amplitudes B and C have opposite signs and are apparently nonzero; but the estimate for α/ν has now far overshoot the correct value (it is again two standard deviations away, but with a much larger standard deviation). The poor performance of this two-correction-term fit — in a case where the two terms $BL^{\approx 0.388}$ and C should have been much *easier* to separate than they were for $q = 3.5$ — suggests that the good result obtained for $q = 3.5$ was indeed a fluke and that the mediocre result obtained for $q = 3.75$ is what should ordinarily be expected.

Finally, for $q = 4$ the true leading behavior is known [19] to be $L(\log L)^{-3/2}$, but with corrections to scaling down by $\log \log L / \log L$, $1 / \log L$, etc. It is clearly hopeless to try to fit to such an ansatz unless one has data for colossally large values of L . It is of course not surprising that fits to $AL^{\alpha/\nu}$ or $AL^{\alpha/\nu} + B$ gave estimates of α/ν near 0.8, far off from the correct value 1; the factor $(\log L)^{3/2}$ is imitating a power $L^{\approx 0.2}$ in our range of L .

7 Data analysis: Dynamic quantities

In this section we analyze the dynamic data by the same general methods as were used in the preceding section to analyze the static data. Our main goal is to estimate the dynamic critical exponents $z_{\text{int},\mathcal{O}}$ associated to the integrated autocorrelation times $\tau_{\text{int},\mathcal{O}}$ for various observables \mathcal{O} .

We proceed as follows: First we discuss the dependence of the autocorrelation times on the number k of active colors (Section 7.1), and we give an overview of the qualitative behavior of the autocorrelation times for different observables (Section 7.2). Then we present a detailed analysis of the dynamic critical exponent $z_{\text{int},\mathcal{E}'}$ (Section 7.3); in particular we discuss the sharpness of the Li–Sokal bound (Section 7.4) and the correctness of the Ossola–Sokal conjecture (Section 7.5). Finally, we analyze briefly the dynamic critical exponent $z_{\text{int},\mathcal{O}}$ for other observables \mathcal{O} (Section 7.6).

7.1 Dependence on k

We began by analyzing the dependence of $\tau_{\text{int},\mathcal{O}}$ on the number k of active colors. Of course we expect that all values of k lie in the same dynamic universality class: that is, we expect that the ratios of $\tau_{\text{int},\mathcal{O}}$ for different k tend to nonzero finite constants as $L \rightarrow \infty$. Moreover, it is intuitively reasonable to think that an update with k active colors does roughly “ k times as much work” as an update with one active color; therefore, we expect that $\tau_{\text{int},\mathcal{O}}$ should be roughly proportional to $1/k$.

We tested these expectations by analyzing the ratios $\tau_{\text{int},\mathcal{O}}(1)/\tau_{\text{int},\mathcal{O}}(k)$ as a function of L for each (q, \mathcal{O}) and each allowable k . In all cases the ratios are fairly close to k , as expected; but in general they are not exactly equal to k . The ratios also show some dependence on L , but tend as $L \rightarrow \infty$ to a limiting value, again as expected. Roughly

speaking, for the smaller values of q the L -dependence is fairly strong, and the ratios are comparatively far from k (which is perhaps not surprising because the values of $\tau_{\text{int},\mathcal{O}}$ are themselves quite small); the limiting values also appear to be different from k , though this conclusion is only tentative because of the strong corrections to scaling. For the larger values of q the L -dependence is weaker, and the ratios are closer to k ; in particular, the limiting values are compatible with k within our statistical errors. In Table 20 we show typical examples of these two behaviors, namely $\mathcal{O} = \mathcal{E}'$ with $q = 2$ and $q = 3.25$. In Table 21 we show our best estimates for the limiting ratios $\tau_{\text{int},\mathcal{E}'}(1)/\tau_{\text{int},\mathcal{E}'}(k)$, obtained by fitting the ratio to a constant and increasing L_{min} until a decent fit is obtained. The behavior for the other observables is qualitatively similar.

Having confirmed that all values of k lie in the same dynamic universality class, we henceforth analyze the data for each value of k separately and then compute a weighted average of the resulting exponent estimates.

7.2 Summary of qualitative behavior

Let us begin by summarizing the qualitative behavior of $\tau_{\text{int},\mathcal{O}}$ for different observables \mathcal{O} :

1) For nearly every triplet (q, k, L) , we find that \mathcal{E}' is the observable (of those we have measured) that has the largest τ_{int} . The only exceptions are $q = 4$, $L = 16$, $1 \leq k \leq 4$ (for which $\tau_{\text{int},\mathcal{S}_2}$ is slightly larger than $\tau_{\text{int},\mathcal{E}'}$) and $q = 4$, $L = 1024$, $k = 1$ (for which $\tau_{\text{int},\mathcal{C}_1}$ is slightly larger than $\tau_{\text{int},\mathcal{E}'}$). But these differences are extremely small and may well represent statistical fluctuations.

2) For every triplet (q, k, L) , we find that \mathcal{C}_2 is the observable (of those we have measured) that has the smallest τ_{int} .

3) For every triplet (q, k, L) we find that

$$\tau_{\text{int},\mathcal{E}'} > \tau_{\text{int},\mathcal{N}}. \quad (7.1)$$

When q is an integer and $k = q$, this inequality is easily proved rigorously for the SW algorithm [17], so it is not surprising that it holds here for CM. However, we do not yet have a rigorous proof (not even in the case when q is an integer and $k < q$).

4) In general, the observables \mathcal{O} that we have measured fall into four groups according to their integrated autocorrelation times $\tau_{\text{int},\mathcal{O}}$:

1. \mathcal{E}' , \mathcal{N} , \mathcal{S}_2 and \mathcal{C}_1 have the largest values of τ_{int} , and they are all fairly close to each other (all are at least ≈ 0.75 times that of \mathcal{E}' , and usually much closer);
2. \mathcal{F}' has an intermediate value of τ_{int} , of order 0.5–0.9 times that of \mathcal{E}' ;
3. \mathcal{C}_3 has a slightly lower value of τ_{int} , of order 0.4–0.8 times that of \mathcal{E}' ;
4. \mathcal{C}_2 has the smallest τ_{int} , of order 0.35–0.8 times that of \mathcal{E}' .

Indeed, for all triplets (q, k, L) we have $\tau_{\text{int},\mathcal{O}_1} > \tau_{\text{int},\mathcal{O}_2} > \tau_{\text{int},\mathcal{O}_3} > \tau_{\text{int},\mathcal{O}_4}$ whenever $\mathcal{O}_1, \mathcal{O}_2, \mathcal{O}_3, \mathcal{O}_4$ belong to groups 1,2,3,4, with the exception that for a few triplets at $q = 4$, $L \geq 256$ we have $\tau_{\text{int},\mathcal{F}'} < \tau_{\text{int},\mathcal{C}_3}$.

These behaviors can be better understood by looking at the normalized autocorrelation functions $\rho_{\mathcal{O}\mathcal{O}}(t)$. A typical example is shown in Figure 3. We see that $\rho_{\mathcal{E}'\mathcal{E}'}(t)$ is nearly a pure exponential, so that $\tau_{\text{int},\mathcal{E}'} \approx \tau_{\text{exp}}$. By contrast, the autocorrelation functions for the observables \mathcal{O} in groups 2, 3 and 4 exhibit an initial fast decay, followed by a decay at the same exponential rate τ_{exp} but with an amplitude $A_{\mathcal{O}}$ that is significantly less than 1. What we do not know is whether $A_{\mathcal{O}}$ tends to a nonzero value as $L \rightarrow \infty$ (in which case we will have $z_{\text{int},\mathcal{O}} = z_{\text{exp}}$) or tends to zero as an inverse power of L (in which case we will have $z_{\text{int},\mathcal{O}} < z_{\text{exp}}$). See Section 7.6 for further analysis of this question; and see [20, Section 5.2] for a more detailed analysis in the case of the Swendsen–Wang dynamics for the three-dimensional Ising model.

In the following subsections we shall fit $\tau_{\text{int},\mathcal{O}}$, for each observable \mathcal{O} , to a variety of ansätze, notably:

- Fits for $z = 0$: $\tau_{\text{int},\mathcal{O}} = A$ or $\tau_{\text{int},\mathcal{O}} = A + BL^{-p}$.
- Fits for $z = 0$ with a multiplicative logarithm: $\tau_{\text{int},\mathcal{O}} = A \log L + B$ or $\tau_{\text{int},\mathcal{O}} = A \log^2 L + B \log L + C$.
- Fits for $z > 0$: $\tau_{\text{int},\mathcal{O}} = AL^z$ or $\tau_{\text{int},\mathcal{O}} = AL^z + B$.

Note that the fits to $A + BL^{-p}$ and $AL^z + B$ are in fact the *same* fit in different notation!

We shall begin (Sections 7.3–7.5) by focusing on the observable \mathcal{E}' , which has the largest autocorrelation time of all the observables we measured. Then (Section 7.6) we shall discuss, more briefly, the other observables, with emphasis on \mathcal{C}_2 .

7.3 Dynamic critical exponent $z_{\text{int},\mathcal{E}'}$

In this subsection we fit the integrated autocorrelation time $\tau_{\text{int},\mathcal{E}'}$ to a variety of ansätze in an effort to estimate the dynamic critical exponent $z_{\text{int},\mathcal{E}'}$. We begin by presenting our fits, in order of increasing q , without much comment. Then we go back and try to interpret what these fits might be telling us about the dynamic critical behavior of the Chayes–Machta algorithm as a function of q .

For $q = 1.25$ the behavior is fairly clear: $\tau_{\text{int},\mathcal{E}'}$ tends to a finite constant as $L \rightarrow \infty$. The fits to the ansatz $\tau_{\text{int},\mathcal{E}'} = A$ are horrible (except of course the fit $L_{\text{min}} = 1024$ that has zero degrees of freedom); but if we fit to $\tau_{\text{int},\mathcal{E}'} = A + BL^{-p}$ we get a decent fit for $L_{\text{min}} = 128$:

$$A = 2.19(8), B = -1.61(5), p = 0.213(35) \quad (\chi^2 = 0.49, 1 \text{ DF}, \text{CL} = 48\%). \quad (7.2)$$

Finally, the fit to AL^z yields an estimated exponent $z \approx 0.05$ but has poor goodness of fit even when $L_{\text{min}} = 256$: $z = 0.053(1)$, $A = 1.27(1)$ with $\chi^2 = 3.76$, 1 DF, CL = 5%.

For $q = 1.5$ the fits to a constant A are again horrible; but if we fit to $A + BL^{-p}$ we get a good fit already for $L_{\text{min}} = 32$:

$$A = 17.09(2.96), B = -15.86(2.92), p = 0.034(7) \quad (\chi^2 = 0.82, 3 \text{ DF}, \text{CL} = 85\%). \quad (7.3)$$

We also tried a fit to $A \log L + B$: a decent fit is obtained for $L_{\min} = 128$, namely

$$A = 0.440(4), B = 1.486(21) \quad (\chi^2 = 0.83, 2 \text{ DF}, \text{CL} = 66\%) . \quad (7.4)$$

A good fit to $A \log^2 L + B \log L + C$ is obtained already for $L_{\min} = 32$, but with a slightly *negative* value of A (which is of course impossible for the actual asymptotics): $A = -0.008(2)$, $B = 0.53(2)$, $C = 1.24(4)$ with $\chi^2 = 0.80$, 3 DF, CL = 85%. Finally, the fit to AL^z yields an estimated exponent $z \approx 0.10$ but again has poor goodness of fit even when $L_{\min} = 256$: $z = 0.104(2)$, $A = 2.20(2)$ with $\chi^2 = 3.84$, 1 DF, CL = 5%.

For $q = 1.75$ (and all larger q) the fit to a constant A is again horrible. The fit to $A \log L + B$ is mediocre even when $L_{\min} = 256$: $A = 1.36(2)$, $B = 0.32(12)$ with $\chi^2 = 2.73$, 1 DF, CL = 10%. A decent fit to $A \log^2 L + B \log L + C$ is obtained already for $L_{\min} = 16$: $A = 0.037(3)$, $B = 0.915(23)$, $C = 1.689(45)$ with $\chi^2 = 4.14$, 4 DF, CL = 39%. The fit to AL^z is good when $L_{\min} = 256$: $z = 0.158(2)$, $A = 3.28(5)$ with $\chi^2 = 0.21$, 1 DF, CL = 65%. The fit to $AL^z + B$ is decent already for $L_{\min} = 16$ ($\chi^2 = 4.63$, 4 DF, CL = 33%), but the χ^2 drops notably from $L_{\min} = 64$ ($\chi^2 = 2.86$) to $L_{\min} = 128$ ($\chi^2 = 0.33$), so that our preferred fit is $L_{\min} = 128$:

$$z = 0.085(26), A = 9.66(4.42), B = -7.56(4.82) \quad (\chi^2 = 0.33, 1 \text{ DF}, \text{CL} = 57\%) . \quad (7.5)$$

For $q \geq 2$ we have data from more than one value of k . For simplicity we discuss here in words only the case $k = 1$; the other cases are qualitatively similar and are reported in Tables 22 and 23.

For $q = 2$ the fit to $A \log L + B$ is poor (CL < 2%) even when $L_{\min} = 256$. The fit to $A \log^2 L + B \log L + C$ is good already for $L_{\min} = 16$: $A = 0.206(6)$, $B = 1.046(53)$, $C = 2.572(103)$ with $\chi^2 = 1.40$, 4 DF, CL = 84%. The fit to AL^z is good for $L_{\min} = 256$: $z = 0.215(3)$, $A = 4.47(9)$ with $\chi^2 = 0.06$, 1 DF, CL = 81%. Finally, the fit to $AL^z + B$ is good already for $L_{\min} = 16$:

$$z = 0.145(4), A = 10.4(5), B = -8.4(6) \quad (\chi^2 = 2.32, 4 \text{ DF}, \text{CL} = 68\%) . \quad (7.6)$$

For $q = 2.25$ the fit to $A \log L + B$ is again poor (CL < 5%) even when $L_{\min} = 256$. The fit to $A \log^2 L + B \log L + C$ is decent already for $L_{\min} = 32$: $A = 0.77(3)$, $B = -0.84(24)$, $C = 7.07(53)$ with $\chi^2 = 3.15$, 3 DF, CL = 37%. The fit to AL^z yields an estimated exponent $z \approx 0.29$ but has mediocre goodness of fit even when $L_{\min} = 256$: $z = 0.286(4)$, $A = 5.35(14)$ with $\chi^2 = 2.16$, 1 DF, CL = 14%. Finally, the fit to $AL^z + B$ is good already for $L_{\min} = 32$:

$$z = 0.235(8), A = 8.91(61), B = -6.68(86) \quad (\chi^2 = 1.62, 3 \text{ DF}, \text{CL} = 66\%) . \quad (7.7)$$

For $q = 2.5$ (and all larger q) the fit to $A \log L + B$ is poor (CL < 3%) even when $L_{\min} = 256$. The fit to $A \log^2 L + B \log L + C$ is decent for $L_{\min} = 128$: $A = 2.7(3)$, $B = -13.7(3.1)$, $C = 37.4(8.6)$ with $\chi^2 = 0.66$, 1 DF, CL = 42%. However, the error bars on B and C are very large in absolute magnitude (and in particular large compared to the value of A), which renders the fit somewhat dubious. The fit to AL^z is good for

$L_{\min} = 256$: $z = 0.353(6)$, $A = 6.35(23)$ with $\chi^2 = 0.02$, 1 DF, CL = 90%. Finally, the fit to $AL^z + B$ is excellent already for $L_{\min} = 32$:

$$z = 0.315(8), A = 9.01(59), B = -6.75(1.00) \quad (\chi^2 = 0.21, 3 \text{ DF}, \text{CL} = 98\%) . \quad (7.8)$$

For $q = 2.75$ the fit to $A \log^2 L + B \log L + C$ is decent for $L_{\min} = 64$: $A = 5.9(3)$, $B = -31.9(2.7)$, $C = 71.0(6.5)$ with $\chi^2 = 2.56$, 2 DF, CL = 28%. But the error bars on B and C are again quite large. The fit to AL^z is good for $L_{\min} = 256$: $z = 0.424(8)$, $A = 7.19(34)$ with $\chi^2 = 0.07$, 1 DF, CL = 80%. Finally, the fit to $AL^z + B$ is excellent already for $L_{\min} = 16$:

$$z = 0.411(5), A = 8.19(30), B = -4.76(57) \quad (\chi^2 = 1.06, 4 \text{ DF}, \text{CL} = 90\%) . \quad (7.9)$$

For $q = 3$ the fit to $A \log^2 L + B \log L + C$ is decent for $L_{\min} = 128$, but with huge error bars: $A = 16.0(1.5)$, $B = -112.6(16.5)$, $C = 257.5(44.5)$ with $\chi^2 = 0.77$, 1 DF, CL = 38%. (The same behavior persists for all larger values of q , with even larger values of the coefficients A, B, C and their error bars; we refrain from reporting the gory results.) The fit to AL^z is good for $L_{\min} = 128$: $z = 0.505(6)$, $A = 7.52(23)$ with $\chi^2 = 1.18$, 2 DF, CL = 56%. Finally, the fit to $AL^z + B$ is excellent already for $L_{\min} = 32$:

$$z = 0.481(10), A = 9.08(63), B = -6.79(1.68) \quad (\chi^2 = 0.84, 3 \text{ DF}, \text{CL} = 84\%) . \quad (7.10)$$

For $q = 3.25$ the fit to AL^z is decent for $L_{\min} = 128$: $z = 0.590(7)$, $A = 7.66(30)$ with $\chi^2 = 3.14$, 2 DF, CL = 21%. Finally, the fit to $AL^z + B$ is decent for $L_{\min} = 64$:

$$z = 0.558(21), A = 9.8(1.4), B = -11.9(6.0) \quad (\chi^2 = 2.93, 2 \text{ DF}, \text{CL} = 23\%) . \quad (7.11)$$

For $q = 3.5$ the fit to AL^z is decent for $L_{\min} = 128$: $z = 0.676(10)$, $A = 7.77(39)$ with $\chi^2 = 1.07$, 2 DF, CL = 58%. Finally, the fit to $AL^z + B$ is decent for $L_{\min} = 64$:

$$z = 0.648(25), A = 9.5(1.6), B = -14.4(8.9) \quad (\chi^2 = 1.15, 2 \text{ DF}, \text{CL} = 56\%) . \quad (7.12)$$

For $q = 3.75$ the fit to AL^z is good already for $L_{\min} = 32$: $z = 0.779(4)$, $A = 7.14(13)$ with $\chi^2 = 0.94$, 4 DF, CL = 92%. Finally, the fit to $AL^z + B$ is excellent already for $L_{\min} = 16$:

$$z = 0.790(9), A = 6.7(3), B = 3.0(1.5) \quad (\chi^2 = 0.33, 4 \text{ DF}, \text{CL} = 99\%) . \quad (7.13)$$

For $q = 4$ the fit to AL^z is good for $L_{\min} = 128$: $z = 0.916(16)$, $A = 5.44(46)$ with $\chi^2 = 0.15$, 2 DF, CL = 93%. Finally, the fit to $AL^z + B$ is excellent already for $L_{\min} = 32$:

$$z = 0.935(18), A = 4.8(5), B = 20.5(5.1) \quad (\chi^2 = 0.66, 3 \text{ DF}, \text{CL} = 88\%) . \quad (7.14)$$

Let us now comment on what we think these fits show.

For $q = 1.25$ it seems fairly clear that $\tau_{\text{int}, \mathcal{E}'}$ converges as $L \rightarrow \infty$ to a finite value, i.e. $z_{\text{int}, \mathcal{E}'} = 0$. For $q = 1.5$ the behavior is unclear: perhaps $\tau_{\text{int}, \mathcal{E}'}$ converges to a finite value, but with extremely strong corrections to scaling (e.g. $A + BL^{-p}$ with $p > 0$ extremely

small); or perhaps it grows logarithmically, like $\log L$ or $\log^2 L$; or perhaps it grows with a very small positive power ($z \lesssim 0.1$) together with very strong corrections to scaling. The evidence points weakly towards the first scenario, but a divergence like $\log L$ or an extremely small positive power of L is also a possibility. For $1.75 \leq q \lesssim 2.25$ a reasonable fit is obtained with the ansatz $AL^z + B \log L + C$; but it seems to us implausible on theoretical grounds that we would have such a logarithmic growth for an entire *interval* of q . Much more likely is that there exists *one* value q_* such that $z = 0$ for $q < q_*$ and $z > 0$ for $q > q_*$, in which case $\tau_{\text{int},\mathcal{E}'}$ might grow logarithmically *at* $q = q_*$ (but only there). Our data suggest that q_* lies between 1.25 and 1.75; our best guess would be ≈ 1.6 , based on linearly interpolating the exponent estimates produced by our fits for $q = 1.5$ and $q = 1.75$.

For all $q \geq 1.75$ we are able to obtain decent fits to the ansätze AL^z and $AL^z + B$ with an exponent $z > 0$; these fits are reported in Tables 22 and 23, respectively, and the results obtained by averaging over k are reported in Table 24. For the smaller values of q in this table, the discrepancy between the fits with and without a constant term B is fairly large: this is not surprising because z is fairly small and hence the effect of the constant term is very strong. As q grows, the discrepancy between the two fits decreases: from ≈ 0.1 at $q = 1.75$ and ≈ 0.07 at $q = 2$ to approximately zero at $q = 3.5$; for $q > 3.5$ the discrepancy has the opposite sign but remains small. Correspondingly, the estimated value of B appears to go through zero (and change sign) at $q \approx 3.5$. We have a slight preference for the fits to $AL^z + B$, for the simple reason that such a constant term must surely be present, if only because the definition of $\tau_{\text{int},\mathcal{O}}$ is somewhat arbitrary (should one include the contribution $\frac{1}{2}$ from $t = 0$ or not?). But our data are insufficient to resolve clearly the discrepancy between the two fits. We therefore choose to report our results for $q \geq 1.75$ in the form

$$\text{best estimate} \pm \text{statistical error} \pm \text{systematic error} , \quad (7.15)$$

where “statistical error” denotes the one-standard-deviation error bar from the fit to $AL^z + B$ (after averaging over k the fits from the chosen values of L_{min}); and “systematic error” is a 68% subjective confidence interval defined as the absolute value of the discrepancy between the fits AL^z and $AL^z + B$ (after averaging over k the fits from the chosen values of L_{min}) plus 0.02. The final results are therefore:

$$q = 1.75: \quad z_{\text{int},\mathcal{E}'} = 0.085 \pm 0.026 \pm 0.094 \quad (7.16a)$$

$$q = 2.00: \quad z_{\text{int},\mathcal{E}'} = 0.143 \pm 0.003 \pm 0.092 \quad (7.16b)$$

$$q = 2.25: \quad z_{\text{int},\mathcal{E}'} = 0.231 \pm 0.008 \pm 0.071 \quad (7.16c)$$

$$q = 2.50: \quad z_{\text{int},\mathcal{E}'} = 0.307 \pm 0.007 \pm 0.066 \quad (7.16d)$$

$$q = 2.75: \quad z_{\text{int},\mathcal{E}'} = 0.408 \pm 0.005 \pm 0.036 \quad (7.16e)$$

$$q = 3.00: \quad z_{\text{int},\mathcal{E}'} = 0.497 \pm 0.003 \pm 0.033 \quad (7.16f)$$

$$q = 3.25: \quad z_{\text{int},\mathcal{E}'} = 0.572 \pm 0.007 \pm 0.035 \quad (7.16g)$$

$$q = 3.50: \quad z_{\text{int},\mathcal{E}'} = 0.689 \pm 0.004 \pm 0.024 \quad (7.16h)$$

$$q = 3.75: \quad z_{\text{int},\mathcal{E}'} = 0.796 \pm 0.004 \pm 0.032 \quad (7.16i)$$

$$q = 4.00: \quad z_{\text{int},\mathcal{E}'} = 0.910 \pm 0.005 \pm 0.032 \quad (7.16j)$$

In Figure 4 we plot these estimates versus q , and compare them with the static exponents α/ν and β/ν . The Ossola–Sokal conjecture $z \geq \beta/\nu$ appears to be violated for $1 \leq q \lesssim 1.95$ (but see Section 7.5 for an alternative fit that is compatible with the conjecture). The Li–Sokal bound $z \geq \alpha/\nu$ is obeyed for $q \neq 4$ and appears to be non-sharp (see Section 7.4 for a more detailed analysis). The apparent violation of the Li–Sokal bound at $q = 4$ is manifestly due to the multiplicative logarithmic corrections: it is known [19] that $C_H \sim L(\log L)^{-3/2}$ but fits to a power law (with or without a constant background) yield an effective exponent ≈ 0.8 (see the last line of Table 19); it is therefore not surprising that $\tau_{\text{int},\mathcal{E}'}$ shows a similar behavior. If one looks directly at the ratio $\tau_{\text{int},\mathcal{E}'}/C_H$ one finds that the Li–Sokal bound (which is after all a rigorous theorem!) is obeyed (see Section 7.4).

For $q = 1.25$ and 1.50 our best estimates suggest that $\tau_{\text{int},\mathcal{E}'}$ is bounded as $L \rightarrow \infty$, i.e. that $z_{\text{int},\mathcal{E}'} = 0$. Our fits to $A + BL^{-p}$ suggest values for the correction exponent p [cf. (7.2)/(7.3)], but we do not know how reliable these estimates are.

Since the autocorrelation function $\rho_{\mathcal{E}'\mathcal{E}'}(t)$ is nearly a pure exponential, we expect that the dynamic critical exponent z_{exp} is either exactly equal or almost exactly equal to $z_{\text{int},\mathcal{E}'}$.

7.4 Sharpness of Li–Sokal bound

The estimates of $z_{\text{int},\mathcal{E}'}$ summarized in Figure 4 suggest that the Li–Sokal bound $z_{\text{int},\mathcal{E}'} \geq \alpha/\nu$ holds *as a strict inequality* over the entire range $1 \leq q < 4$, i.e. that it is *non-sharp by a power*. But this conclusion is weakened by the fact that our fits of the specific heat C_H give estimates of α/ν that deviate significantly from the known exact values (Table 19). It is therefore of interest to study directly the ratio $\tau_{\text{int},\mathcal{E}'}/C_H$, in an effort to fit its behavior as $L \rightarrow \infty$ to one of the following ansätze:

- 1) Asymptotically constant with additive corrections to scaling $A + BL^{-p}$.
- 2) A logarithmic growth, either as $A \log L + B$ or as $A \log^p L$.
- 3) A power-law growth AL^p or $AL^p + B$.

Unfortunately our time-series analysis does not produce statistically valid error bars for composite static-dynamic quantities such as $\tau_{\text{int},\mathcal{E}'}/C_H$. We therefore conducted the analysis in this subsection under the crude assumption that the statistical fluctuations on our estimators of $\tau_{\text{int},\mathcal{E}'}$ and C_H are uncorrelated. In fact it is likely that these fluctuations are *positively* correlated, so that the true error bars on the ratio $\tau_{\text{int},\mathcal{E}'}/C_H$ are *smaller* than we have supposed. If so, this means that the true confidence level of our fits is *smaller* than what we report.¹⁷

The fits to $A + BL^{-p}$ with $p > 0$ were always bad: either they had a horrible confidence level, or they converged to a value $p < 0$ (indicating that the true leading behavior is a power-law *growth*). We therefore focussed on comparing the logarithmic-growth and power-law-growth scenarios. We chose $A \log L + B$ and AL^p as the ansätze in order to compare fits with an equal number of free parameters. The results are shown in

¹⁷ This failure to provide statistically valid error bars is embarrassing. We should have used the batch-means method [17, Section 4.2] to obtain such error bars. Unfortunately, the raw data from our simulations are no longer accessible, so we are unable to conduct such a reanalysis.

Table 25. We see that both fits are in general good (though the confidence levels may be overestimated as noted above). However, the power-law fits are in general better. In particular, there are no cases in which the power-law fit has a confidence level less than 25%; but there are quite a few cases in which the logarithmic fit exhibits such a low confidence level (sometimes much lower). We therefore conclude that the fits to $\tau_{\text{int},\mathcal{E}'}/C_H$ also provide weak evidence that the Li–Sokal bound is non-sharp by a power.

7.5 Test of Ossola–Sokal conjecture

In the Introduction we argued that the Ossola–Sokal conjecture $z_{\text{CM}} \geq \beta/\nu$ is probably false, on the grounds that it fails for $q = 1$ (where $z_{\text{CM}} = 0$ and $\beta/\nu > 0$) and that z_{CM} is presumably a continuous function of q . But this latter assumption is far from certain: it is possible, for instance, that $z_{\text{CM}} = \beta/\nu$ exactly for all q near 1, but with an amplitude that vanishes as $q \downarrow 1$. In this subsection we would like to test this scenario against our data for $1.25 \leq q \leq 2$.

We first tried fits to $\tau_{\text{int},\mathcal{E}'} = AL^{\beta/\nu} + B$. We then tried fits to $\tau_{\text{int},\mathcal{E}'} = AL^{\beta/\nu} + B + CL^{-p}$ where $p > 0$ is fixed and A, B, C are free. Let us report our results from these fits in decreasing order of q :

1) For $q = 2$ ($k = 1$) the fit to $AL^{\beta/\nu} + B$ is decent already for $L_{\text{min}} = 32$ ($\chi^2 = 3.90$, 4 DF, CL = 42%) and better for $L_{\text{min}} = 64$:

$$A = 13.27(7), B = -11.83(13) \quad (\chi^2 = 1.51, 3 \text{ DF}, \text{CL} = 68\%). \quad (7.17)$$

This behavior is not surprising, because our fit to $AL^z + B$ with z free yielded $z = 0.145(4)$ with $L_{\text{min}} = 16$, which is not very far from $\beta/\nu = 0.125$.

In Figure 5 we plot the results of our fits to $AL^{\beta/\nu} + B + CL^{-p}$ as a function of p , for $L_{\text{min}} = 16$ and 32:

- For $L_{\text{min}} = 16$ an excellent confidence level is obtained over the whole range $0 < p < 2$ (and indeed beyond), with an optimum at $p \approx 0.692$ (CL = 92%). The estimated amplitudes A are positive and very far from zero; at the optimum we have $A = 13.44(9)$. As $p \rightarrow \infty$ the amplitude A tends to a value ≈ 13 , which is close to that obtained from the fit to $AL^{\beta/\nu} + B$.
- For $L_{\text{min}} = 32$ an excellent confidence level is again obtained over the whole range $0 < p < 2$ (and indeed beyond), with an optimum at $p \approx 0.228$ (CL = 84%) but with a very broad peak. The estimated amplitudes A are again positive and very far from zero; at the optimum we have $A = 13.71(30)$. As $p \rightarrow \infty$ the amplitude A again tends to ≈ 13 .

2) For $q = 1.75$ the fit to $AL^{\beta/\nu} + B$ is decent already for $L_{\text{min}} = 128$ ($\chi^2 = 2.31$, 2 DF, CL = 32%) and excellent for $L_{\text{min}} = 256$:

$$A = 5.36(8), B = -2.62(17) \quad (\chi^2 = 0.002, 1 \text{ DF}, \text{CL} = 97\%). \quad (7.18)$$

Once again this behavior is not surprising, because our fit to $AL^z + B$ with z free yielded $z = 0.085(26)$ with $L_{\text{min}} = 128$, which is not very far from $\beta/\nu \approx 0.121$.

In Figure 6 we plot the results of our fits to $AL^{\beta/\nu} + B + CL^{-p}$ as a function of p , for $L_{\min} = 32$ and 64:

- For $L_{\min} = 32$ a decent confidence level is obtained for $p \lesssim 0.6$, with an optimum at $p \approx 0.056$ (CL = 41%). The estimated amplitudes A are positive and far from zero; at the optimum we have $A = 3.51(24)$. As $p \rightarrow \infty$ the amplitude A tends to a value ≈ 5.8 , which is close to that obtained from the fit to $AL^{\beta/\nu} + B$.
- For $L_{\min} = 64$ a decent confidence level is obtained over the entire range $0 < p \leq 2$ (or even beyond), with an optimum at $p \approx 1.321$ (CL = 96%). The estimated amplitudes A are again positive and far from zero, and in fact quite close to those obtained from $L_{\min} = 32$. At the optimum, we have $A = 5.28(7)$.

3) For $q = 1.5$ the fit to $AL^{\beta/\nu} + B$ is poor even for $L_{\min} = 256$ (CL = 3%). In Figure 7 we plot the results of our fits to $AL^{\beta/\nu} + B + CL^{-p}$ as a function of p , for $L_{\min} = 32$ and 64:

- For $L_{\min} = 32$ a decent confidence level is obtained for $p \lesssim 0.3$, but with the optimum attained at the ridiculously small value $p \approx 0.004$ (CL = 86%). Also, the estimated amplitude A is negative for $p \lesssim 0.033$, which is obviously impossible. However, for $0.08 \lesssim p \lesssim 0.3$ a decent fit is obtained with an amplitude A that is positive and far from zero.
- For $L_{\min} = 64$ a decent confidence level is obtained for $0 < p \lesssim 0.9$, with an optimum at $p \approx 0.228$ (CL = 86%). The estimated amplitudes A are again negative for $p \lesssim 0.038$ but positive and far from zero for $p \gtrsim 0.1$. At the optimum, we have $A = 1.11(8)$.

4) For $q = 1.25$ the fit to $AL^{\beta/\nu} + B$ is poor even for $L_{\min} = 256$ (CL = 1%). The fits to $AL^{\beta/\nu} + B + CL^{-p}$ are poor (CL < 6%) for $L_{\min} = 32$ and 64 for all $p > 0$. For $L_{\min} = 128$, however, we are able to obtain decent fits over the whole range $0 < p \lesssim 2$, as shown in Figure 8. The optimum lies at $p \approx 0.695$ (CL = 99.9997%). The estimated amplitudes A are negative for $p \lesssim 0.211$ but positive and far from zero for $p \gtrsim 0.4$. At the optimum, we have $A = 0.28(2)$.

The foregoing fits show that the Ossola–Sokal conjecture $z_{\text{CM}} \geq \beta/\nu$ is *not* ruled out by our data at $1.25 \leq q \leq 2$. Indeed, our data are consistent with the possibility that $z_{\text{CM}} = \beta/\nu$ exactly for $1 < q \lesssim 2$, but with an amplitude that vanishes as $q \downarrow 1$, perhaps proportional to $q - 1$ (the fits for $q = 1.25$ and 1.50 are consistent with this latter behavior).

7.6 Dynamic critical exponents $z_{\text{int},\mathcal{O}}$ for other \mathcal{O}

Let us now look briefly at the dynamic critical exponents $z_{\text{int},\mathcal{O}}$ for observables \mathcal{O} other than \mathcal{E}' . For $\mathcal{O} = \mathcal{N}, \mathcal{S}_2, \mathcal{C}_1$, the values of $\tau_{\text{int},\mathcal{O}}$ are very close to those of $\tau_{\text{int},\mathcal{E}'}$, so the estimates of $z_{\text{int},\mathcal{O}}$ will be nearly the same; little would be gained by going through these fits in detail. Instead, it seems sensible to look at the observable that has the *smallest*

autocorrelation time, namely \mathcal{C}_2 — the idea being that if any differences in $z_{\text{int},\mathcal{O}}$ between different observables are to be detected, they will be detected here.

From Figure 3 we see that the autocorrelation function of \mathcal{E}' is nearly a pure exponential (and this is so for all q, k, L), so that $\tau_{\text{int},\mathcal{E}'} \approx \tau_{\text{exp}}$ and hence $z_{\text{int},\mathcal{E}'} = z_{\text{exp}}$ or nearly so. The autocorrelation function of \mathcal{C}_2 , by contrast, exhibits an initial fast decay, followed by a decay at the *same* exponential rate τ_{exp} as for the other observables but with an amplitude $A_{\mathcal{C}_2}$ that is significantly less than 1 (e.g. around 0.4 in the plot shown). The key question is whether this amplitude tends to a nonzero value when $L \rightarrow \infty$ (in which case we will have $z_{\text{int},\mathcal{C}_2} = z_{\text{exp}}$) or tends to zero as an inverse power of L (in which case we will have $z_{\text{int},\mathcal{C}_2} < z_{\text{exp}}$).¹⁸

In Tables 26 and 27 we show the fits for $\tau_{\text{int},\mathcal{C}_2}$ to the ansätze AL^z and $AL^z + B$. In Table 28 we show the results for $z_{\text{int},\mathcal{C}_2}$ obtained by averaging over k .

The estimates for $z_{\text{int},\mathcal{C}_2}$ are indeed less than those for $z_{\text{int},\mathcal{E}'}$, by an amount that is ≈ 0.1 for $q \approx 2$ and tends to zero as $q \uparrow 4$. The question is: Are these differences real, or are they artifacts of corrections to scaling at small L ? The fact that the differences are smaller for $q \gtrsim 3$, where the autocorrelation times are larger, suggests that perhaps the differences will disappear as $L \rightarrow \infty$ but that at small q we have to go to larger L to see this. But this is far from clear; we will only know the truth by doing simulations at significantly larger values of L .

8 Discussion

In this paper we have studied the dynamic critical behavior of the Chayes–Machta algorithm as a function of q over the whole range $1.25 \leq q \leq 4$. We have obtained estimates of the dynamic critical exponent $z_{\text{int},\mathcal{E}'}$ as a function of q : see (7.16), Table 24 and Figure 4. Since the autocorrelation function $\rho_{\mathcal{E}'\mathcal{E}'}(t)$ is nearly a pure exponential, we also expect that the dynamic critical exponent z_{exp} is either exactly equal or almost exactly equal to $z_{\text{int},\mathcal{E}'}$.

By simultaneously studying the whole range of values of q , we were able to gain some insights that would not have been available had we studied only a single value of q (such as the Ising value $q = 2$) or even all integer values of q as in past studies of the Swendsen–Wang algorithm. For instance:

1) The autocorrelation time $\tau_{\text{int},\mathcal{E}'}$ at $q = 2$ can be plausibly fit with the ansatz $A \log^2 L + B \log L + C$, suggesting that the Li–Sokal bound might be sharp modulo a logarithm; this agrees with the conclusions of the paper [16], where the data were in fact found to slightly favor the non-sharp-by-a-logarithm ansatz over the non-sharp-by-a-power ansatz. But we now find that the good fit to $A \log^2 L + B \log L + C$ persists over the whole range $1.75 \leq q \lesssim 2.25$. And it seems to us implausible on theoretical grounds that we would have such a logarithmic growth for an entire *interval* of q ; rather, we expect that there exists *one* value q_\star such that $z = 0$ for $q < q_\star$ and $z > 0$ for $q > q_\star$, with a possible (poly)logarithmic growth *at* $q = q_\star$. Our data suggest that q_\star lies between 1.25

¹⁸ See [20, Section 5.2] for a more detailed analysis of this kind, for the Swendsen–Wang dynamics for the three-dimensional Ising model.

and 1.75, with our best guess being around 1.6. If this scenario is correct, it follows that the Li–Sokal bound is non-sharp by a power for $q_* < q \leq 2$. This then suggests (but of course does not prove) that it might be non-sharp by a power over the whole interval $q_* < q < 4$ (possibly reverting to non-sharp by a logarithm at $q = 4$).

2) By considering the Ossola–Sokal conjecture $z_{\text{CM}} \geq \beta/\nu$ simultaneously for all q , we can see immediately that it fails at $q = 1$ (where $z_{\text{CM}} = 0$ but $\beta/\nu > 0$) and hence fails also for q near 1 *if* the dynamic critical exponent z_{CM} is a continuous function of q . Indeed, our pure power-law fits suggest that the conjecture fails for $1 \leq q \lesssim 1.95$. (In particular, if $q_* > 1$ as just suggested, then the conjecture fails spectacularly in the interval $1 \leq q < q_*$, where $z_{\text{CM}} = 0$ but $\beta/\nu > 0$.) However — and perhaps surprisingly — our data are also compatible with an alternative scenario in which $z_{\text{CM}} = \beta/\nu$ exactly for all q near 1, but with an amplitude that vanishes as $q \downarrow 1$ (Section 7.5).

However, the behavior of the Chayes–Machta autocorrelation time for $1 < q < 2$ is still unclear: though our data strongly suggest that $\tau_{\text{int}, \mathcal{E}'}$ diverges as $L \rightarrow \infty$ for q slightly below 2, and is nondivergent as $L \rightarrow \infty$ for q slightly above 1, we cannot rule out the possibility that the data at $L \leq 1024$ are misleading and that the true asymptotic behavior is different from what we conjecture. Future work at larger values of L would of course be desirable.

Likewise, though our data suggest that the Li–Sokal bound is non-sharp by a power for $1.6 \lesssim q < 4$, it is also true that the exponent estimates have been dropping over time as data becomes available at larger values of L and as we try ansätze other than a pure power law (see Table 24 for the effect of the ansatz). Our data suggest most clearly the non-sharpness of the Li–Sokal bound (when the non-sharpness is measured in units of the standard deviation of our estimate) at $q = 2.75$ and $q = 3$. At these values of q , the critical slowing-down is strong enough that interference from the regular background term is less important than it is at smaller q (i.e. the AL^z and $AL^z + B$ fits show less discrepancy) but modest enough that we can have reasonably good data on large lattices (contrary to the situation at larger q); furthermore, the correction-to-scaling exponent Δ_1 is still fairly large. It would therefore be of great interest to perform high-precision simulations at these values of q , going to very high values of L .

Acknowledgments

The authors would like to thank Youjin Deng and Jonathan Machta for many helpful discussions. We would also like to thank Mulin Ding for helping us to recover some of the data from this project.

This research was supported in part by U.S. National Science Foundation grants PHY–0116590 and PHY–0424082.

References

- [1] K. Binder, ed., *Monte Carlo Methods in Statistical Physics*, 2nd ed. (Springer-Verlag, Berlin, 1986).

- [2] K. Binder, ed., *Applications of the Monte Carlo Method in Statistical Physics*, 2nd ed. (Springer-Verlag, Berlin, 1987).
- [3] K. Binder, ed., *The Monte Carlo Method in Condensed Matter Physics*, 2nd ed. (Springer-Verlag, Berlin, 1995).
- [4] P.C. Hohenberg and B.I. Halperin, *Rev. Mod. Phys.* **49**, 435 (1977).
- [5] A. D. Sokal, Monte Carlo methods in Statistical Mechanics: Foundations and new algorithms, in C. DeWitt-Morette, P. Cartier and A. Folacci, eds., *Functional Integration: Basics and Applications* (1996 Cargèse summer school), pp. 131–192 (Plenum, New York, 1997).
- [6] R. H. Swendsen and J.-S. Wang, *Phys. Rev. Lett.* **58**, 86 (1987).
- [7] R. B. Potts, *Proc. Cambridge Philos. Soc.* **48**, 106 (1952).
- [8] F. Y. Wu, *Rev. Mod. Phys.* **54**, 235 (1982) and erratum **55**, 315 (1983).
- [9] F. Y. Wu, *J. Appl. Phys.* **55**, 2421 (1984).
- [10] P. W. Kasteleyn and C. M. Fortuin, *J. Phys. Soc. Japan* **26** (Suppl.), 11 (1969).
- [11] C. M. Fortuin and P. W. Kasteleyn, *Physica* **57**, 536 (1972).
- [12] C. M. Fortuin, *Physica* **58**, 393 (1972).
- [13] C. M. Fortuin, *Physica* **59**, 545 (1972).
- [14] R.G. Edwards and A.D. Sokal, *Phys. Rev. D* **38**, 2009 (1988).
- [15] G. Grimmett, *The Random-Cluster Model* (Springer-Verlag, New York, 2006).
- [16] J. Salas and A.D. Sokal, Universal amplitude ratios in the critical two-dimensional Ising model on a torus, cond-mat/9904038v1. For space reasons, this material was deleted from the published version of this paper [*J. Stat. Phys.* **98**, 551 (2000)].
- [17] J. Salas and A.D. Sokal, *J. Stat. Phys.* **87**, 1 (1997), hep-lat/9605018.
- [18] J. Salas and A.D. Sokal, *J. Stat. Phys.* **85**, 297 (1996), hep-lat/9511022.
- [19] J. Salas and A.D. Sokal, *J. Stat. Phys.* **88**, 567 (1997), hep-lat/9607030.
- [20] G. Ossola and A.D. Sokal, *Nucl. Phys. B* **691**, 259 (2004), hep-lat/0402019.
- [21] W. Klein, T. Ray and P. Tamayo, *Phys. Rev. Lett.* **62**, 163 (1989).
- [22] T. Ray, P. Tamayo and W. Klein, *Phys. Rev. A* **39**, 5949 (1989).
- [23] P.D. Coddington and C.F. Baillie, *Phys. Rev. Lett.* **68**, 962 (1992).

- [24] N. Persky, R. Ben-Av, I. Kanter and E. Domany, Phys. Rev. E **54**, 2351 (1996), cond-mat/9603134.
- [25] L. Chayes and J. Machta, Physica A **254**, 477 (1998).
- [26] H.W.J. Blöte, Y. Deng, X. Qian and A.D. Sokal, in preparation,
- [27] Y. Deng, T. M. Garoni and A. D. Sokal, Dynamic critical behavior of the Chayes-Machta algorithm for the random-cluster model, II. Three dimensions, in preparation.
- [28] Y. Deng, T. M. Garoni, J. Machta and A. D. Sokal, Dynamic critical behavior of the Chayes-Machta algorithm for the random-cluster model, III. Complete graph, in preparation.
- [29] Y. Deng, T. M. Garoni, J. Machta, G. Ossola, M. Polin and A. D. Sokal, Phys. Rev. Lett. **99**, 055701 (2007), arXiv:0705.2751 [cond-mat.stat-mech].
- [30] R. J. Baxter, *Exactly Solved Models in Statistical Mechanics* (Academic Press, London–New York, 1982).
- [31] V. Beffara and H. Duminil-Copin, The self-dual point of the two-dimensional random-cluster model is critical for $q \geq 1$, arXiv:1006.5073 [math.PR].
- [32] B. Nienhuis, J. Stat. Phys. **34**, 731 (1984).
- [33] B. Nienhuis, in *Phase Transitions and Critical Phenomena*, vol. 11, C. Domb and J.L. Lebowitz, eds. (Academic Press, New York–London, 1987), section IV.C.
- [34] M.P.M. den Nijs, Phys. Rev. B **27**, 1674 (1983).
- [35] X.-J. Li and A. D. Sokal, Phys. Rev. Lett. **63**, 827 (1989).
- [36] D. J. Amit and V. Martín-Mayor, *Field Theory, the Renormalization Group, and Critical Phenomena*, 3rd ed. (World Scientific, Singapore, 2005).
- [37] S. Caracciolo, R. G. Edwards, A. Pelissetto and A. D. Sokal, Nucl. Phys. B **403**, 475 (1993), hep-lat/9205005.
- [38] F. Cooper, B. Freedman and D. Preston, Nucl. Phys. B **210** [FS6], 210 (1982).
- [39] M. B. Priestley, *Spectral Analysis and Time Series*, 2 vols. (Academic, London, 1981).
- [40] T. W. Anderson, *The Statistical Analysis of Time Series* (Wiley, New York, 1971).
- [41] N. Madras and A. D. Sokal, J. Stat. Phys. **50**, 109 (1988).
- [42] G. Ossola and A.D. Sokal, Phys. Rev. E **70**, 027701 (2004), hep-lat/0403010.
- [43] P. L’Ecuyer, Math. Comp. **68**, 249 (1999).
- [44] H. Guo and D. Jasnow, Phys. Rev. B **35**, 1846 (1987); **39**, 753 (E) (1989).

- [45] X. Feng, Y. Deng and H.W.J. Blöte, Phys. Rev. E **78**, 031136 (2008), arXiv:0901.1370 [cond-mat.stat-mech].
- [46] H.W.J. Blöte and M.P.M. den Nijs, Phys. Rev. B **37**, 1766 (1988).
- [47] P. Di Francesco, H. Saleur and J.-B. Zuber, Nucl. Phys. B **290** [FS20], 527 (1987).
- [48] P. Di Francesco, H. Saleur and J.-B. Zuber, Europhys. Lett. **5**, 95 (1988).
- [49] J. Salas and A.D. Sokal, J. Stat. Phys. **98**, 551 (2000), cond-mat/9904038.
- [50] A.E. Ferdinand and M.E. Fisher, Phys. Rev. **185**, 832 (1969).
- [51] J. Salas, J. Phys. A **34**, 1311 (2001), cond-mat/0009054.

q	α/ν	β/ν	γ/ν	Δ_1
1.25	-0.35527	0.11118	1.77764	1.80702
1.50	-0.22663	0.11678	1.76644	1.63551
1.75	-0.10929	0.12131	1.75738	1.47905
2.00	0.00000	0.12500	1.75000	1.33333
2.25	0.10363	0.12798	1.74404	1.19517
2.50	0.20357	0.13034	1.73932	1.06191
2.75	0.30168	0.13212	1.73576	0.93110
3.00	0.40000	0.13333	1.73333	0.80000
3.25	0.50126	0.13393	1.73214	0.66499
3.50	0.61007	0.13377	1.73246	0.51991
3.75	0.73760	0.13242	1.73517	0.34986
4.00	1.00000	0.12500	1.75000	0.00000

Table 2: Exact values of the static critical exponents, rounded to five decimal places.

L	$q = 1.25$	$q = 1.50$	$q = 1.75$	$q = 2.00$
16	0.5011732(38)	0.5025161(59)	0.5040267(83)	0.5056788(68)
32	0.5005202(20)	0.5011648(32)	0.5019472(47)	0.5028427(41)
64	0.5002301(10)	0.5005395(17)	0.5009352(26)	0.5014281(24)
128	0.5001022(5)	0.5002494(9)	0.5004485(14)	0.5007133(14)
256	0.5000444(3)	0.5001146(5)	0.5002159(8)	0.5003559(8)
512	0.5000199(2)	0.5000530(3)	0.5001046(6)	0.5001763(6)
1024	0.5000089(2)	0.5000243(3)	0.5000510(5)	0.5000884(6)

L	$q = 2.25$	$q = 2.50$	$q = 2.75$	$q = 3.00$
16	0.5075026(91)	0.5094773(117)	0.5115651(149)	0.5138241(136)
32	0.5038896(56)	0.5050706(76)	0.5064185(101)	0.5078851(97)
64	0.5020129(34)	0.5027090(49)	0.5035416(68)	0.5045052(68)
128	0.5010481(21)	0.5014567(31)	0.5019755(45)	0.5025847(47)
256	0.5005396(12)	0.5007837(19)	0.5010878(29)	0.5014847(33)
512	0.5002817(10)	0.5004183(17)	0.5006029(26)	0.5008522(32)
1024	0.5001446(10)	0.5002238(17)	0.5003359(28)	0.5004888(35)

L	$q = 3.25$	$q = 3.50$	$q = 3.75$	$q = 4.00$
16	0.5161911(167)	0.5186811(202)	0.5213781(243)	0.5240486(230)
32	0.5095378(124)	0.5113335(157)	0.5132856(197)	0.5154722(196)
64	0.5056256(92)	0.5069004(122)	0.5083371(162)	0.5100231(169)
128	0.5033402(67)	0.5042207(95)	0.5052769(133)	0.5065189(148)
256	0.5019717(49)	0.5025922(74)	0.5033613(111)	0.5043157(132)
512	0.5011757(51)	0.5015847(82)	0.5021351(128)	0.5028279(170)
1024	0.5006989(59)	0.5009736(100)	0.5013665(173)	0.5018837(242)

Table 3: Static data for $\langle \mathcal{N} \rangle$, from the Monte Carlo simulations at the critical point of the 2-dimensional random cluster model, as a function of L and q , obtained by combining the data for all available k values for each q . The quoted error bar corresponds to one standard deviation.

L	$q = 1.25$	$q = 1.50$	$q = 1.75$	$q = 2.00$
16	0.5533 ± 0.0004	1.0380 ± 0.0006	1.4902 ± 0.0008	1.9285 ± 0.0006
32	0.6180 ± 0.0004	1.1940 ± 0.0006	1.7753 ± 0.0009	2.3779 ± 0.0008
64	0.6672 ± 0.0004	1.3284 ± 0.0007	2.0348 ± 0.0010	2.8226 ± 0.0010
128	0.7058 ± 0.0004	1.4420 ± 0.0007	2.2767 ± 0.0012	3.2651 ± 0.0012
256	0.7360 ± 0.0004	1.5366 ± 0.0007	2.4957 ± 0.0013	3.7062 ± 0.0014
512	0.7594 ± 0.0006	1.6200 ± 0.0011	2.7016 ± 0.0020	4.1456 ± 0.0023
1024	0.7768 ± 0.0010	1.6911 ± 0.0018	2.8922 ± 0.0035	4.5918 ± 0.0043

L	$q = 2.25$	$q = 2.50$	$q = 2.75$	$q = 3.00$
16	2.3666 ± 0.0008	2.8023 ± 0.0011	3.2511 ± 0.0014	3.7039 ± 0.0013
32	3.0210 ± 0.0011	3.7149 ± 0.0016	4.4747 ± 0.0022	5.3043 ± 0.0022
64	3.7224 ± 0.0015	4.7651 ± 0.0022	5.9700 ± 0.0033	7.3834 ± 0.0035
128	4.4734 ± 0.0019	5.9631 ± 0.0031	7.8056 ± 0.0049	10.1121 ± 0.0057
256	5.2731 ± 0.0024	7.3397 ± 0.0042	10.0718 ± 0.0072	13.6991 ± 0.0092
512	6.1406 ± 0.0043	8.9200 ± 0.0081	12.8590 ± 0.0141	18.4085 ± 0.0206
1024	7.0693 ± 0.0085	10.7582 ± 0.0171	16.2779 ± 0.0344	24.6869 ± 0.0521

L	$q = 3.25$	$q = 3.50$	$q = 3.75$	$q = 4.00$
16	4.1724 ± 0.0017	4.6485 ± 0.0022	5.1301 ± 0.0027	5.6282 ± 0.0027
32	6.1993 ± 0.0030	7.1820 ± 0.0040	8.2551 ± 0.0054	9.4058 ± 0.0058
64	9.0259 ± 0.0052	10.9483 ± 0.0076	13.1591 ± 0.0111	15.6961 ± 0.0128
128	12.9732 ± 0.0091	16.5492 ± 0.0144	20.9891 ± 0.0229	26.4882 ± 0.0294
256	18.5468 ± 0.0158	24.9710 ± 0.0274	33.5950 ± 0.0481	45.0709 ± 0.0680
512	26.3990 ± 0.0392	37.7809 ± 0.0751	54.1813 ± 0.1423	78.3598 ± 0.2298
1024	37.3057 ± 0.1063	56.9881 ± 0.2229	87.9462 ± 0.4814	136.9444 ± 0.8705

Table 4: Static data for C_H , from the Monte Carlo simulations at the critical point of the 2-dimensional random cluster model, as a function of L and q , obtained by combining the data for all available k values for each pair (q, L) . The quoted error bar corresponds to one standard deviation.

L	$q = 1.25$	$q = 1.50$	$q = 1.75$	$q = 2.00$
16	145.2585 ± 0.0075	142.6486 ± 0.0106	140.8411 ± 0.0140	139.6098 ± 0.0107
32	497.8233 ± 0.0265	485.2393 ± 0.0382	476.2855 ± 0.0515	469.9356 ± 0.0405
64	1706.4867 ± 0.0932	1650.6023 ± 0.1357	1610.1083 ± 0.1860	1581.4235 ± 0.1495
128	5850.3427 ± 0.3249	5614.3344 ± 0.4780	5442.1190 ± 0.6643	5319.5479 ± 0.5429
256	20054.6950 ± 1.1280	19099.3800 ± 1.6687	18399.0050 ± 2.3542	17890.2105 ± 1.9519
512	68770.5920 ± 5.3616	64981.2580 ± 7.9347	62211.4880 ± 11.2476	60146.9825 ± 9.8673
1024	235766.3800 ± 30.2818	221047.8000 ± 45.1926	210455.2400 ± 64.7251	202355.8500 ± 56.1135

L	$q = 2.25$	$q = 2.50$	$q = 2.75$	$q = 3.00$
16	138.8711 ± 0.0134	138.5052 ± 0.0163	138.3926 ± 0.0195	138.5876 ± 0.0170
32	465.8207 ± 0.0515	463.3878 ± 0.0642	462.5502 ± 0.0791	462.6740 ± 0.0708
64	1561.0853 ± 0.1941	1548.2598 ± 0.2482	1542.4292 ± 0.3129	1541.8545 ± 0.2886
128	5232.5878 ± 0.7205	5173.4167 ± 0.9438	5144.4281 ± 1.2191	5134.3089 ± 1.1567
256	17520.7785 ± 2.6405	17280.0615 ± 3.5374	17129.3300 ± 4.7118	17087.6517 ± 4.5949
512	58713.4455 ± 13.4485	57681.1135 ± 18.6703	57059.7820 ± 23.9577	56845.9733 ± 25.6428
1024	196609.0350 ± 78.3919	192554.3100 ± 109.9204	190128.7000 ± 153.6076	189071.0300 ± 159.4872

L	$q = 3.25$	$q = 3.50$	$q = 3.75$	$q = 4.00$
16	138.9566 ± 0.0199	139.5084 ± 0.0231	140.3091 ± 0.0266	141.0928 ± 0.0242
32	464.1562 ± 0.0851	466.4774 ± 0.1019	469.6013 ± 0.1210	473.9444 ± 0.1140
64	1546.5943 ± 0.3570	1555.8520 ± 0.4412	1569.0339 ± 0.5429	1588.4126 ± 0.5280
128	5150.8298 ± 1.4817	5182.9838 ± 1.8976	5238.2491 ± 2.4158	5312.8763 ± 2.4510
256	17123.9467 ± 6.0699	17256.6300 ± 8.0307	17479.6003 ± 10.6954	17798.6190 ± 11.3951
512	56959.4603 ± 35.1990	57362.2313 ± 48.4641	58221.5237 ± 65.2645	59402.9003 ± 75.5415
1024	189355.8433 ± 223.7014	190717.4067 ± 322.6179	194007.2267 ± 466.2996	198760.7775 ± 550.8406

Table 5: Static data for χ , from the Monte Carlo simulations at the critical point of the 2-dimensional random cluster model, as a function of L and q , obtained by combining the data for all available k values for each pair (q, L) . The quoted error bar corresponds to one standard deviation.

L	$q = 1.25$	$q = 1.50$	$q = 1.75$	$q = 2.00$
16	0.92329(10)	0.91489(13)	0.91142(17)	0.91137(13)
32	0.91903(10)	0.91064(13)	0.90705(17)	0.90702(13)
64	0.91784(10)	0.90927(14)	0.90559(18)	0.90596(14)
128	0.91755(10)	0.90869(14)	0.90492(19)	0.90553(15)
256	0.91727(10)	0.90868(14)	0.90482(20)	0.90511(16)
512	0.91748(14)	0.90867(20)	0.90500(27)	0.90433(24)
1024	0.91729(23)	0.90855(33)	0.90595(46)	0.90467(40)

L	$q = 2.25$	$q = 2.50$	$q = 2.75$	$q = 3.00$
16	0.91427(16)	0.91952(19)	0.92604(22)	0.93484(20)
32	0.91015(17)	0.91564(21)	0.92363(26)	0.93262(23)
64	0.90856(18)	0.91384(23)	0.92198(29)	0.93200(27)
128	0.90866(20)	0.91375(26)	0.92226(33)	0.93190(32)
256	0.90774(21)	0.91372(29)	0.92091(38)	0.93187(37)
512	0.90817(32)	0.91313(45)	0.92086(57)	0.93186(61)
1024	0.90777(56)	0.91280(78)	0.92117(109)	0.93191(114)

L	$q = 3.25$	$q = 3.50$	$q = 3.75$	$q = 4.00$
16	0.94453(23)	0.95554(27)	0.96872(31)	0.98129(29)
32	0.94431(28)	0.95731(33)	0.97163(40)	0.98913(38)
64	0.94428(33)	0.95874(41)	0.97494(51)	0.99544(50)
128	0.94522(40)	0.95967(52)	0.97789(66)	0.99884(67)
256	0.94465(49)	0.96087(65)	0.98047(86)	1.00431(92)
512	0.94516(84)	0.96028(115)	0.98054(155)	1.00374(178)
1024	0.94561(160)	0.95999(229)	0.98103(329)	1.00762(386)

Table 6: Static data for ξ/L , from the Monte Carlo simulations at the critical point of the 2-dimensional random cluster model, as a function of L and q , obtained by combining the data for all available k values for each q . The quoted error bar corresponds to one standard deviation.

L	$q = 1.25$	$q = 1.50$	$q = 1.75$	$q = 2.00$
16	186.2505 ± 0.0063	184.4023 ± 0.0090	183.1015 ± 0.0119	182.1899 ± 0.0092
32	689.6841 ± 0.0241	680.2851 ± 0.0349	673.4366 ± 0.0472	668.4742 ± 0.0373
64	2554.0565 ± 0.0912	2509.5209 ± 0.1337	2476.5244 ± 0.1844	2452.6604 ± 0.1491
128	9458.3576 ± 0.3426	9256.6841 ± 0.5088	9106.1186 ± 0.7136	8996.7788 ± 0.5878
256	35023.7950 ± 1.2827	34147.6420 ± 1.9207	33487.5700 ± 2.7425	32997.3910 ± 2.2970
512	129717.7400 ± 6.5774	125972.7400 ± 9.8879	123159.5900 ± 14.2165	121001.7950 ± 12.6325
1024	480361.5500 ± 40.1000	464676.1500 ± 60.9749	453086.4700 ± 88.8330	443892.0650 ± 78.1385

L	$q = 2.25$	$q = 2.50$	$q = 2.75$	$q = 3.00$
16	181.6159 ± 0.0114	181.3067 ± 0.0140	181.1556 ± 0.0168	181.2307 ± 0.0147
32	665.1430 ± 0.0477	663.0250 ± 0.0597	662.0820 ± 0.0738	661.7617 ± 0.0663
64	2435.0770 ± 0.1948	2423.3282 ± 0.2505	2417.2209 ± 0.3176	2415.0313 ± 0.2944
128	8916.5343 ± 0.7865	8859.1099 ± 1.0381	8828.1239 ± 1.3495	8811.6847 ± 1.2878
256	32630.0710 ± 3.1391	32381.5370 ± 4.2429	32211.1000 ± 5.6996	32145.2913 ± 5.5950
512	119466.6650 ± 17.4240	118314.9800 ± 24.4583	117572.5400 ± 31.6963	117255.6470 ± 34.1426
1024	437205.8550 ± 110.7533	432342.1300 ± 157.0958	429266.3250 ± 222.0290	427635.5230 ± 232.5611

L	$q = 3.25$	$q = 3.50$	$q = 3.75$	$q = 4.00$
16	181.4135 ± 0.0172	181.7222 ± 0.0200	182.2158 ± 0.0231	182.6714 ± 0.0212
32	662.5142 ± 0.0800	663.8117 ± 0.0962	665.6519 ± 0.1145	668.4296 ± 0.1084
64	2417.0586 ± 0.3658	2422.3096 ± 0.4545	2430.5493 ± 0.5611	2443.8329 ± 0.5482
128	8818.7426 ± 1.6581	8836.6149 ± 2.1356	8874.0274 ± 2.7312	8926.2274 ± 2.7887
256	32146.4423 ± 7.4382	32235.6990 ± 9.8938	32400.5450 ± 13.2437	32647.2718 ± 14.1668
512	117238.6570 ± 47.2276	117484.8100 ± 65.4957	118192.9730 ± 88.6774	119114.2730 ± 103.0354
1024	427561.8030 ± 328.2653	428396.6700 ± 476.5507	431327.5100 ± 691.8068	435425.1580 ± 822.7561

Table 7: Static data for C_1 , from the Monte Carlo simulations at the critical point of the 2-dimensional random cluster model, as a function of L and q , obtained by combining the data for all available k values for each q . The quoted error bar corresponds to one standard deviation.

L	$q = 1.25$	$q = 1.50$	$q = 1.75$	$q = 2.00$
16	1.3601 ± 0.0008	2.6552 ± 0.0022	4.5086 ± 0.0048	7.0555 ± 0.0093
32	1.4516 ± 0.0009	2.9749 ± 0.0026	5.2959 ± 0.0060	8.6748 ± 0.0127
64	1.5433 ± 0.0010	3.2988 ± 0.0030	6.1255 ± 0.0075	10.4931 ± 0.0167
128	1.6225 ± 0.0011	3.6209 ± 0.0034	7.0060 ± 0.0093	12.4925 ± 0.0217
256	1.7014 ± 0.0012	3.9284 ± 0.0039	7.8884 ± 0.0110	14.7173 ± 0.0278
512	1.7679 ± 0.0016	4.2341 ± 0.0060	8.8097 ± 0.0176	17.0928 ± 0.0493
1024	1.8281 ± 0.0028	4.5295 ± 0.0109	9.8139 ± 0.0340	19.8144 ± 0.0982

L	$q = 2.25$	$q = 2.50$	$q = 2.75$	$q = 3.00$
16	10.5266 ± 0.0169	15.0260 ± 0.0288	20.8370 ± 0.0469	28.2660 ± 0.0739
32	13.4708 ± 0.0243	20.0908 ± 0.0443	29.2540 ± 0.0778	41.3643 ± 0.1309
64	17.0098 ± 0.0346	26.6206 ± 0.0675	40.4635 ± 0.1264	60.2637 ± 0.2298
128	21.2642 ± 0.0483	34.7971 ± 0.1008	55.3810 ± 0.2025	87.1456 ± 0.3990
256	26.1625 ± 0.0657	44.9461 ± 0.1479	75.4692 ± 0.3214	124.4389 ± 0.6808
512	32.0642 ± 0.1234	57.4369 ± 0.3026	101.4174 ± 0.7096	175.6975 ± 1.6194
1024	38.6893 ± 0.2657	73.2671 ± 0.6912	135.6123 ± 1.7396	246.8774 ± 4.2833

L	$q = 3.25$	$q = 3.50$	$q = 3.75$	$q = 4.00$
16	37.4020 ± 0.1125	48.7655 ± 0.1673	62.7027 ± 0.2440	79.4340 ± 0.3475
32	57.1966 ± 0.2126	78.7249 ± 0.3431	106.2816 ± 0.5379	142.0782 ± 0.8310
64	87.3178 ± 0.4006	126.1715 ± 0.6960	181.3644 ± 1.1991	253.4333 ± 1.9791
128	134.4255 ± 0.7644	206.2906 ± 1.4542	312.1399 ± 2.7062	462.6885 ± 4.8818
256	202.0761 ± 1.4086	329.0069 ± 2.9261	534.9698 ± 6.0685	875.8576 ± 12.7193
512	309.5691 ± 3.7861	532.7875 ± 8.5469	933.1742 ± 19.8120	1652.8786 ± 46.7469
1024	446.2539 ± 10.4070	822.7567 ± 26.0508	1581.9426 ± 69.4509	3049.0566 ± 186.3115

Table 8: Estimates of $\tau_{\text{int},\mathcal{E}'}$ from the Monte Carlo simulations at the critical point of the 2-dimensional random cluster model, as a function of L and q , for $k = 1$. The quoted error bar corresponds to one standard deviation.

L	$q = 1.25$	$q = 1.50$	$q = 1.75$	$q = 2.00$
16	1.2040 ± 0.0007	2.2847 ± 0.0019	3.8600 ± 0.0041	6.0689 ± 0.0080
32	1.2656 ± 0.0008	2.5269 ± 0.0022	4.5125 ± 0.0052	7.4842 ± 0.0110
64	1.3202 ± 0.0009	2.7598 ± 0.0025	5.1783 ± 0.0063	9.0496 ± 0.0144
128	1.3614 ± 0.0009	2.9810 ± 0.0028	5.8732 ± 0.0078	10.7689 ± 0.0187
256	1.4015 ± 0.0010	3.1840 ± 0.0032	6.5651 ± 0.0092	12.6943 ± 0.0240
512	1.4325 ± 0.0013	3.3804 ± 0.0048	7.2791 ± 0.0146	14.7495 ± 0.0425
1024	1.4560 ± 0.0022	3.5685 ± 0.0086	8.0614 ± 0.0279	17.1123 ± 0.0848

L	$q = 2.25$	$q = 2.50$	$q = 2.75$	$q = 3.00$
16	9.1341 ± 0.0147	13.1592 ± 0.0252	18.4381 ± 0.0415	25.2445 ± 0.0660
32	11.7916 ± 0.0213	17.8549 ± 0.0394	26.3710 ± 0.0701	37.7574 ± 0.1195
64	15.0067 ± 0.0306	23.9303 ± 0.0607	37.0129 ± 0.1156	55.9353 ± 0.2133
128	18.8651 ± 0.0428	31.6032 ± 0.0916	51.3588 ± 0.1878	82.0584 ± 0.3757
256	23.3330 ± 0.0586	41.2200 ± 0.1356	70.7459 ± 0.3013	118.5736 ± 0.6487
512	28.7842 ± 0.1107	53.1546 ± 0.2800	96.0301 ± 0.6719	169.0612 ± 1.5582
1024	34.9401 ± 0.2400	68.3955 ± 0.6452	129.5483 ± 1.6618	239.4339 ± 4.1541

L	$q = 3.25$	$q = 3.50$	$q = 3.75$	$q = 4.00$
16	33.6892 ± 0.1013	44.2837 ± 0.1520	57.2882 ± 0.2229	73.0397 ± 0.3195
32	52.7843 ± 0.1962	73.3099 ± 0.3195	99.7789 ± 0.5050	134.2543 ± 0.7852
64	82.0705 ± 0.3765	119.8115 ± 0.6609	173.5483 ± 1.1474	244.1495 ± 1.9066
128	128.1915 ± 0.7289	198.6992 ± 1.4006	302.8677 ± 2.6258	451.5682 ± 4.7645
256	194.9751 ± 1.3591	320.3198 ± 2.8488	524.1844 ± 5.9461	862.6987 ± 12.5282
512	301.2867 ± 3.6848	522.8481 ± 8.3875	921.2799 ± 19.5595	1638.0215 ± 46.3267
1024	437.3916 ± 10.2003	812.1417 ± 25.7147	1568.8474 ± 68.8760	3032.3859 ± 185.2928

Table 9: Estimates of $\tau_{\text{int},\mathcal{N}}$ from the Monte Carlo simulations at the critical point of the 2-dimensional random cluster model, as a function of L and q , for $k = 1$. The quoted error bar corresponds to one standard deviation.

L	$q = 1.25$	$q = 1.50$	$q = 1.75$	$q = 2.00$
16	1.3386 ± 0.0008	2.6034 ± 0.0021	4.4205 ± 0.0047	6.9286 ± 0.0091
32	1.4078 ± 0.0009	2.8602 ± 0.0025	5.0735 ± 0.0058	8.3286 ± 0.0122
64	1.4676 ± 0.0010	3.0892 ± 0.0028	5.7122 ± 0.0070	9.8003 ± 0.0156
128	1.5118 ± 0.0010	3.2941 ± 0.0031	6.3331 ± 0.0084	11.2921 ± 0.0196
256	1.5495 ± 0.0011	3.4664 ± 0.0034	6.8843 ± 0.0096	12.8477 ± 0.0243
512	1.5770 ± 0.0015	3.6264 ± 0.0051	7.4316 ± 0.0149	14.3819 ± 0.0415
1024	1.6009 ± 0.0024	3.7573 ± 0.0090	7.9652 ± 0.0276	16.0737 ± 0.0796

L	$q = 2.25$	$q = 2.50$	$q = 2.75$	$q = 3.00$
16	10.3488 ± 0.0166	14.8081 ± 0.0284	20.5896 ± 0.0464	28.0138 ± 0.0733
32	12.9917 ± 0.0235	19.4472 ± 0.0429	28.4240 ± 0.0756	40.4259 ± 0.1279
64	15.9573 ± 0.0325	25.1767 ± 0.0639	38.5615 ± 0.1205	57.9953 ± 0.2212
128	19.3490 ± 0.0439	32.1053 ± 0.0930	51.5394 ± 0.1884	82.2076 ± 0.3764
256	23.0132 ± 0.0578	40.1938 ± 0.1322	68.5937 ± 0.2922	115.2704 ± 0.6306
512	27.2615 ± 0.1049	49.7110 ± 0.2619	89.9306 ± 0.6292	159.7078 ± 1.4720
1024	31.7864 ± 0.2183	61.4579 ± 0.5798	116.7935 ± 1.4982	220.6996 ± 3.8291

L	$q = 3.25$	$q = 3.50$	$q = 3.75$	$q = 4.00$
16	37.2039 ± 0.1119	48.6233 ± 0.1669	62.6624 ± 0.2439	79.6370 ± 0.3484
32	56.2252 ± 0.2090	77.8100 ± 0.3391	105.4646 ± 0.5338	141.5583 ± 0.8279
64	84.5549 ± 0.3879	123.3440 ± 0.6804	178.5750 ± 1.1806	250.9246 ± 1.9595
128	128.5492 ± 0.7310	199.5134 ± 1.4064	305.0319 ± 2.6446	457.0131 ± 4.8219
256	190.1111 ± 1.3252	315.2552 ± 2.8038	520.8366 ± 5.9082	860.9974 ± 12.5035
512	287.5530 ± 3.5168	506.8770 ± 8.1313	898.2129 ± 19.0697	1617.6331 ± 45.7501
1024	408.0224 ± 9.5154	777.6178 ± 24.6216	1526.7086 ± 67.0260	2980.4947 ± 182.1220

Table 10: Estimates of $\tau_{\text{int},\mathcal{S}_2}$ from the Monte Carlo simulations at the critical point of the 2-dimensional random cluster model, as a function of L and q , for $k = 1$. The quoted error bar corresponds to one standard deviation.

L	$q = 1.25$	$q = 1.50$	$q = 1.75$	$q = 2.00$
16	1.1821 ± 0.0007	2.1678 ± 0.0018	3.5450 ± 0.0038	5.4257 ± 0.0072
32	1.2066 ± 0.0007	2.2716 ± 0.0020	3.8255 ± 0.0044	6.0790 ± 0.0089
64	1.2285 ± 0.0008	2.3601 ± 0.0021	4.1069 ± 0.0050	6.7601 ± 0.0108
128	1.2433 ± 0.0008	2.4422 ± 0.0023	4.3807 ± 0.0058	7.4396 ± 0.0129
256	1.2563 ± 0.0009	2.5088 ± 0.0025	4.6063 ± 0.0064	8.1526 ± 0.0154
512	1.2672 ± 0.0012	2.5784 ± 0.0036	4.8445 ± 0.0097	8.8373 ± 0.0255
1024	1.2756 ± 0.0019	2.6249 ± 0.0063	5.0706 ± 0.0176	9.5914 ± 0.0475

L	$q = 2.25$	$q = 2.50$	$q = 2.75$	$q = 3.00$
16	7.9521 ± 0.0128	11.2607 ± 0.0216	15.5512 ± 0.0350	21.1189 ± 0.0552
32	9.2758 ± 0.0168	13.7011 ± 0.0302	19.8378 ± 0.0528	28.2005 ± 0.0892
64	10.7242 ± 0.0218	16.6498 ± 0.0422	25.3352 ± 0.0791	38.0837 ± 0.1452
128	12.3646 ± 0.0281	20.2411 ± 0.0587	32.2903 ± 0.1181	51.5226 ± 0.2359
256	14.1174 ± 0.0354	24.2638 ± 0.0798	41.3352 ± 0.1761	70.0114 ± 0.3830
512	16.1705 ± 0.0622	29.0610 ± 0.1531	52.5554 ± 0.3677	94.2286 ± 0.8685
1024	18.3806 ± 0.1262	34.7041 ± 0.3274	66.1941 ± 0.8491	128.1428 ± 2.2233

L	$q = 3.25$	$q = 3.50$	$q = 3.75$	$q = 4.00$
16	28.0987 ± 0.0845	36.7802 ± 0.1262	47.5330 ± 0.1850	60.6406 ± 0.2653
32	39.3515 ± 0.1463	54.7327 ± 0.2386	74.6290 ± 0.3777	100.4741 ± 0.5877
64	55.6487 ± 0.2553	82.1045 ± 0.4529	119.8880 ± 0.7926	170.2119 ± 1.3292
128	81.4775 ± 0.4633	127.4713 ± 0.8986	197.8031 ± 1.7149	300.7931 ± 3.1737
256	116.2497 ± 0.8103	196.8057 ± 1.7503	330.7032 ± 3.7514	557.2872 ± 8.0930
512	171.9805 ± 2.1034	308.7344 ± 4.9527	557.6357 ± 11.8390	1014.8762 ± 28.7029
1024	239.5051 ± 5.5854	471.3493 ± 14.9243	943.8663 ± 41.4379	1849.8784 ± 113.0361

Table 11: Estimates of $\tau_{\text{int}, \mathcal{F}}$ from the Monte Carlo simulations at the critical point of the 2-dimensional random cluster model, as a function of L and q , for $k = 1$. The quoted error bar corresponds to one standard deviation.

L	$q = 1.25$	$q = 1.50$	$q = 1.75$	$q = 2.00$
16	1.3101 ± 0.0008	2.5278 ± 0.0021	4.2775 ± 0.0046	6.6989 ± 0.0088
32	1.3708 ± 0.0008	2.7571 ± 0.0024	4.8684 ± 0.0056	7.9857 ± 0.0117
64	1.4224 ± 0.0009	2.9585 ± 0.0027	5.4412 ± 0.0067	9.3266 ± 0.0149
128	1.4596 ± 0.0009	3.1373 ± 0.0030	5.9956 ± 0.0079	10.6786 ± 0.0186
256	1.4918 ± 0.0010	3.2868 ± 0.0033	6.4856 ± 0.0091	12.0813 ± 0.0229
512	1.5155 ± 0.0014	3.4287 ± 0.0048	6.9711 ± 0.0139	13.4617 ± 0.0388
1024	1.5364 ± 0.0023	3.5411 ± 0.0085	7.4506 ± 0.0258	14.9718 ± 0.0742

L	$q = 2.25$	$q = 2.50$	$q = 2.75$	$q = 3.00$
16	10.0086 ± 0.0161	14.3476 ± 0.0275	20.0130 ± 0.0451	27.2880 ± 0.0714
32	12.4722 ± 0.0225	18.7396 ± 0.0414	27.4966 ± 0.0731	39.3047 ± 0.1244
64	15.2204 ± 0.0310	24.0900 ± 0.0611	37.1348 ± 0.1160	56.1933 ± 0.2143
128	18.3474 ± 0.0416	30.5895 ± 0.0886	49.4474 ± 0.1808	79.3969 ± 0.3635
256	21.6896 ± 0.0544	38.1134 ± 0.1254	65.5494 ± 0.2792	111.0562 ± 0.6076
512	25.5866 ± 0.0984	46.9593 ± 0.2474	85.7120 ± 0.5997	153.1954 ± 1.4120
1024	29.7135 ± 0.2041	57.6989 ± 0.5443	110.7213 ± 1.4203	211.5007 ± 3.6695

L	$q = 3.25$	$q = 3.50$	$q = 3.75$	$q = 4.00$
16	36.4019 ± 0.1095	47.7804 ± 0.1640	61.9085 ± 0.2409	79.1044 ± 0.3461
32	54.9946 ± 0.2045	76.5469 ± 0.3336	104.2901 ± 0.5278	141.5283 ± 0.8278
64	82.5872 ± 0.3789	121.5950 ± 0.6708	177.0526 ± 1.1706	251.4255 ± 1.9634
128	125.2155 ± 0.7120	196.1776 ± 1.3829	303.5483 ± 2.6317	461.4449 ± 4.8687
256	185.1345 ± 1.2905	310.3888 ± 2.7605	518.9183 ± 5.8864	868.1885 ± 12.6080
512	280.0361 ± 3.4249	500.1480 ± 8.0233	900.8537 ± 19.1258	1637.5816 ± 46.3143
1024	395.2831 ± 9.2183	762.0676 ± 24.1293	1519.4102 ± 66.7056	3054.3411 ± 186.6344

Table 12: Estimates of τ_{int,C_1} from the Monte Carlo simulations at the critical point of the 2-dimensional random cluster model, as a function of L and q , for $k = 1$. The quoted error bar corresponds to one standard deviation.

L	$q = 1.25$	$q = 1.50$	$q = 1.75$	$q = 2.00$
16	1.0547 ± 0.0007	1.8490 ± 0.0015	2.9362 ± 0.0031	4.3973 ± 0.0058
32	1.0744 ± 0.0007	1.9293 ± 0.0017	3.1495 ± 0.0036	4.8826 ± 0.0071
64	1.0920 ± 0.0007	1.9968 ± 0.0018	3.3571 ± 0.0041	5.3808 ± 0.0086
128	1.1020 ± 0.0007	2.0563 ± 0.0020	3.5553 ± 0.0047	5.8582 ± 0.0102
256	1.1120 ± 0.0008	2.1031 ± 0.0021	3.7110 ± 0.0052	6.3568 ± 0.0120
512	1.1195 ± 0.0010	2.1560 ± 0.0030	3.8788 ± 0.0078	6.8290 ± 0.0197
1024	1.1265 ± 0.0017	2.1835 ± 0.0052	4.0403 ± 0.0140	7.3298 ± 0.0363

L	$q = 2.25$	$q = 2.50$	$q = 2.75$	$q = 3.00$
16	6.3209 ± 0.0102	8.8061 ± 0.0169	12.0317 ± 0.0271	16.1764 ± 0.0423
32	7.3082 ± 0.0132	10.6241 ± 0.0234	15.2020 ± 0.0404	21.3897 ± 0.0677
64	8.3609 ± 0.0170	12.7509 ± 0.0323	19.1601 ± 0.0599	28.6341 ± 0.1092
128	9.5115 ± 0.0216	15.2680 ± 0.0442	24.1050 ± 0.0881	38.1520 ± 0.1747
256	10.7245 ± 0.0269	18.0907 ± 0.0595	30.4051 ± 0.1295	51.3142 ± 0.2807
512	12.1338 ± 0.0467	21.4336 ± 0.1129	38.3258 ± 0.2682	68.1149 ± 0.6278
1024	13.6414 ± 0.0937	25.2171 ± 0.2379	47.5954 ± 0.6105	92.1484 ± 1.5988

L	$q = 3.25$	$q = 3.50$	$q = 3.75$	$q = 4.00$
16	21.3907 ± 0.0643	27.8259 ± 0.0955	35.8844 ± 0.1397	45.7629 ± 0.2002
32	29.7129 ± 0.1105	41.2669 ± 0.1799	56.1696 ± 0.2843	76.2426 ± 0.4459
64	41.7815 ± 0.1917	61.7907 ± 0.3409	90.4411 ± 0.5979	129.5723 ± 1.0118
128	60.2645 ± 0.3427	95.1785 ± 0.6709	148.7277 ± 1.2894	231.9678 ± 2.4475
256	85.4706 ± 0.5958	145.8670 ± 1.2973	249.9941 ± 2.8358	429.9691 ± 6.2441
512	125.2840 ± 1.5322	229.6477 ± 3.6840	425.3373 ± 9.0302	810.2299 ± 22.9150
1024	174.4576 ± 4.0685	348.2103 ± 11.0253	724.6440 ± 31.8135	1487.0973 ± 90.8685

Table 13: Estimates of $\tau_{\text{int}, \mathcal{C}_2}$ from the Monte Carlo simulations at the critical point of the 2-dimensional random cluster model, as a function of L and q , for $k = 1$. The quoted error bar corresponds to one standard deviation.

L	$q = 1.25$	$q = 1.50$	$q = 1.75$	$q = 2.00$
16	1.0627 ± 0.0007	1.9037 ± 0.0015	3.0988 ± 0.0033	4.7417 ± 0.0063
32	1.0882 ± 0.0007	2.0070 ± 0.0017	3.3763 ± 0.0039	5.3802 ± 0.0079
64	1.1096 ± 0.0007	2.0948 ± 0.0019	3.6466 ± 0.0045	6.0321 ± 0.0096
128	1.1247 ± 0.0007	2.1761 ± 0.0021	3.9002 ± 0.0051	6.6878 ± 0.0116
256	1.1379 ± 0.0008	2.2400 ± 0.0022	4.1293 ± 0.0058	7.3441 ± 0.0139
512	1.1487 ± 0.0011	2.3012 ± 0.0032	4.3459 ± 0.0087	7.9879 ± 0.0230
1024	1.1573 ± 0.0018	2.3518 ± 0.0056	4.5466 ± 0.0158	8.6848 ± 0.0430

L	$q = 2.25$	$q = 2.50$	$q = 2.75$	$q = 3.00$
16	6.9598 ± 0.0112	9.8960 ± 0.0190	13.7462 ± 0.0310	18.6750 ± 0.0488
32	8.2349 ± 0.0149	12.2476 ± 0.0270	17.8387 ± 0.0474	25.5572 ± 0.0809
64	9.6298 ± 0.0196	15.0431 ± 0.0382	23.1057 ± 0.0722	35.0341 ± 0.1336
128	11.1923 ± 0.0254	18.4369 ± 0.0534	29.6671 ± 0.1085	47.6201 ± 0.2180
256	12.8179 ± 0.0322	22.2087 ± 0.0731	38.1085 ± 0.1623	65.1028 ± 0.3562
512	14.7338 ± 0.0567	26.6674 ± 0.1405	48.6601 ± 0.3405	87.6815 ± 0.8081
1024	16.7174 ± 0.1148	31.8749 ± 0.3007	61.5270 ± 0.7892	118.9944 ± 2.0645

L	$q = 3.25$	$q = 3.50$	$q = 3.75$	$q = 4.00$
16	24.9741 ± 0.0751	32.8814 ± 0.1128	42.7608 ± 0.1664	54.9178 ± 0.2403
32	35.7876 ± 0.1330	50.1792 ± 0.2187	68.8743 ± 0.3486	94.4193 ± 0.5522
64	51.7567 ± 0.2374	77.0195 ± 0.4249	113.3164 ± 0.7492	163.7752 ± 1.2789
128	76.0751 ± 0.4326	120.8170 ± 0.8516	190.4901 ± 1.6515	297.1283 ± 3.1350
256	109.5690 ± 0.7638	188.0194 ± 1.6722	321.0373 ± 3.6417	553.7972 ± 8.0423
512	162.8091 ± 1.9912	298.8569 ± 4.7942	551.3396 ± 11.7054	1044.3142 ± 29.5354
1024	226.4912 ± 5.2819	452.2253 ± 14.3188	928.5042 ± 40.7635	1950.0423 ± 119.1566

Table 14: Estimates of $\tau_{\text{int},\mathcal{C}_3}$ from the Monte Carlo simulations at the critical point of the 2-dimensional random cluster model, as a function of L and q , for $k = 1$. The quoted error bar corresponds to one standard deviation.

q	Fits to $\xi/L = x^*$					Fits to $\xi/L = x^* + BL^{-p}$							Δ_1 (exact)
	L_{\min}	x^*	χ^2	DF	CL(%)	L_{\min}	x^*	B	p	χ^2	DF	CL(%)	
1.25	256	0.91734(8)	1.48	2	48	16	0.91735(7)	0.900(243)	1.81(10)	2.53	4	64	1.80702
1.50	128	0.90867(9)	0.17	3	98	16	0.90857(10)	0.563(173)	1.62(11)	0.77	4	94	1.63551
1.75	128	0.90496(12)	5.19	3	16	16	0.90487(14)	0.582(228)	1.62(14)	6.93	4	14	1.47905
2.00	512	0.90442(20)	0.54	1	46	32	0.90387(74)	0.017(9)	0.49(21)	4.12	3	25	1.33333
2.25	256	0.90786(17)	1.30	2	52	[16]	0.90799(16)	0.465(184)	1.55(15)	8.19	4	8	1.19517
2.50	64	0.91369(14)	3.36	4	50	16	0.91335(21)	0.396(195)	1.50(18)	3.69	4	45	1.06191
2.75	256	0.92092(30)	0.06	2	97	16	0.92085(45)	0.066(33)	0.92(20)	5.96	4	20	0.93110
3.00	64	0.93193(17)	0.13	4	100	16	0.93184(23)	0.704(1.120)	1.97(59)	0.02	4	100	0.80000
3.25	128	0.94503(29)	0.97	3	81	—	—	—	—	—	—	—	0.66499
3.50	256	0.96069(55)	0.30	2	86	16	0.96223(198)	-0.025(9)	0.47(23)	1.21	4	88	0.51991
3.75	256	0.98051(73)	0.03	2	99	32	0.98591(540)	-0.060(27)	0.41(23)	1.19	3	75	0.34986
4.00	256	1.00434(80)	0.84	2	66	16	1.01323(335)	-0.100(9)	0.41(7)	4.81	4	31	0.00000

Table 15: Fits for ξ/L . The quoted error bar corresponds to one standard deviation. L_{\min} in brackets indicates a poor fit (confidence level $< 10\%$).

Fits to $\chi = AL^{\gamma/\nu}$									
q	L_{\min}	γ/ν	A	χ^2	DF	CL(%)	γ/ν (exact)	deviation	dev(σ)
1.25	256	1.77773(9)	1.0496(6)	1.40	1	24	1.77764	0.00009	1.0
1.50	128	1.76639(8)	1.0645(5)	0.30	2	86	1.76644	-0.00005	-0.6
1.75	128	1.75759(12)	1.0768(7)	2.34	2	31	1.75738	0.00022	1.8
2.00	128	1.74969(11)	1.0937(6)	2.54	2	28	1.75000	-0.00031	-2.9
2.25	256	1.74428(26)	1.1039(17)	1.37	1	24	1.74404	0.00024	0.9
2.50	256	1.73902(37)	1.1209(24)	0.01	1	94	1.73932	-0.00030	-0.8
2.75	128	1.73575(28)	1.1316(17)	0.85	2	65	1.73576	-0.00001	-0.03
3.00	128	1.73438(28)	1.1371(17)	0.72	2	70	1.73333	0.00105	3.8
3.25	128	1.73341(37)	1.1460(23)	0.30	2	86	1.73214	0.00127	3.4
3.50	256	1.73304(99)	1.1571(67)	0.01	1	93	1.73246	0.00058	0.6
3.75	128	1.73745(67)	1.1431(40)	1.46	2	48	1.73517	0.00229	3.4
4.00	256	1.73968(152)	1.1502(101)	0.44	1	51	1.75000	-0.01032	-6.8

Table 16: Fits of the susceptibility χ to a pure power law. The quoted error bar corresponds to one standard deviation. L_{\min} in brackets indicates a poor fit (confidence level $< 10\%$). The final two columns show the deviation of the estimated γ/ν from the known exact value, in absolute terms and in units of its standard deviation.

q	Fits to $\chi/L^{\gamma/\nu} = A$					Fits to $\chi/L^{\gamma/\nu} = A + BL^{-p}$							Δ_1 (exact)
	L_{\min}	A	χ^2	DF	CL(%)	L_{\min}	A	B	p	χ^2	DF	CL(%)	
1.25	256	1.05017(5)	2.38	2	30	16	1.05013(8)	0.011(5)	0.87(19)	4.72	4	32	1.80702
1.50	128	1.06417(6)	0.70	3	87	16	1.06379(53)	0.003(1)	0.34(30)	1.55	4	82	1.63551
1.75	64	1.07811(7)	7.16	4	13	—	—	—	—	—	—	—	1.47905
2.00	512	1.09148(15)	0.50	1	48	[16]	1.09195(8)	-0.231(316)	1.88(50)	15.63	4	0.4	1.33333
2.25	256	1.10545(13)	2.19	2	33	[16]	1.10565(15)	-0.078(43)	1.22(21)	7.84	4	10	1.19517
2.50	128	1.11875(14)	2.34	3	51	16	1.11912(26)	-0.062(22)	0.94(14)	3.96	4	41	1.06191
2.75	128	1.13159(18)	0.85	3	84	16	1.13192(29)	-0.161(51)	1.12(12)	5.80	4	21	0.93110
3.00	256	1.14415(25)	1.71	2	43	16	1.14541(49)	-0.086(12)	0.73(6)	0.43	4	98	0.80000
3.25	512	1.15559(63)	0.25	1	62	16	1.15656(67)	-0.111(14)	0.70(6)	2.74	4	60	0.66499
3.50	256	1.16102(46)	0.35	2	84	16	1.16365(96)	-0.119(15)	0.65(6)	0.99	4	91	0.51991
3.75	256	1.15852(61)	0.42	2	81	16	1.16358(199)	-0.080(9)	0.48(7)	0.79	4	94	0.34986
4.00	[512]	1.07693(124)	2.97	1	8	—	—	—	—	—	—	—	0.00000

Table 17: Fits for $\chi/L^{\gamma/\nu}$ with γ/ν set to its exact value (1.10). The quoted error bar corresponds to one standard deviation. L_{\min} in brackets indicates a poor fit (confidence level $< 10\%$).

Fits to $C_1 = AL^{d-\beta/\nu}$									
q	L_{\min}	β/ν	A	χ^2	DF	CL(%)	β/ν (exact)	deviation	dev(σ)
1.25	256	0.11111(6)	0.9896(3)	1.29	1	26	0.11118	-0.00007	-1.2
1.50	16	0.11681(2)	0.9958(1)	2.01	5	85	0.11678	0.00003	1.6
1.75	128	0.12115(8)	1.0004(4)	2.21	2	33	0.12131	-0.00016	-2.1
2.00	128	0.12518(7)	1.0080(4)	2.04	2	36	0.12500	0.00018	2.7
2.25	256	0.12787(17)	1.0118(10)	1.20	1	27	0.12798	-0.00011	-0.6
2.50	128	0.13033(13)	1.0177(7)	1.48	2	48	0.13034	-0.00001	-0.10
2.75	128	0.13230(18)	1.0237(10)	1.65	2	44	0.13212	0.00018	1.0
3.00	64	0.13283(11)	1.0245(5)	1.24	3	74	0.13333	-0.00050	-4.6
3.25	128	0.13366(24)	1.0295(13)	0.86	2	65	0.13393	-0.00027	-1.1
3.50	64	0.13315(19)	1.0289(9)	2.39	3	50	0.13377	-0.00062	-3.3
3.75	32	0.13174(15)	1.0263(7)	1.74	4	78	0.13242	-0.00067	-4.4
4.00	256	0.13200(104)	1.0357(62)	0.54	1	46	0.12500	0.00700	6.8

Table 18: Fits of the mean size C_1 of the largest cluster to a pure power law. The quoted error bar corresponds to one standard deviation. L_{\min} in brackets indicates a poor fit (confidence level $< 10\%$). The final two columns show the deviation of the estimated β/ν from the known exact value, in absolute terms and in units of its standard deviation.

q	Fits to $C_H = AL^{\alpha/\nu}$						Fits to $C_H = AL^{\alpha/\nu} + B$							α/ν (exact)	dev	dev(σ)
	L_{\min}	α/ν	A	χ^2	DF	CL(%)	L_{\min}	α/ν	A	B	χ^2	DF	CL(%)			
1.25	[256]	0.0406(9)	0.588(3)	16.40	1	5×10^{-3}	16	-0.3675(49)	-0.791(6)	0.839(2)	1.82	4	77	-0.35527	-0.012	-2.5
1.50	[256]	0.0712(8)	1.036(5)	30.87	1	3×10^{-6}	128	-0.1977(186)	-1.933(23)	2.182(59)	0.37	1	54	-0.22663	0.029	1.6
1.75	[256]	0.1089(8)	1.366(7)	31.62	1	2×10^{-6}	128	-0.0965(135)	-5.413(347)	5.665(440)	0.15	1	70	-0.10929	0.013	0.9
2.00	[256]	0.1569(6)	1.554(6)	43.28	1	5×10^{-9}	(see text)	—	—	—	—	—	—	0(log)	—	—
2.25	[256]	0.2143(8)	1.608(8)	36.65	1	1×10^{-7}	128	0.1108(65)	5.856(558)	-5.554(640)	0.45	1	50	0.10363	0.007	1.1
2.50	[256]	0.2778(10)	1.573(10)	9.47	1	0.2	64	0.2025(32)	3.421(109)	-3.176(150)	0.73	2	69	0.20357	-0.001	-0.3
2.75	[256]	0.3488(13)	1.457(11)	7.44	1	0.6	32	0.2995(18)	2.293(33)	-2.001(54)	0.39	3	94	0.30168	-0.002	-1.2
3.00	256	0.4254(13)	1.295(10)	0.42	1	52	32	0.3947(15)	1.681(18)	-1.296(37)	2.14	3	54	0.40000	-0.005	-3.6
3.25	[256]	0.5063(17)	1.120(11)	2.94	1	9	32	0.4902(16)	1.275(14)	-0.771(38)	3.04	3	39	0.50126	-0.011	-6.8
3.50	64	0.5952(7)	0.921(3)	0.94	3	82	64	0.5945(35)	0.925(22)	-0.020(102)	0.90	2	64	0.61007	-0.016	-4.5
3.75	256	0.6920(31)	0.724(13)	0.69	1	41	128	0.7095(86)	0.635(38)	1.149(369)	0.03	1	86	0.73760	-0.028	-3.3
4.00	256	0.7998(35)	0.534(11)	0.35	1	55	128	0.8338(85)	0.416(24)	2.713(392)	0.53	1	47	1 ($\log^{-3/2}$)	-0.166	-19.6

Table 19: Fits for the specific heat C_H . The quoted error bar corresponds to one standard deviation. L_{\min} in brackets indicates a poor fit (confidence level $< 10\%$). The final two columns show the deviation of the estimated α/ν (from the fit $AL^{\alpha/\nu} + B$) from the known exact value, in absolute terms and in units of its standard deviation.

L	$q = 2$	$q = 3.25$
16	2.143(3)	2.020(7)
32	2.123(4)	2.013(9)
64	2.100(4)	1.990(11)
128	2.080(4)	2.015(14)
256	2.069(5)	1.991(17)
512	2.047(7)	2.034(30)
1024	2.051(12)	1.953(56)

Table 20: Ratios $\tau_{\text{int},\mathcal{E}'}(k=1)/\tau_{\text{int},\mathcal{E}'}(k=2)$ as a function of L for $q = 2$ and $q = 3.25$. Error bars are one standard deviation.

Fits to $\tau_{\text{int},\mathcal{E}'}(1)/\tau_{\text{int},\mathcal{E}'}(k) = A$						
q	k	L_{min}	A	χ^2	DF	CL(%)
2.00	2	512	2.048(6)	0.09	1	76
2.25	2	256	2.036(5)	0.51	2	77
2.50	2	128	2.022(5)	0.02	3	100
2.75	2	128	2.006(6)	0.87	3	83
3.00	2	32	2.015(5)	3.63	5	60
3.25	2	32	2.005(6)	5.40	5	37
3.50	2	16	2.015(5)	6.74	6	35
3.75	2	16	2.014(6)	1.68	6	95
4.00	2	16	2.011(7)	2.75	6	84
3.00	3	256	3.011(16)	0.66	2	72
3.25	3	64	3.012(11)	3.18	4	53
3.50	3	64	3.014(13)	3.67	4	45
3.75	3	16	3.034(9)	2.32	6	89
4.00	3	64	2.988(19)	1.66	4	80
4.00	4	64	4.002(25)	3.01	4	56

Table 21: Estimates for the limiting ratios $\tau_{\text{int},\mathcal{E}'}(1)/\tau_{\text{int},\mathcal{E}'}(k)$ as $L \rightarrow \infty$ from fits to a constant A . Error bars are one standard deviation.

Fits to $\tau_{\text{int},\mathcal{E}'} = AL^z$							
q	k	L_{min}	$z_{\text{int},\mathcal{E}'}$	A	χ^2	DF	CL(%)
1.25	1	[256]	0.053(1)	1.27(1)	3.76	1	5
1.50	1	[256]	0.104(2)	2.20(2)	3.84	1	5
1.75	1	256	0.158(2)	3.28(5)	0.21	1	65
2.00	1	256	0.215(3)	4.47(9)	0.06	1	81
2.00	2	[256]	0.224(2)	2.06(3)	6.91	1	0.9
2.25	1	256	0.286(4)	5.35(14)	2.16	1	14
2.25	2	[256]	0.287(3)	2.62(5)	10.68	1	0.1
2.50	1	256	0.353(6)	6.35(23)	0.02	1	90
2.50	2	256	0.353(4)	3.15(8)	0.06	1	80
2.75	1	256	0.424(8)	7.19(34)	0.07	1	80
2.75	2	[256]	0.421(5)	3.66(12)	3.02	1	8
3.00	1	128	0.505(6)	7.52(23)	1.18	2	56
3.00	2	128	0.516(4)	3.55(8)	1.46	2	48
3.00	3	256	0.505(6)	2.51(9)	0.04	1	84
3.25	1	128	0.590(7)	7.66(30)	3.14	2	21
3.25	2	256	0.585(10)	3.96(23)	0.003	1	96
3.25	3	256	0.585(8)	2.64(13)	0.02	1	90
3.50	1	128	0.676(10)	7.77(39)	1.07	2	58
3.50	2	16	0.693(2)	3.54(2)	2.39	5	79
3.50	3	64	0.695(3)	2.33(4)	0.05	3	100
3.75	1	32	0.779(4)	7.14(13)	0.94	4	92
3.75	2	32	0.784(3)	3.46(4)	1.63	4	80
3.75	3	128	0.798(7)	2.14(8)	0.70	2	71
4.00	1	128	0.916(16)	5.44(46)	0.15	2	93
4.00	2	128	0.909(12)	2.84(17)	0.75	2	69
4.00	3	64	0.890(5)	2.09(5)	1.58	3	66
4.00	4	256	0.938(17)	1.18(12)	0.06	1	81

Table 22: Estimates for $z_{\text{int},\mathcal{E}'}$ from fits to $\tau_{\text{int},\mathcal{E}'} = AL^z$. Error bars are one standard deviation. L_{min} in brackets indicates a poor fit (confidence level $< 10\%$).

Fits to $\tau_{\text{int},\mathcal{E}'} = AL^z + B$								
q	k	L_{min}	$z_{\text{int},\mathcal{E}'}$	A	B	χ^2	DF	CL(%)
1.25	1	128	-0.213(35)	-1.61(5)	2.19(8)	0.49	1	48
1.50	1	32	-0.034(7)	-15.86(2.92)	17.09(2.96)	0.82	3	85
1.75	1	128	0.085(26)	9.66(4.42)	-7.56(4.82)	0.33	1	57
2.00	1	16	0.145(4)	10.37(51)	-8.44(57)	2.32	4	68
2.00	2	32	0.141(5)	5.48(32)	-4.83(36)	1.32	3	72
2.25	1	32	0.235(8)	8.92(61)	-6.68(86)	1.62	3	65
2.25	2	[128]	0.200(19)	6.37(1.31)	-6.45(1.89)	3.44	1	6
2.50	1	32	0.315(8)	9.01(59)	-6.75(1.00)	0.21	3	98
2.50	2	64	0.294(11)	5.38(48)	-5.23(85)	0.91	2	63
2.75	1	16	0.411(5)	8.19(30)	-4.76(57)	1.06	4	90
2.75	2	128	0.348(24)	6.87(1.40)	-9.62(3.28)	0.47	1	49
3.00	1	32	0.481(10)	9.08(63)	-6.79(1.68)	0.84	3	84
3.00	2	16	0.500(4)	4.00(11)	-2.15(25)	1.35	4	85
3.00	3	16	0.497(3)	2.72(6)	-1.71(13)	2.40	4	66
3.25	1	64	0.558(21)	9.75(1.44)	-11.92(5.96)	2.93	2	23
3.25	2	32	0.577(8)	4.24(22)	-2.93(78)	0.71	3	87
3.25	3	64	0.565(12)	3.10(26)	-3.51(1.12)	0.22	2	90
3.50	1	64	0.648(25)	9.50(1.56)	-14.38(8.87)	1.15	2	56
3.50	2	16	0.691(6)	3.57(11)	-0.13(40)	2.27	4	69
3.50	3	32	0.689(8)	2.42(11)	-0.66(55)	0.34	3	95
3.75	1	16	0.790(9)	6.69(32)	2.96(1.49)	0.33	4	99
3.75	2	16	0.800(6)	3.15(10)	2.21(50)	1.62	4	81
3.75	3	16	0.795(5)	2.15(6)	1.10(28)	2.91	4	57
4.00	1	32	0.935(18)	4.76(48)	20.52(5.09)	0.66	3	88
4.00	2	32	0.925(13)	2.54(18)	7.49(1.85)	0.59	3	90
4.00	3	16	0.902(6)	1.94(6)	2.60(36)	2.07	4	72
4.00	4	128	0.993(36)	0.80(19)	18.49(6.33)	0.07	1	79

Table 23: Estimates for $z_{\text{int},\mathcal{E}'}$ from fits to $\tau_{\text{int},\mathcal{E}'} = AL^z + B$. Error bars are one standard deviation. L_{min} in brackets indicates a poor fit (confidence level $< 10\%$).

q	Fits to $\tau_{\text{int},\mathcal{E}'} = AL^z$		Fits to $\tau_{\text{int},\mathcal{E}'} = AL^z + B$		Difference	α/ν (exact)	β/ν (exact)
	L_{min}	z	L_{min}	z			
1.25	—	—	128	-0.213(35)	—	-0.35527	0.11118
1.50	—	—	32	-0.034(7)	—	-0.22663	0.11678
1.75	256	0.158(2)	128	0.085(26)	0.074	-0.10929	0.12131
2.00	256	0.215(3)	16–32	0.143(3)	0.072	0.00000	0.12500
2.25	256	0.286(4)	32	0.235(8)	0.051	0.10363	0.12798
2.50	256	0.353(3)	32–64	0.307(7)	0.046	0.20357	0.13034
2.75	256	0.424(8)	16–128	0.408(5)	0.016	0.30168	0.13212
3.00	128–256	0.511(3)	16–32	0.497(3)	0.013	0.40000	0.13333
3.25	128–256	0.587(5)	32–64	0.572(7)	0.015	0.50126	0.13393
3.50	16–128	0.693(1)	16–64	0.689(4)	0.004	0.61007	0.13377
3.75	32–128	0.784(2)	16	0.796(4)	-0.012	0.73760	0.13242
4.00	64–256	0.898(4)	16–128	0.910(5)	-0.012	1.00000	0.12500

Table 24: Summary of estimates for $z_{\text{int},\mathcal{E}'}$, averaged over all values of k for which the confidence level is $\geq 10\%$. Error bars are one standard deviation.

q	k	L_{\min}	$\tau/C_H = A \log L + B$			$\tau/C_H = AL^p$		
			A	B	CL(%)	p	A	CL(%)
1.75	1	256	0.159(8)	2.28(5)	9	0.049(3)	2.41(4)	14
2.00	1	128	0.224(8)	2.74(4)	23	0.056(2)	2.91(3)	44
2.00	2	128	0.125(3)	1.23(1)	8	0.064(1)	1.34(1)	30
2.00	2	256	0.134(5)	1.18(3)	59	0.067(2)	1.32(2)	36
2.25	1	128	0.337(13)	3.11(7)	22	0.068(3)	3.42(5)	45
2.25	1	256	0.373(25)	2.89(14)	86	0.072(5)	3.33(9)	69
2.25	2	128	0.178(5)	1.45(2)	30	0.073(2)	1.63(2)	25
2.50	1	64	0.410(13)	3.86(6)	33	0.069(2)	4.19(4)	79
2.50	1	128	0.438(22)	3.71(12)	62	0.071(3)	4.13(8)	85
2.50	2	64	0.215(5)	1.85(2)	15	0.073(2)	2.02(2)	76
2.50	2	256	0.244(14)	1.68(8)	55	0.077(4)	1.97(5)	74
2.75	1	64	0.531(21)	4.55(10)	30	0.073(3)	4.99(7)	65
2.75	1	128	0.584(35)	4.26(19)	89	0.078(5)	4.87(12)	88
2.75	2	64	0.286(7)	2.15(3)	62	0.079(2)	2.41(2)	36
3.00	1	32	0.619(20)	5.63(9)	61	0.073(2)	6.05(6)	89
3.00	1	64	0.660(32)	5.42(15)	100	0.075(4)	5.98(10)	90
3.00	2	64	0.354(11)	2.57(5)	32	0.081(2)	2.89(4)	82
3.00	2	128	0.383(19)	2.41(10)	94	0.084(4)	2.83(6)	98
3.00	3	64	0.240(6)	1.68(3)	28	0.083(2)	1.90(2)	80
3.00	3	128	0.257(11)	1.59(6)	98	0.085(3)	1.88(3)	82
3.25	1	32	0.833(30)	6.30(13)	22	0.083(3)	6.91(9)	41
3.25	1	64	0.907(48)	5.93(23)	55	0.086(4)	6.79(15)	38
3.25	2	32	0.421(11)	3.12(4)	48	0.084(2)	3.43(3)	99
3.25	2	64	0.443(17)	3.01(8)	81	0.084(3)	3.42(5)	98
3.25	3	64	0.311(9)	1.92(4)	85	0.089(3)	2.22(3)	28
3.25	3	128	0.302(17)	1.97(9)	84	0.083(4)	2.30(5)	66
3.50	1	64	1.208(74)	6.51(35)	62	0.095(6)	7.77(21)	31
3.50	1	128	1.071(134)	7.25(71)	86	0.081(10)	8.41(44)	80
3.50	2	64	0.623(26)	3.15(12)	17	0.100(4)	3.80(7)	50
3.50	2	256	0.827(102)	1.97(58)	47	0.119(14)	3.39(28)	59
3.50	3	32	0.387(9)	2.24(4)	43	0.097(2)	2.56(2)	99
3.50	3	64	0.405(14)	2.15(7)	69	0.097(3)	2.57(4)	98
3.75	1	32	1.475(67)	7.73(28)	81	0.103(4)	9.01(17)	92
3.75	2	32	0.767(23)	3.69(10)	52	0.107(3)	4.39(6)	79
3.75	2	64	0.816(39)	3.45(18)	84	0.108(5)	4.38(10)	64
3.75	3	32	0.502(13)	2.49(5)	0.9	0.106(3)	2.93(3)	35
3.75	3	128	0.624(41)	1.85(21)	84	0.117(7)	2.76(11)	54
4.00	1	64	2.264(174)	6.66(80)	52	0.127(9)	9.49(41)	74
4.00	1	128	2.680(336)	4.43(1.70)	92	0.139(17)	8.89(78)	76
4.00	2	32	1.021(35)	3.90(14)	24	0.122(4)	4.89(8)	85
4.00	2	64	1.133(61)	3.36(28)	90	0.126(7)	4.78(15)	89
4.00	3	32	0.696(19)	2.55(8)	19	0.124(3)	3.24(4)	58
4.00	3	64	0.757(33)	2.25(15)	75	0.126(5)	3.21(8)	44
4.00	4	32	0.516(12)	1.91(5)	14	0.123(3)	2.42(3)	77
4.00	4	64	0.554(22)	1.73(10)	52	0.124(5)	2.41(5)	63

Table 25: Fits for the ratio $\tau_{\text{int},\mathcal{E}'}/C_H$. The quoted error bar corresponds to one standard deviation.

Fits to $\tau_{\text{int},\mathcal{C}_2} = AL^z$							
q	k	L_{min}	$z_{\text{int},\mathcal{C}_2}$	A	χ^2	DF	CL(%)
1.25	1	256	0.010(1)	1.05(1)	0.05	1	82
1.50	1	[256]	0.030(2)	1.78(2)	10.00	1	0.2
1.75	1	128	0.062(1)	2.63(2)	0.39	2	82
2.00	1	256	0.103(3)	3.59(7)	0.01	1	91
2.00	2	[256]	0.114(2)	1.56(2)	4.85	1	3
2.25	1	128	0.174(3)	4.08(6)	0.40	2	82
2.25	2	[256]	0.175(3)	1.94(4)	6.66	1	1
2.50	1	128	0.243(3)	4.69(8)	0.37	2	83
2.50	2	128	0.248(2)	2.22(3)	0.15	2	93
2.75	1	16	0.334(1)	4.77(2)	1.99	5	85
2.75	2	256	0.325(5)	2.49(8)	0.70	1	40
3.00	1	32	0.419(2)	5.00(5)	1.12	4	89
3.00	2	64	0.428(2)	2.36(3)	0.69	3	87
3.00	3	16	0.431(1)	1.54(1)	2.29	5	81
3.25	1	64	0.521(4)	4.80(10)	3.49	3	32
3.25	2	32	0.518(2)	2.42(2)	1.98	4	74
3.25	3	64	0.528(3)	1.52(2)	1.01	3	80
3.50	1	64	0.625(6)	4.60(12)	1.34	3	72
3.50	2	256	0.664(14)	1.82(14)	0.53	1	47
3.50	3	128	0.645(6)	1.36(4)	0.94	2	63
3.75	1	128	0.757(13)	3.78(25)	0.23	2	89
3.75	2	128	0.755(8)	1.90(9)	0.28	2	87
3.75	3	128	0.763(7)	1.20(5)	0.47	2	79
4.00	1	128	0.897(16)	2.99(25)	0.17	2	92
4.00	2	128	0.890(12)	1.54(9)	0.96	2	62
4.00	3	128	0.880(9)	1.09(5)	1.25	2	54
4.00	4	256	0.935(17)	0.59(6)	0.04	1	85

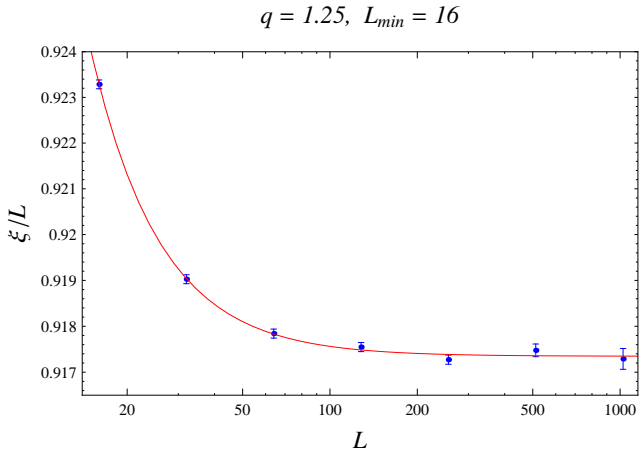
Table 26: Estimates for $z_{\text{int},\mathcal{C}_2}$ from fits to $\tau_{\text{int},\mathcal{C}_2} = AL^z$. Error bars are one standard deviation. L_{min} in brackets indicates a poor fit (confidence level $< 10\%$).

Fits to $\tau_{\text{int},\mathcal{C}_2} = AL^z + B$								
q	k	L_{min}	$z_{\text{int},\mathcal{C}_2}$	A	B	χ^2	DF	CL(%)
1.25	1	64	-0.189(89)	-0.19(1)	1.18(3)	0.58	2	75
1.50	1	[128]	-0.170(97)	-1.03(4)	2.51(22)	6.63	1	1
1.75	1	128	0.047(67)	3.77(6.81)	-1.19(7.02)	0.34	1	56
2.00	1	64	0.006(26)	104.55(437.90)	-102.03(438.13)	0.85	2	65
2.00	2	64	0.019(17)	16.72(16.04)	-15.66(16.12)	1.97	2	37
2.25	1	16	0.118(8)	8.25(80)	-5.12(87)	2.58	4	63
2.25	2	16	0.124(5)	3.81(24)	-2.45(26)	5.01	4	29
2.50	1	16	0.216(7)	6.24(40)	-2.55(51)	1.16	4	88
2.50	2	128	0.240(30)	2.41(72)	-0.31(1.17)	0.07	1	79
2.75	1	16	0.326(7)	5.04(27)	-0.43(43)	0.89	4	93
2.75	2	128	0.252(31)	5.00(1.47)	-5.15(2.47)	0.00	1	98
3.00	1	16	0.431(8)	4.58(23)	1.01(45)	2.18	4	70
3.00	2	16	0.434(5)	2.25(8)	0.34(15)	1.10	4	89
3.00	3	16	0.428(4)	1.57(4)	-0.06(9)	1.82	4	77
3.25	1	16	0.547(8)	3.97(19)	3.28(50)	5.53	4	24
3.25	2	32	0.524(9)	2.34(14)	0.26(43)	1.62	3	65
3.25	3	16	0.546(5)	1.34(4)	0.71(10)	1.14	4	89
3.50	1	16	0.650(9)	3.87(19)	4.42(64)	2.10	4	72
3.50	2	128	0.726(39)	1.15(31)	8.41(3.26)	0.04	1	84
3.50	3	16	0.665(5)	1.18(3)	1.51(12)	0.24	4	99
3.75	1	16	0.774(10)	3.32(17)	7.53(80)	0.65	4	96
3.75	2	16	0.779(7)	1.61(6)	3.73(27)	0.98	4	91
3.75	3	128	0.748(37)	1.34(34)	-1.65(3.86)	0.28	1	60
4.00	1	32	0.940(19)	2.23(23)	18.11(2.55)	0.30	3	96
4.00	2	32	0.918(13)	1.27(10)	7.06(95)	1.35	3	72
4.00	3	32	0.909(11)	0.89(5)	4.14(53)	0.79	3	85
4.00	4	128	1.009(37)	0.34(8)	12.03(2.97)	0.24	1	62

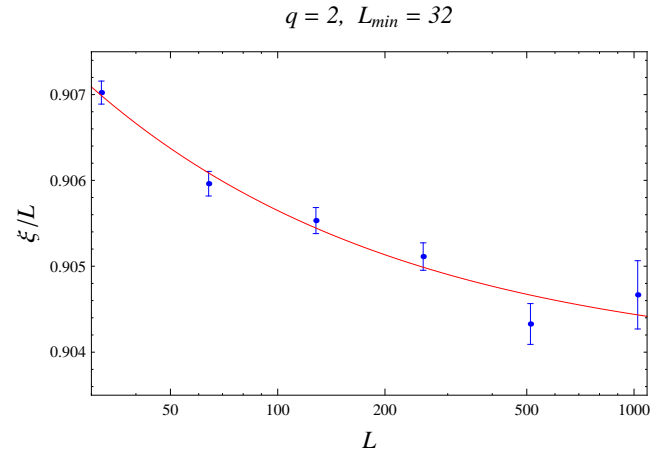
Table 27: Estimates for $z_{\text{int},\mathcal{C}_2}$ from fits to $\tau_{\text{int},\mathcal{C}_2} = AL^z + B$. Error bars are one standard deviation. L_{min} in brackets indicates a poor fit (confidence level $< 10\%$).

q	Fits to $\tau_{\text{int},\mathcal{C}_2} = AL^z$			Fits to $\tau_{\text{int},\mathcal{C}_2} = AL^z + B$		
	L_{min}	z	$z_{\mathcal{C}_2} - z_{\mathcal{E}'}$	L_{min}	z	$z_{\mathcal{C}_2} - z_{\mathcal{E}'}$
1.25	256	0.010(1)	—	64	-0.189(89)	0.024
1.50	—	—	—	—	—	—
1.75	128	0.062(1)	-0.096	128	0.047(67)	-0.038
2.00	256	0.103(3)	-0.112	64	0.016(14)	-0.127
2.25	128	0.174(3)	-0.112	16	0.122(4)	-0.113
2.50	128	0.247(2)	-0.106	16–128	0.217(7)	-0.090
2.75	16–256	0.333(1)	-0.091	16–128	0.322(7)	-0.086
3.00	16–64	0.429(1)	-0.082	16	0.431(3)	-0.066
3.25	32–64	0.522(1)	-0.065	16–32	0.543(4)	-0.029
3.50	64–256	0.637(4)	-0.056	16–128	0.662(4)	-0.027
3.75	128	0.759(5)	-0.025	16–128	0.777(5)	-0.019
4.00	128–256	0.892(6)	-0.006	32–128	0.921(7)	0.011

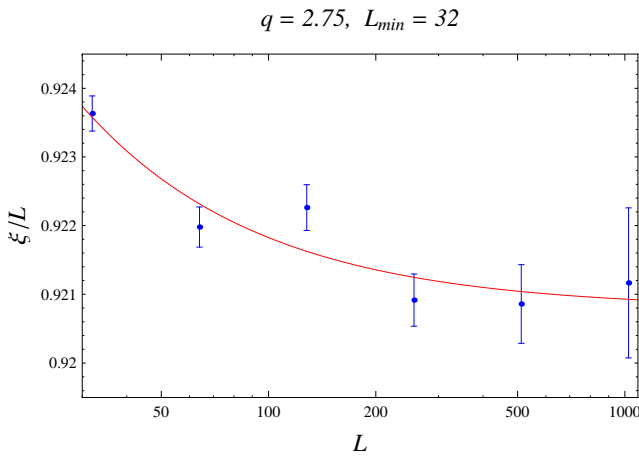
Table 28: Summary of estimates for $z_{\text{int},\mathcal{C}_2}$, averaged over all values of k for which the confidence level is $\geq 10\%$. Error bars are one standard deviation. The last column of each group shows $z_{\text{int},\mathcal{C}_2} - z_{\text{int},\mathcal{E}'}$ from the corresponding fits.



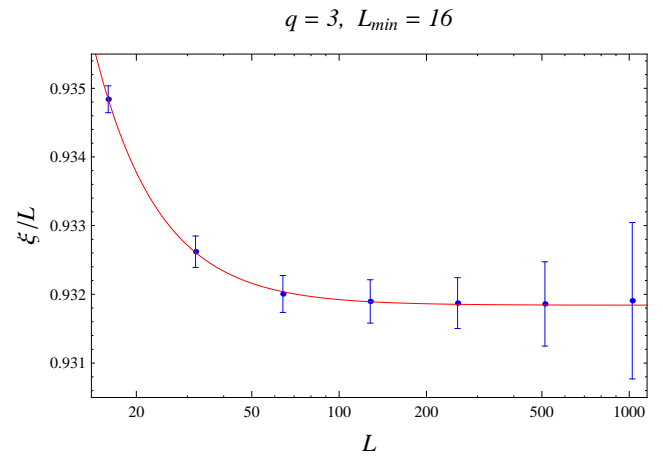
(a)



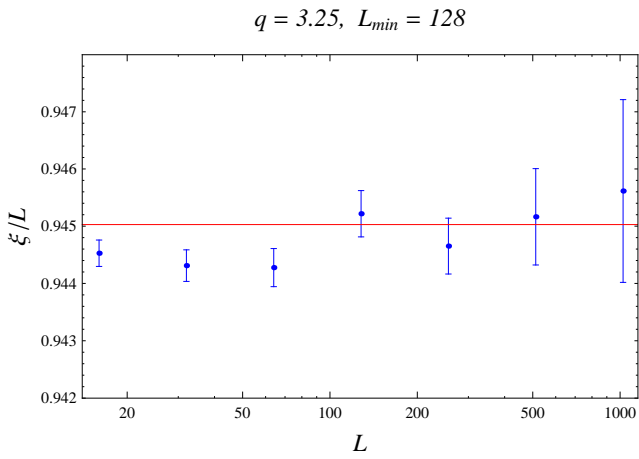
(b)



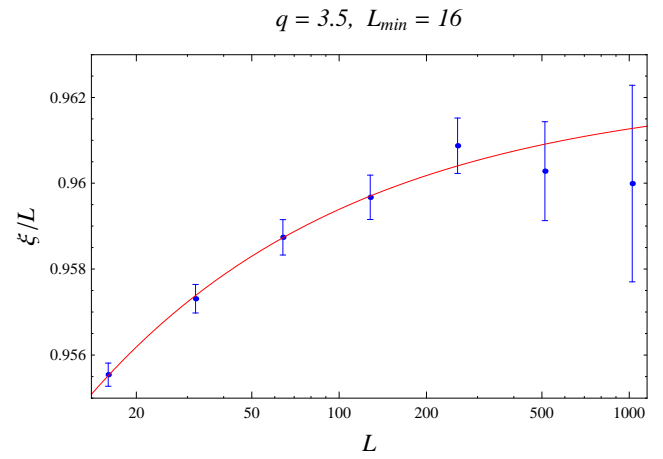
(c)



(d)



(e)



(f)

Figure 1: Fits of ξ/L to $x^* + BL^{-p}$. (a) $q = 1.25$, (b) $q = 2$, (c) $q = 2.75$, (d) $q = 3$, (e) $q = 3.25$, (f) $q = 3.5$. For $q = 3.25$ the fit is actually to a constant x^* .

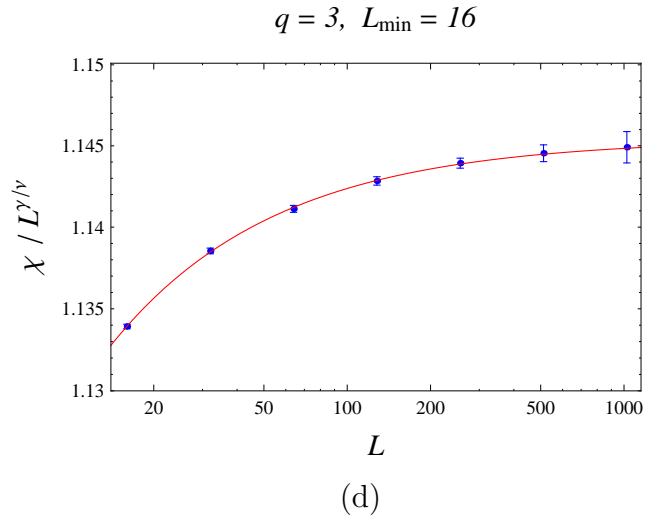
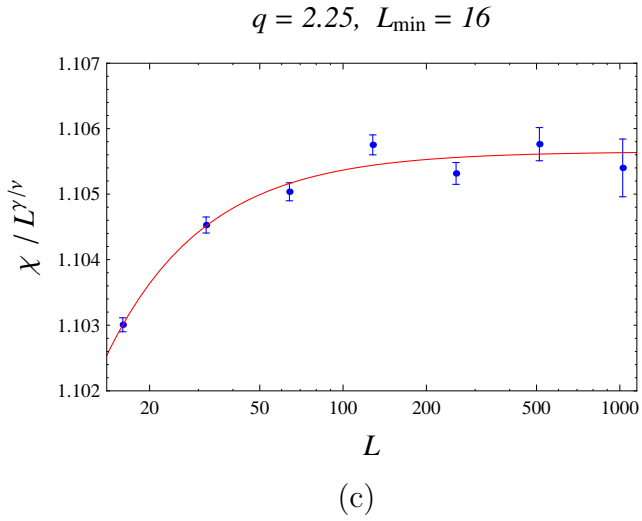
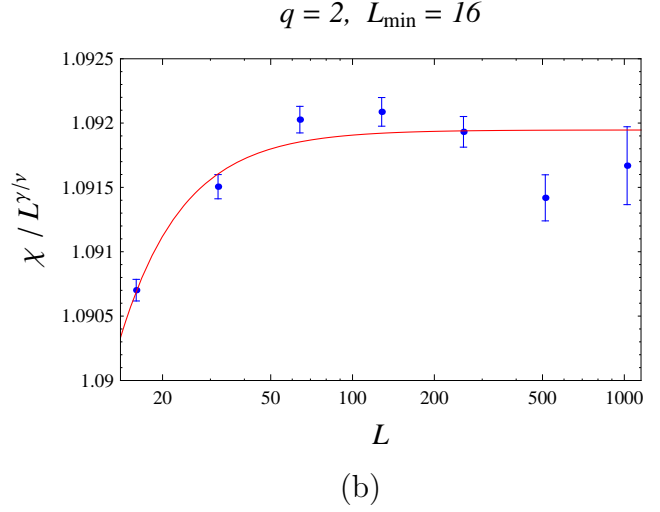
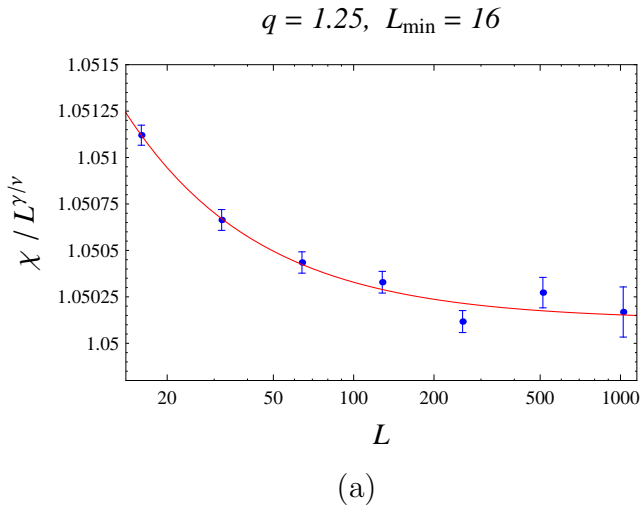


Figure 2: Fits of $\chi/L^{\gamma/\nu}$ to $A + BL^{-p}$. (a) $q = 1.25$, (b) $q = 2$, (c) $q = 2.25$, (d) $q = 3$.

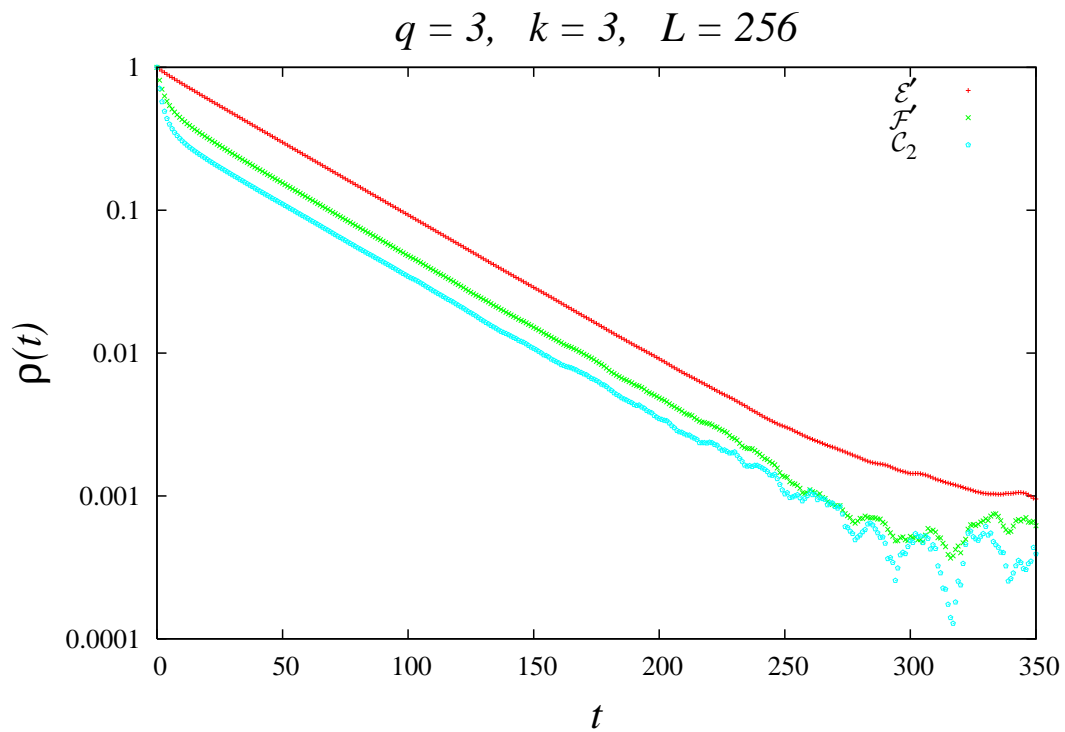


Figure 3: Normalized autocorrelation function $\rho_{\mathcal{O}\mathcal{O}}(t)$ for the observables $\mathcal{O} = \mathcal{E}'$, \mathcal{F}' and \mathcal{C}_2 , in the case $q = 3$, $k = 3$, $L = 256$.

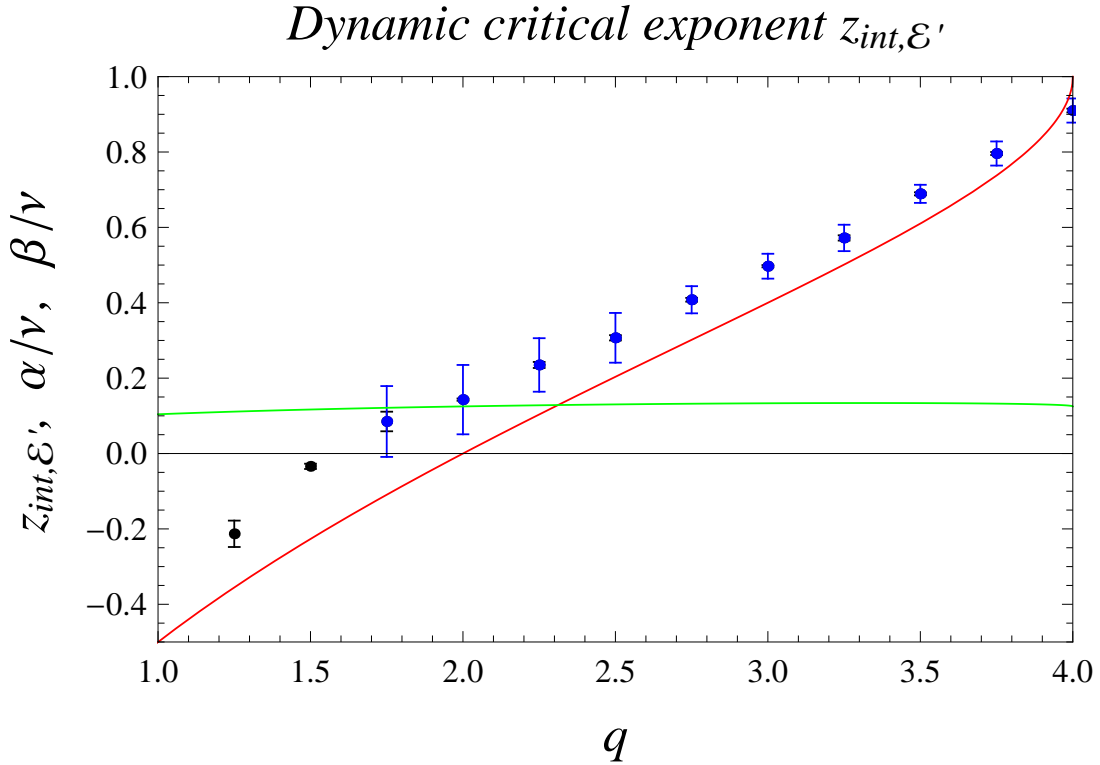
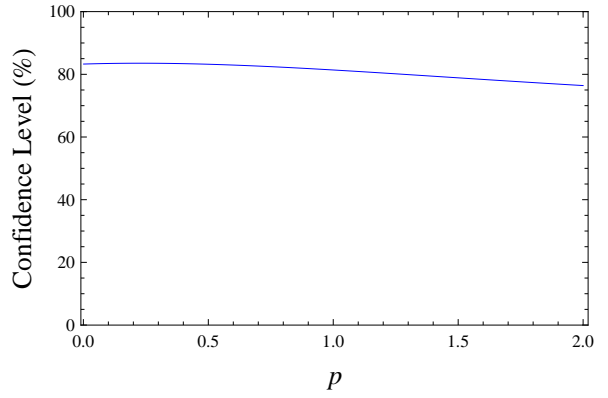
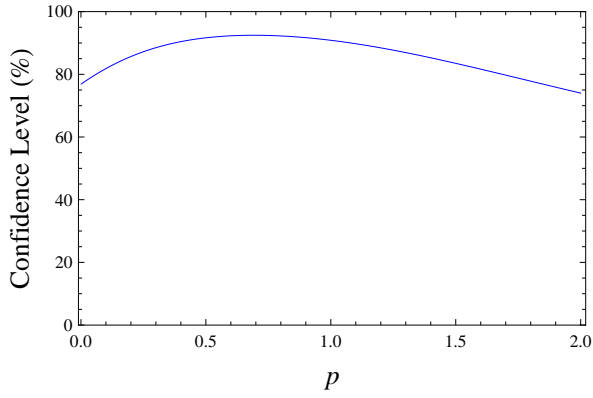
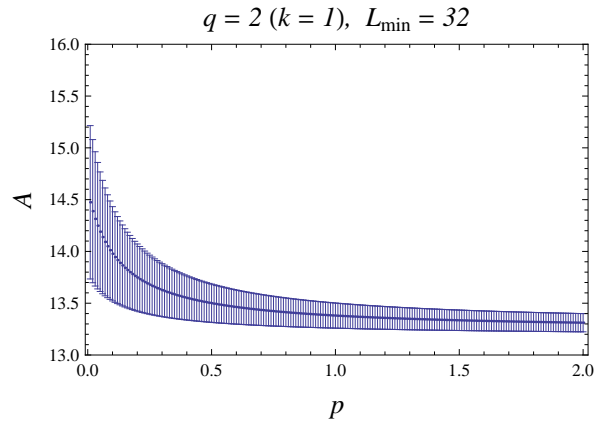
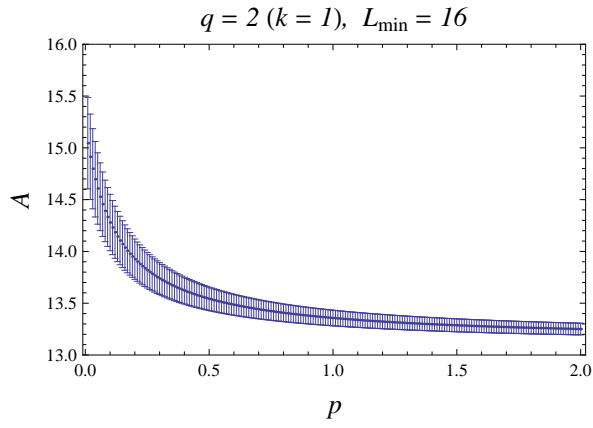


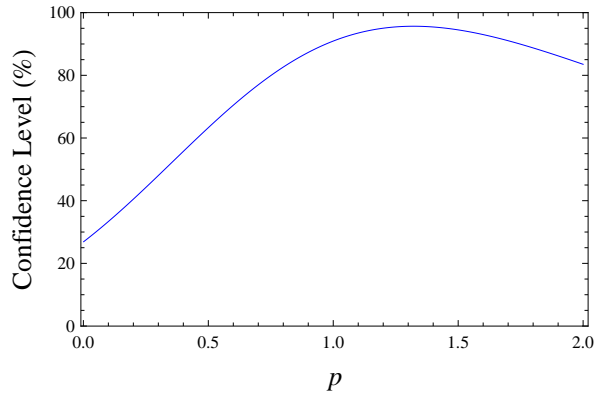
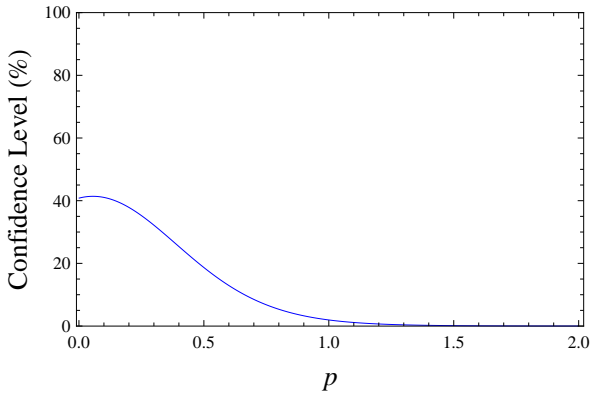
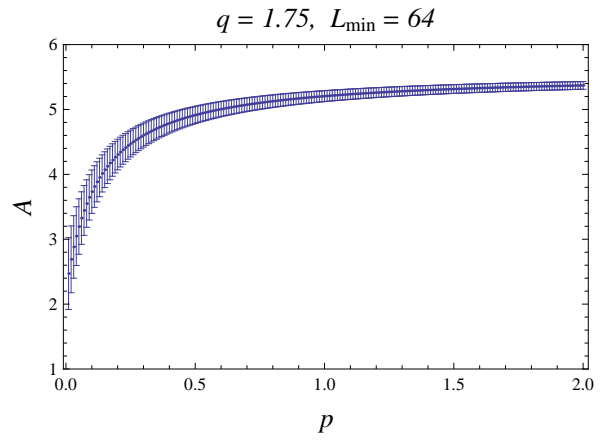
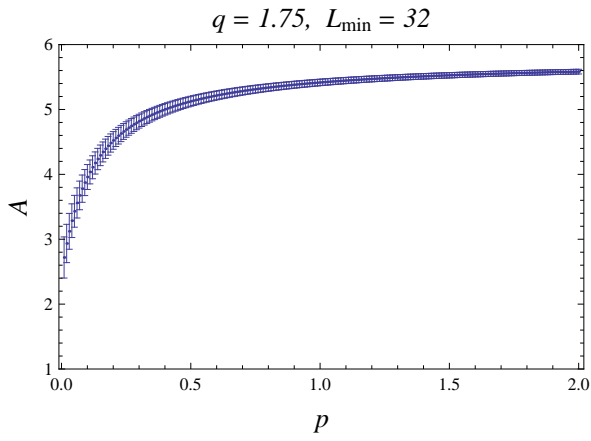
Figure 4: Our best estimates of the dynamic critical exponent $z_{int,\mathcal{E}'}$. The purely statistical error bar is indicated in black and is usually about the same size as the symbol; the combined statistical and systematic error bar is indicated in blue. (For $q = 1.25, 1.50$ we are unable to estimate the systematic errors.) The static exponents α/ν and β/ν are shown for comparison (red and green curves, respectively).



(a)

(b)

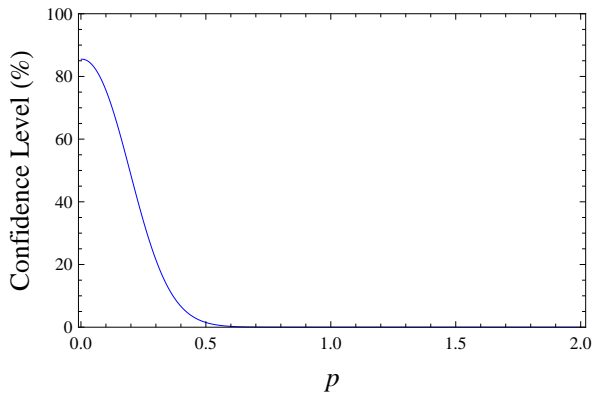
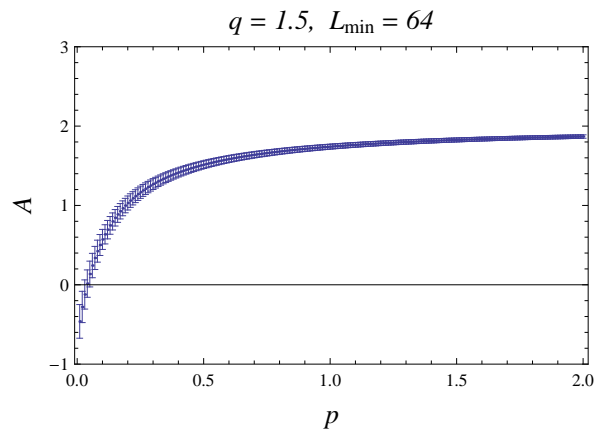
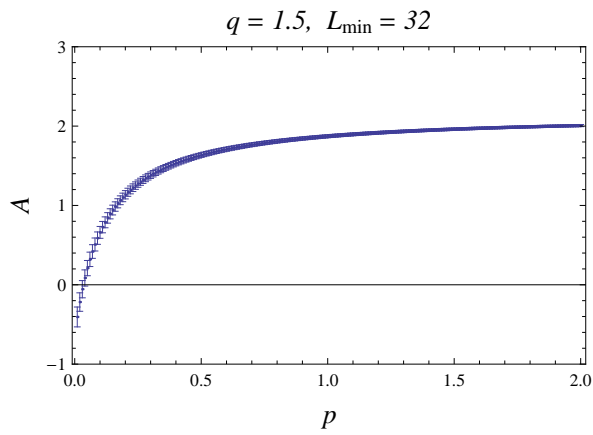
Figure 5: Fits to $\tau_{\text{int},\mathcal{E}'} = AL^{\beta/\nu} + B + CL^{-p}$ for $q = 2 (k = 1)$. (a) $L_{\min} = 16$, (b) $L_{\min} = 32$.



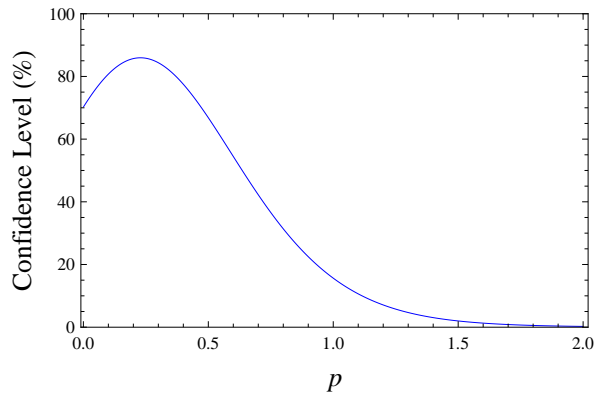
(a)

(b)

Figure 6: Fits to $\tau_{\text{int},\mathcal{E}'} = AL^{\beta/\nu} + B + CL^{-p}$ for $q = 1.75$. (a) $L_{\min} = 32$, (b) $L_{\min} = 64$.



(a)



(b)

Figure 7: Fits to $\tau_{\text{int},\mathcal{E}'} = AL^{\beta/\nu} + B + CL^{-p}$ for $q = 1.5$. (a) $L_{\min} = 32$, (b) $L_{\min} = 64$.

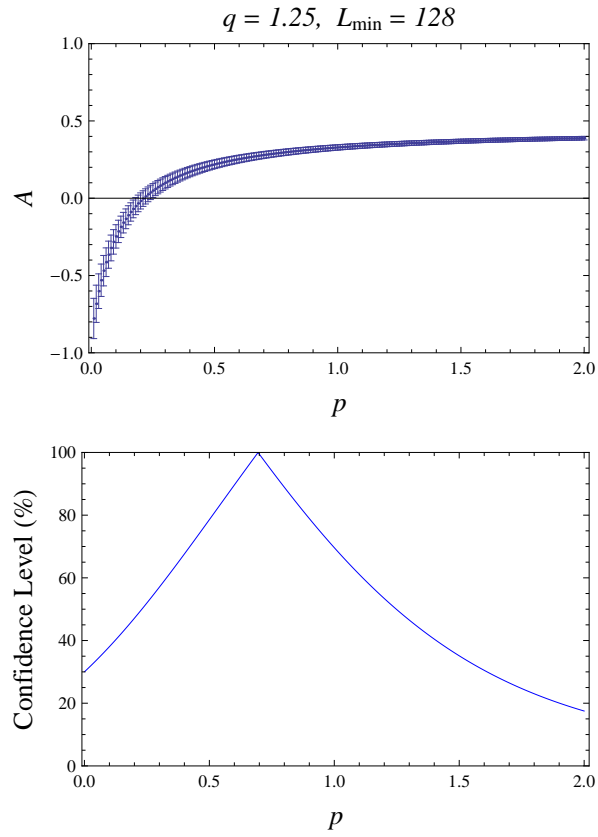


Figure 8: Fits to $\tau_{\text{int},\varepsilon'} = AL^{\beta/\nu} + B + CL^{-p}$ for $q = 1.25$, with $L_{\min} = 128$.